Comprehensive Assessment of Nanoparticle Delivery after Experimental Traumatic Brain Injury

by

Vimala Nagabhushana Bharadwaj

A Dissertation Presented in Partial Fulfillment
of the Requirements for the Degree
Doctor of Philosophy

Approved April 2018 by the
Graduate Supervisory Committee:

Sarah E. Stabenfeldt. Co-chair
Vikram D. Kodibagkar, Co-chair
Jeffery Kleim
Yanqinq Tian
Jonathan Lifshitz
Trent Anderson

ARIZONA STATE UNIVERSITY

May 2018

ABSTRACT

Traumatic brain injury (TBI) is a leading cause of disability worldwide with 1.7 million TBIs reported annually in the United States. Broadly, TBI can be classified into focal injury, associated with cerebral contusion, and diffuse injury, a widespread injury pathology. TBI results in a host of pathological alterations and may lead to a transient blood-brain-barrier (BBB) breakdown. Although the BBB dysfunction after TBI may provide a window for therapeutic delivery, the current drug delivery approaches remains largely inefficient due to rapid clearance, inactivation and degradation. One potential strategy to address the current therapeutic limitations is to employ nanoparticle (NP)-based technology to archive greater efficacy and reduced clearance compared to standard drug administration. However, NP application for TBI is challenging not only due to the transient temporal resolution of the BBB breakdown, but also due to the heterogeneous (focal/diffuse) aspect of the disease itself. Furthermore, recent literature suggests sex of the animal influences neuroinflammation/outcome after TBI; yet, the influence of sex on BBB integrity following TBI and subsequent NP delivery has not been previously investigated. The overarching hypothesis for this thesis is that TBI-induced compromised BBB and leaky vasculature will enable delivery of systemically injected NPs to the injury penumbra. This study specifically explored the feasibility and the temporal accumulation of NPs in preclinical mouse models of focal and diffuse TBI. Key findings from these studies include the following. (1) After focal TBI, NPs ranging from 20-500nm exhibited peak accumulation within the injury penumbra acutely (1h) post-injury. (2) A smaller delayed peak of NP accumulation (40nm) was observed sub-acutely (3d) after focal brain injury. (3) Mild diffuse TBI simulated with a mild closed head injury model did not display any measurable NP accumulation after 1h post-injury. (4) In contrast, a moderate diffuse model (fluid percussion injury) demonstrated peak accumulation at 3h post-injury with up to 500 nm size NPs accumulating in cortical tissue. (5) Robust NP accumulation (40nm) was found in female mice compared to the males at 24h and 3d following focal brain injury. Taken together, these results demonstrate the potential for NP delivery at acute and sub-acute time points after TBI by exploiting the compromised BBB. Results also reveal a potential sex dependent component of BBB disruption leading to altered NP accumulation. The applications of this research are far-

reaching ranging from theranostic delivery to personalized NP delivery for effective therapeutic outcome.

DEDICATION

I dedicate this work to my mother, Bharati Rao. I am grateful for your unconditional love and support to make this possible. I would like to thank my dad, Nagabhushana Rao for his love, guidance and support through the years. I would like to thank my brother Shashank for his unwavering encouragement, inimitable set of advice and motivation over the years. Cheers to my sister-in-law, Aparna for always being there for me and making this journey enjoyable. I would like to thank my husband, Charan for his incredible patience, love and support. My stability, health and happiness are wholly indebted to you. In the recent years, I am extremely grateful for the love, support and encouragement of my loving parents, Sudha and Prakash.

ACKNOWLEDGMENTS

I would like to thank my Ph.D. advisors and mentors, Drs. Sarah E. Stabenfeldt and Vikram D. Kodibagkar. Thank you both for sculpting my research skills and instilling critical thinking. I shall always be grateful for your constant encouragement and insightful thinking, constructive criticism and for always being available to address any concerns. I would like to thank my dissertation committee members, Drs. Jeffery Kleim, Yanqinq Tian, Jonathan Lifshitz, and Trent Anderson for their encouragement. I appreciate their continued guidance and helpful inputs to shape my work and expand my scientific perspective.

I would like to thank the facilities/resources at Arizona State University. Especially, I appreciate the Bioimaging facility/Keck division (Arizona State University) and Dr. Debra Baluch for use/assistance with confocal imaging. I appreciate CLAS-Life Sciences Electron Microscope and Mr. David Lowry for use/training in transmission electron microscopy. I appreciate Dr. Meldrum for the use of dynamic light scattering instrument. I express my sincere thanks to Dr. Jason Newbern for his guidance/training in using confocal microscope and all the valuable advice.

Over the past few years, our collaborators at University of Arizona-College of Medicine, Phoenix have been integral to the success of this work through their contribution of knowledge, time and resources. I truly appreciate Dr. Shenfeng Qiu for his assistance and guidance with the two-photon microcopy and I am thankful for letting me use the animal stereotaxic mount. I would like to thank Dr. Trent Anderson and his lab members, especially Chen Wu for performing mild closed head injuries and supporting the two-photon microscope experiments. I extend my thanks to Dr. Jonathan Lifshitz and his lab, especially Dr. Rachel Rowe, Dr. Jordan Harrison for performing the fluid percussion injuries. Also, I would like to thank Katie Giordano for supply/maintenance of the transgenic animals used for two-photon experiments.

I want to acknowledge all the lab members of Stabenfeldt and Probe lab for their continued help and support. Specifically, thanks to Crystal Willingham, Amanda Witten, Briana Martinez, Kassondra Hickey and Connor Copeland for contributing to a healthy/supportive lab environment and managing the lab. Thanks to Amanda Witten for spending hours of her time for

creating incredible artistic illustrations/figures used in this work. Special thanks to graduates, undergraduates and high school students for their contributions to this work and/or helping me build my mentoring skills- Jordan Todd, Kyle Offenbacher, Jacob Irwin and Alisha Kodibagkar; I have learnt a lot from each one of them. Thanks to my BME friends from various labs for a truly enjoyable environment both at and outside of work. In particular, I would like to thank Drs. Caroline Addington, Dipankar Dutta, Rohini Vidya Shankar, Shubhangi Agarwal, Aprinda Indahlastari, Priya Nair and Sai Pavan Taraka Grandhi. I would also extend my thanks to Nutandev Bikkamane Jayadev, Swathy Sampath Kumar and Stephanie Ong. I am extremely grateful to Dr. Jagannatha Rao (Dayanada Sagar Institutions) and Dr. Vincent Pizziconi (ASU) for their continued career mentoring and advising through these years.

I would like to mention my appreciation for the staff at SBHSE for taking care of all the administrative matters in a friendly and timely manner, in particular Laura Hawes, Tamera Cameroon, Tomi St John and Jessica Jensen. This work was supported by the Flinn foundation (1976, VDK, SES, JL, PDA) and National Institutes of Health (IDP2HD084067; SES). I also extend my thanks to School of Biological and Health Systems Engineering and the Graduate and Professional Student Association at ASU for their travel support for several conferences.

TABLE OF CONTENTS

Page

LIST OF TABLES

LIST OF FIGURES

PREFACE

The work represented in this dissertation document has been previously published in the form of a review article[1] (Chapter 1) and an original research article[2] (Chapters 2). These published works have been expanded upon and adapted for use in this dissertation document.

CHAPTER 1

INTRODUCTION

1.1 Epidemiology of Traumatic Brain Injury

Diagnosis and treatment of acquired brain injuries remain a considerable challenge, particularly of traumatic brain injury (TBI)[3-7]. TBI is a leading cause of disability worldwide[8] with 1.7 million TBIs reported annually in the United States[9]. TBI accounts for an estimated 235,000 hospitalizations yearly in the US, with 80,000 of these cases resulting in lasting disability[10]. TBI is the leading cause of mortality and morbidity for persons under 45 years of age[11]. Moreover, brain injuries affect a large patient population, with major physical and emotional suffering for patients and their relatives and at a significant cost to the society[9,12-14]. These injuries may not only lead to substantial tissue damage with an irreversible functional loss, they also lead to disruption of the intricate neural circuits and connections involved in cognitive, sensor-motor functions[15,16].

1.2 Pathophysiology of TBI

TBI is damage to the brain that occurs as a result of direct and indirect damage due to a traumatic event such as falls and traffic accidents[17]. Brain injury characterized by structural failure and neurologic dysfunction begins at the time of initial injury and lasts from hours to weeks[18,19]. The initial mechanism of injury results in a cascade of neural and vascular events, which eventually lead to the clinical syndrome of TBI[18,19] (Figure 1.1.).

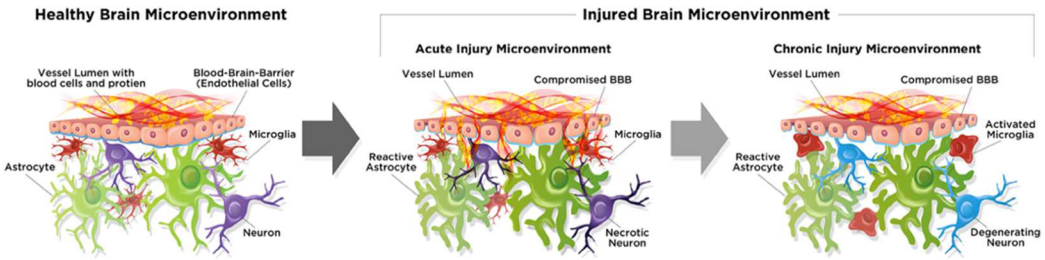

Figure 1.1 Microenvironment of a healthy and injured brain: pathological changes after brain injury. Healthy brain microenvironment consists of an intact BBB with healthy astrocytes, microglia, and neurons. Brain-injured microenvironment may shift to an altered state that evolves

over time and may include compromised BBB, reactive astrocyte, activated microglia, and necrotic/degenerating neurons.

1.2.1 Response phases of TBI

The pathology of TBI leads to immediate and delayed injury response phases, Fig 1.2. The immediate primary injury is due to the external impact and is considered untreatable, but preventable. On the macroscopic level, such damage includes shearing of white-matter tracts, focal contusions, hematomas, and diffuse swelling[12,15,20]. The pathology that follows the primary injury is known as the secondary injury including inflammation, receptor-mediated damage, oxidative damage and calcium-mediated damage[12,15,20]. Each type of head injury might initiate such pathophysiological mechanisms with variable extent and duration[12,15,20]. The secondary process develops over hours and days, thus allowing a time window for intervention.

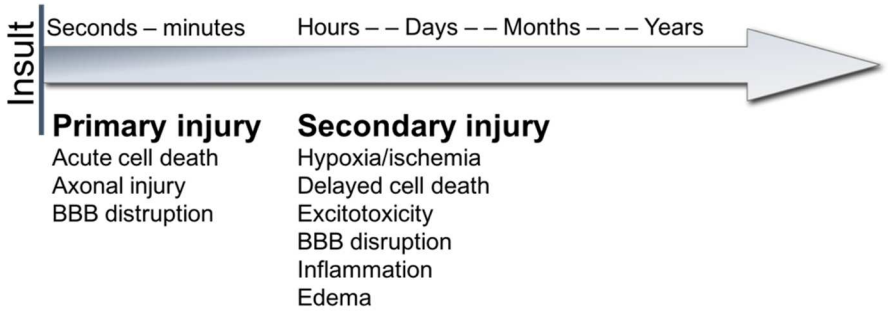

Figure 1.2 Temporal phases of TBI response: the mechanical impact leads to the primary injury due to immediate mechanical damage that occurs at the time of the injury. Secondary injury occurs due to the biochemical and physiological events from the primary injury.

1.2.2 Blood-brain barrier (BBB) dysfunction

TBI causes a widespread release of inflammatory cytokines and other inflammatory mediator results in oxidative stress and upregulates endothelial expression of cell adhesion molecules[15,21]. Consequently, an influx of inflammatory cells into the brain parenchyma further

progresses the injury and incites excitotoxicity and neuronal loss[15,21]. In some cases of TBI, the microvessel disruption caused by the impact rapidly activates the coagulation cascade forming intravascular thrombi in capillaries of the pericontusional area[17,21]. Platelet and leukocyte-platelet aggregates have also been observed within pial and parenchymal venules after injury. Such aggregates may lead to reduced cerebral blood flow in pericontusional brain tissue with a potential risk for secondary ischemic injury. Ischemia causes a reduction in oxygen accessibility and ionic gradient failure that results due to energy depletion in the neuronal cells through interruption of the ATP-dependent Na^+/K^+-ATPase and Ca^{2+}-ATPase activity. When the ionic balance is disrupted, cations in the extracellular fluid (e.g. Na^+) accumulate inside the cells finally leading to cytotoxic edema[22,23]. Moreover, Na^+ uptake causes extensive plasma membrane depolarization and eventually bringing additional Ca^{2+} into the cell[22]. An influx of Ca^{2+} stimulates the release of neurotransmitters such as glutamate or dopamine into the synapse, leads to neurotoxic shock and ensuing neuronal cell death and development of an ischemic core[24]. Consequently, calcium homeostasis in the central nervous system (CNS) is disrupted leading to the generation of mitochondrial reactive oxygen species (ROS) and a host of catalytic enzymes that damage proteins and DNA[22,24]. Collectively, these neurochemical events contribute to lipid peroxidation and disruption of the BBB[23-25].

The BBB is one of the most vital components of a physiological normal brain creating a restrictive barrier between the CNS and the rest of the body[17]. The BBB performs the major function as physical and transports barrier to monitor the influx of substances from blood via paracellular/transcellular diffusion and/or transport proteins[26]. After TBI, the shearing forces generated by head trauma imparts mechanical damage to endothelial cells and may lead to acute BBB permeability and extravasation of plasma protein and red blood cells[15,17,27]. Studies have shown immediate and delayed dysfunction in the BBB/gliovascular unit after TBI[15,21,28-30]. In cases of focal injury, the immediate (minutes to hours) BBB breakdown can be a combination of the direct mechanical impact leading to the cerebrovascular walls disruption and the functional changes occurring at the BBB[15,21]. The delayed (days) BBB opening can arise

due to inflammation-related mechanisms, astrocytic dysfunction and metabolic disturbances[15,21]. The BBB dysfunction at the delayed time point is mainly associated with dysregulation of tight junction proteins[15,31]. Tight junction protein complexes situated between endothelial cells control BBB permeability by limiting paracellular diffusion; key tight junction proteins include junctional adhesion molecules, occludin, claudins and membrane-associated guanylate kinase-like proteins (ZO-1,-2,-3) [32]. Oxidative stress due to ROS and free radical production after brain trauma alter the critical organization of tight junctions proteins at the BBB resulting in increased paracellular leakage[15,33]. Additionally, astrocytes influence the BBB disruption after brain injury by mechanisms such as the opening of paracellular channels, physical disruption of astrocyte-endothelial junctions and digestion of BBB matrix proteins[34,35]. Conclusively, a better understanding of the brain injury pathology and the BBB permeability is instrumental in developing improved therapeutic interventions. The BBB dysfunction (initial and delayed opening) enables blood-borne substances that are normally restricted, such as proteins, red blood cells to enter the brain parenchyma. The BBB disruption may provide opportunities for therapeutic delivery via nanoparticles (NPs). The strategies for therapeutic interventions via NP delivery are aimed at salvaging the pericontusional/penumbra area for possible neuroprotection and neurovascular unit preservation.

1.2.3 Sex dependence and BBB disruption

The role sex differences in the treatment and outcome of brain injury is a growing area of research. Numerous studies have shown sexual dimorphism in the anatomical structure, cerebral blood flow and neural organization in the brain [36-40]. For example, studies have confirmed a higher cerebral blood flow in females compared to males[41-43]. One of the studies focused on the role sex hormones such as estrogens play in the neural organization of the cerebral cortex, cell-mediated immunity, axonal and dendritic growth and synapse formation[39]. However, the complexity of neural structure and function with respect to sex has not been fully elucidated.

Of particular interest to the TBI field, it is not known if the permeability of BBB (specifically after TBI) is regulated differently in females and males. Seizure studies have demonstrated

female rats showed pronounced extravasation of Evans-blue (BBB permeability tracer) compared to the male rats[40,44-46]. Specifically, Evans-blue was injected 5 minutes before administering seizures in rats and were perfused after 30mins to analyze the tissue[44]. Furthermore, TBI studies have investigated the sex differences in the degree of tissue injury showing more severe cerebral edema, a significant cause of secondary brain injury, in males compared to females[47,48]. Furthermore, Roof *et. al.* showed that reduction in edema severity with progesterone treatment was also associated with improved BBB integrity[47,48]. Another aspect of BBB permeability is the close association with the neuroinflammatory response after TBI[21]. Recently, Villapol's group reported a sex-dependent inflammatory response after TBI (mouse model). Specifically, they observed a less robust neuroinflammatory profile in female mice compared to a pronounced activation in male mice[49]. Taken together, understanding how sex affects the BBB permeability after TBI is a critical step toward developing not only effective but also personalized TBI treatment.

1.3 Types of TBI and Animal Models

In clinical settings, TBIs are classified based on the presence or absence of focal lesions as focal or diffuse. Injuries may be considered predominantly heterogeneous with both focal and diffuse components, but most injuries are heterogeneous with a combination of both the components[20]. Lesions such as contusion, subdural hematoma, epidural hematoma, and intraparenchymal hemorrhage are considered focal injury[20]. The diffuse injury is associated with axonal injury, hypoxic-ischemic injury and microvascular injury that affect widely distributed anatomic regions[20]. The pathophysiological heterogeneity observed in TBI patients may arise from the mechanism of primary injury (the location, nature, and severity) and the effects of other factors such as age, health, sex, genetics, and medication/drug use[50]. Animal models have been developed to improve our understanding of the complex molecular cascade involved in clinical TBI[51]. In preclinical setting, a single animal model may not be able to fully recapitulate all the aspects of human TBI[52,53]. For successful clinical translation, multiple TBI animal models must be incorporated to develop new strategies.

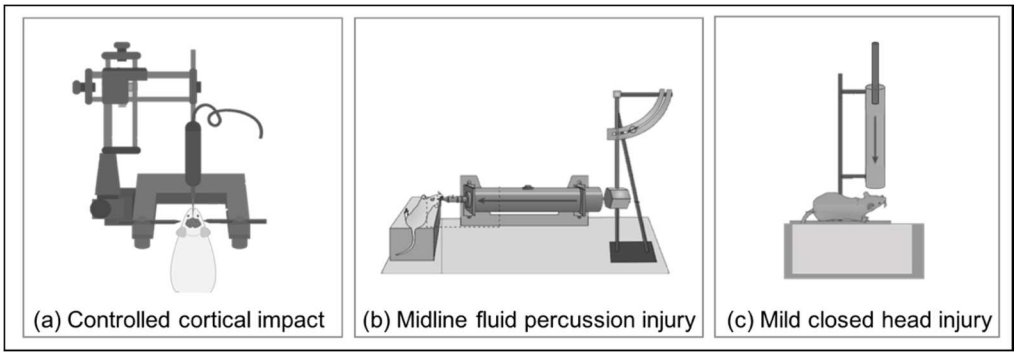

Figure 1.3 Animal models of traumatic brain injury: Focal injury model: Controlled cortical impact is schematically depicted in panel (a). The two types of commonly used diffuse injury models are depicted in panel (b) midline fluid percussion injury and (c) mild closed head injury models. (modified/reprinted by permission from Springer Nature, [41]).

1.3.1 Focal brain injuries

Focal injuries are thought to be responsible for two-thirds of brain injury-related deaths[18]. Clinically, the focal injuries are associated with contusions, epidural hematomas and skull fracture[53,54]. Focal injuries are typically induced due to penetrating object to the skull, such as gunshot wound, or a blow. Such injuries typically result in macroscopically visible damage at the impact site. Experimental focal brain injuries in rodents can be induced by techniques such as controlled cortical impact (CCI) [51,53,55]. Here, a pneumatically or electromagnetic driven impactor is used at a specific velocity and depth, through a craniectomy to deform the brain[51,53,55], Fig 1.3 (a). CCI produces contusion with hemorrhagic and necrotic contusion with cortical tissue loss, acute subdural hematoma, axonal injury, concussion, cytotoxic and vasogenic edema and BBB dysfunction[51,53,56,57].

1.3.2 Diffuse brain injuries

Clinically, the hallmark of diffuse injury is diffuse axonal injury (DIA) encompassing a spectrum of injuries of severe injuries result in vegetative/highly dysfunctional outcomes but also those mild brain injuries of concussive type[18]. Indeed, DIA is thought to be one of the most common pathologic features of TBI[9,53,58,59]. The main outcome of dynamic deformation of

white matter tracts during trauma is the disruption of axonal transport, leading to axonal swellings within a few hours of trauma[53]. One of the widely used diffuse injury models is midline fluid percussion injury and mild closed head injury.

1.3.2.1 Midline fluid percussion injury (FPI)

The midline FPI models a closed head injury and the applied mechanical forces are the hydraulic pressure produced by a device[51,53,60,61]. The pressure fluid pulse is delivered onto the intact dura through a craniectomy that lies along the midline suture. The procedure does breach the cranial vault, but the skull is sealed to the injury device, thus restoring a closed system[51,53,60,61], Fig 1.3 (b). Midline FPI leads to bilateral cortical alterations, cerebrovascular changes, hypertension, elevated intracranial pressure, BBB permeability[51,53,60,61]. Histopathological findings display association with petechial hemorrhage in the brain parenchyma, subarachnoid hemorrhage and axonal damage[60,61].

1.3.2.2 Mild closed head injury (mCHI)

About 70-90% of all TBIs are mild head trauma, most common among professional athletes engaged in contact and collision sports[51,60,62]. The primary cause of mTBI in sports is the application of both linear and rotational acceleration and impact deceleration forces to the brain[62]. Such impacts cause non-penetrating diffuse damage rather than focal injury[62]. A modified model of weight-drop model, termed as mild closed head injury (mCHI) is known to produce a diffuse brain injury[63]. The study reports recapitulating the nature of CHI where animal is unrestrained and under goes linear and rotational impact forces[63], Fig 1.3 (c). The mild CHI model is known to produce several of the cognitive and behavioral outcomes associated with clinical mTBI[63,64].

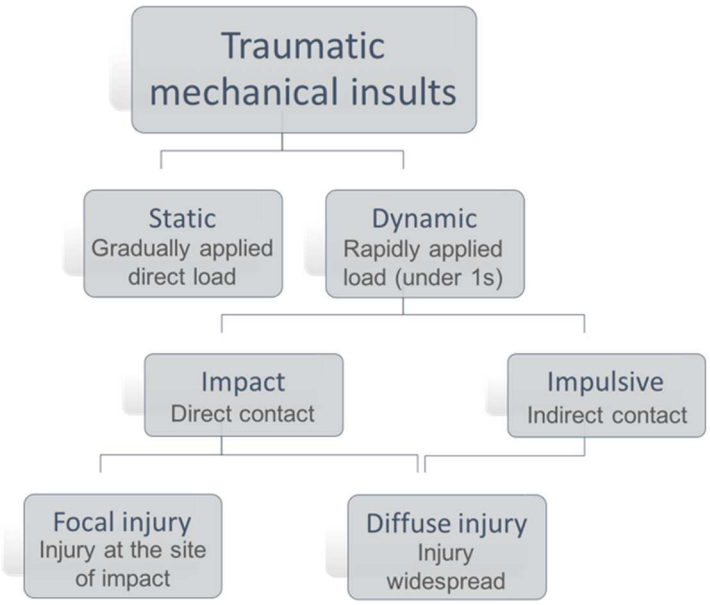

Figure 1.4 Traumatic mechanical insults: The two broad categories of the mechanical impact, static and dynamic, can induce traumatic brain injury. Dynamic loading is the most common type, can be further classified as impact and impulsive loading. The insult parameters and the mechanical response will dictate the types of injury (focal and/or diffuse TBI).

1.3.3 Traumatic mechanical insults

At a mechanistic level, TBI can be mechanically induced by blunt or penetrating impacts, inertial loading or non-impact blast waves. Such mechanical impact induces a mechanical response at the cell and tissue level that ultimately cause pathophysiological injury response. The point at which an external load causes tissue damage, known as the threshold is dependent on the type and duration of the load[54]. The mechanical conditions (insult parameters) can broadly be categorized, (Fig 1.4), into static and dynamic loading[54,65]. Static loading is gradually applied direct load and dynamic loading is rapidly applied load[54,65]. Dynamic loading is the most common type and can be further classified into impact loading and impulsive loading[54,65]. Impact loading is where a direct impact occurs on the head. Depending on the magnitude of the force and area of the impact, impact loading can result in either focal or diffuse injury[54,66]. Impulsive loading occurs due to indirect loads and leads to diffuse injury[54]. In this study, we use

mice models to simulate the different models of focal and diffuse TBI for pre-clinical study. We use controlled cortical impact to model focal brain injury and fluid percussion injury as well as mild closed head injury to model diffuse brain TBI.

1.3.5 Inference

The complex cascade of events in the pathophysiology that ensues after brain injury limits effective diagnostic and therapeutic options available[16]. Moreover, access to the brain is typically regulated by the blood-brain barrier (BBB) thus presenting a formidable obstacle for small and macromolecular therapeutics to enter the brain[75]. Therefore, diagnosis/treatment via systemic administration or local delivery of drugs is largely inefficient[76]. Despite these challenges, the potential benefits of nanotechnologies for brain injury applications are tremendous and may eventually offer the novel clinical opportunities to address current limitations.

1.4 Drug Delivery and Nanoparticles

Drug delivery can be defined as the process of delivery a drug/bioactive agent within the therapeutic threshold for dosing and time in a safe and reproducible manner[67,68]. However, for many drugs ideal dosing to the target tissue(s) are not met with standard approaches (i.e. oral or intravenous dosing of free drug). Therefore, it is critical to improve drug delivery methods using current advances in drug discovery and rational design[67,68]. Drug dosing and delivery mechanisms are limited by small molecule 1) aggregation due to poor solubility, 2) elevated toxicity and dosage, 3) nonspecific delivery, 4) in vivo degradation and 5) short circulation half-lives[67,68]. Additionally, one of the main limitations of clinical failure specifically for TBI is lower drug efficacy due to drug clearance, inactivation and, degradation[52,69,70,69,71]. One strategy to improve drug efficacy is by encapsulating small molecules/drugs into nanoparticles (NPs)[68,72-74]. The advantages of using NPs as a drug delivery system include the ability of easy manipulation of the NP particle size and surface characteristics to achieve both passive and active drug delivery after administration[68,72-74]. Moreover, NPs can be used to achieve an increase in drug therapeutic efficacy, reduce side effects, and preserve drug activity[68,72-74].

1.5 Nanoparticle Delivery after TBI

Nanoparticles (NPs) as defined for pharmaceutical purposes are solid colloidal particles ranging from 1 and 1000 nm in size[73,77,78] and are utilized for various biomedical applications due to their pharmacological attributes[79,80]. Their small size and mobility enable NPs to access a wide range of tissues and cells for both extracellular and intracellular delivery. Administration of NPs through the microcirculation is a viable approach for facilitating drug delivery to the brain, since the diameter of the smallest capillaries is approximately 5-6 μm[81]. NPs can be used to deliver hydrophilic/hydrophobic drugs, proteins, vaccines, biological macromolecules, gene delivery, etc[82]. Engineered NPs have the potential to revolutionize the diagnosis and treatment of many diseases due to their unique function and structural organization[83,84]. Over two-dozen NPs systems have been approved by the US Food and Drug Administration (FDA) for clinic to either treat or diagnose diseases with additional formulations in clinical trials[85,86]. One advantage of nanomaterials is the potential interaction with biological systems at a molecular and supra-molecular level. Such interactions may be tailored to induce desired physiological responses in cells while reducing undesirable systemic side effects[87].

For a NP delivery system to achieve the desired benefits, the residence time in the bloodstream must be long enough for the NP to reach or recognize its site of action. However, the major obstacle to the realization of this goal is NP clearance from the bloodstream where previous studies report only 1-5% of injected NPs may actually reach their intended target site[88,89]. The main NP clearance mechanisms are the same as the body's removal of foreign material from the bloodstream. These coordinated mechanisms include opsonization, renal clearance, and sequestration in the mononuclear phagocytic system (MPS), previously known as the reticuloendothelial system. Phagocytic recognition and clearance is dependent on initial particle opsonization and as such recent research has focused on developing methods to effectively slow this process resulting in increased blood circulation half-life[90]. Key NP parameters identified to help evade clearance mechanisms include surface modification, size,

charge and shape[88]. Furthermore, we note that recent reviews have addressed the complex response of the MPS and NP clearance[88,91] that are only briefly mentioned in the sections below.

1.5.1 Composition

Nanoparticles can be synthesized using various materials and protocols where the parameters of which are trailered to design the desired NPs. Most essential characteristics for drug delivery considerations are size, payload encapsulation efficiency, zeta potential and payload release characteristics[68,72,79,81]. The ideal properties of NPs for brain drug delivery are not only to be nontoxic, biodegradable and biocompatible, but also have physical stability in blood with prolonged blood circulation and ability to cross BBB[68,73,74,92]. Different NPs used for brain injury applications include polymeric NPs (liposomes, dendrimers, chitosan) [93-96], lipid NPs[97], inorganic NPs (silica, metals) [98,99] and hybrid NPs[100,101].

1.5.2 Surface modification

Surface modification of NPs is a key parameter used to escape clearance mechanisms, particularly opsonization. Seminal studies demonstrated masking of NPs from opsonization by conjugating the hydrophilic polymer polyethylene glycol (PEG) onto NP surface[102-104]. PEG substantially reduces nonspecific interactions with proteins through its hydrophilicity and steric repulsion effects, which results in reduced opsonization[105]. For example, Lu *et. al*., demonstrated markedly prolonged blood circulation of PEGylated liposomal doxorubicin compared to native liposomes. Specifically, the elimination half-time of regular and PEGylated liposomes were ~26 and ~46 h, respectively, thus nearly doubled by simply PEGylating the NP surface[103]. Similarly, Sadzuka *et. al*., observed prolonged plasma circulation of liposomes and increase of drug accumulation in the tumor by employing PEGylated liposomes[106]. Therefore, PEGylation dramatically influence the NP delivery to improve NP circulation half-life.

1.5.3 Size

Small molecules (< 1kDa) such as free drug and contrast agents are removed from blood circulation via renal clearance by glomerular filtration into the urine. Glomerular filtration is dictated largely by a molecular size with a cut-off for compounds smaller than 5-6 nm[107]. For systemic delivery, the upper size limit of NPs size is about 5-8 μm dictated by the smallest diameter of lung micro-capillaries[108]. Larger particles carry the risk of clogging the vessels inducing embolism[108]. Generally, for brain delivery NPs ranging from 20 – 100 nm are used for leveraging minimal clearance NPs[104,109,110]. Studies have shown a clear inverse correlation between NP size and BBB penetration[2,111]. We previously reported NP delivery to the brain via the transiently breached BBB due to focal brain trauma. The study demonstrated the ability of smaller NPs (20, 40 nm) for prolonged access to the injured brain compared to larger NPs (100, 500 nm) [2]. To this end, for systemic brain delivery, the NP size plays an important role for enabling prolonged blood circulation and access to the brain.

1.5.4 Charge

Another key parameter to consider for systemic delivery of NPs is the surface charge, which influences clearance and stability in circulation. Here one must consider the impact blood proteins and cells have on the stability of NPs *in vivo.* For example, i*n vitro* studies limited to NPs suspended in saline or deionized water require a high zeta potential of more than 30 mV (either positive or negative) to maintain the stability and prevent aggregation. [112,113] Yet, systemically delivered positively charged NPs *in vivo* readily form aggregates with the negatively charged serum proteins and often cause embolism(s) in the lung capillaries[108]. Generally, negative NPs (~ - 40 mV) exhibit strong MPS uptake and positive NPs (~ + 40 mV) induce serum protein aggregation[104,114]. NPs with neutral charge (within +/- 10 mV) exhibit the least MPS interaction and the longest circulation *in vivo*[104,114]. Specifically, for brain delivery studies have shown that highly positive NPs (~ + 45 mV) cause immediate toxicity with BBB disruption[115]. On the other hand, neutral and moderately negative NPs did not show toxic effect and can be utilized for brain delivery[115].

1.5.5 Shape

The morphology and shape of the NPs also contributes significantly to cellular uptake, transport and biodistribution[116]. The shape of NPs is significant in cellular uptake and internalization pathway[117]. Round shape/ spherical NPs are the most common due to their ease of synthesis and fast rate of endocytosis while other shapes (rod, cube, disk) have gained attention for their advantage in cellular internalization and efficiency of drug loading[118]. For example, NPs with disc or rod or spherical shape of size 150-200 nm, display enhanced cellular uptake and internalization in cells via clathrin-mediated endocytosis[119]. In contrast to NPs larger than 200 nm are preferentially taken up via macropinocytosis or phagocytic pathway[119]. However, it is noted that at some level, both mechanisms could happen simultaneously[119]. Furthermore, shape-induced NP enhancement of vascular targeting in the brain via receptor mediated delivery was confirmed by Kolhar and group[120]. Specifically, the rod shaped polystyrene NPs decorated with an anti-transferrin receptor antibody showed 7-fold increase in brain accumulation compared to NPs with spherical shape with the same surface chemistry[120]. Regional distribution of NPs within the brain following systemic injection has also been linked with NP shape. Chaturbedy et al demonstrated the preferred regional localization of iron oxide NPs with various shapes (sphere, biconcave, spindle, and nanotube) across the cerebral cortex and cerebellum *in vivo*[121].

Taken together, systemically delivered NPs eventually will be cleared through renal clearance, phagocytosis or by the MPS (either by the liver and/or the spleen uptake). The studies outlined above and summarized in (Table 1.1) describe strategies aimed at slowing this process by escaping different clearance mechanisms leading to prolonged blood circulation and delivery to the brain.

Factors	**Parameter**	**Outcome**
Surface modification	PEGylation	Optimal for prolonged circulation[103],[106]

Size	70-200 nm	Optimal for prolonged circulation[104,109,110,122]
	20-100 nm	Optimal for brain delivery[2,109,110,123]
	> 300 nm	Prone to splenic uptake[114]
	~ 5 nm	Prone to renal clearance[107]
Charge	Neutral	Reduced MPS uptake and optimal for brain delivery[104,114],[115]
	Positive	Agglomeration[104,114]
	Negative	MPS uptake[104,114]
Shape	Spherical	Easy to prepare[118]
	Ab coated rod	Increased brain accumulation[120]

Table 1.1 Summary of factors affecting the biodistribution and pharmacokinetics of nanoparticles for systemic delivery (optimal NP size for brain delivery pertains to injured brain).

1.6 Strategies for Nanoparticle Delivery to the Brain: Mechanisms of Delivery via Systemic Administration

The blood brain barrier (BBB) is comprised of brain capillary endothelial cells (BCEC) and other cell types such as neuronal cells, pericytes, and astrocytes[124]. The tight junctions among BCECs play significant roles in maintaining homeostasis by preventing unregulated transport into/out of the brain[33]. BBB provides about one of the largest surface area (~ 20 m^2) between the periphery and CNS, thereby generating a key access route for most endogenous and drug delivery molecules[124]. In addition, foreign molecules are also transported from brain to blood via efflux mechanism to mitigate toxicity and maintain homeostasis in the brain[125]. Therefore,

NP delivery to the brain at large needs to consider strategies to first cross the BBB to enhance the NP delivery to the brain. Such strategies may be broadly classified into passive and active delivery approaches.

1.6.1 Passive delivery

Passive delivery of NPs in the brain predominately relies on the functional state of the BBB. Particular pathological events such as inflammation or hypoxia (typically due to tumor, infarct, and/or trauma) has previously been shown to disrupt the normally tightly regulated BBB to produce leaky blood vessels[126]. Such permeable blood vessels provide an opportunity for the systemically circulating NPs extravasate and spontaneously accumulate in the interstitial space[2,126-128]. In tumor literature particularly, such passive NP delivery is known as enhanced permeability and retention (EPR) effect, where NPs enter the tumor interstitial space and are retained due to compromised lymphatic filtration[126]. Analogous to tumor microenvironments, a dysfunctional BBB occurs after brain injury or neuroinflammation diseases can lead to opening of the tight junctions resulting in a leaky vasculature[15,110]. The NPs may accumulate in the brain parenchyma due to increased paracellular permeability through the leaky vasculature[92,110]. However, the BBB permeability is transient and the timing of the NP delivery needs to be fine-tuned to take advantage of these changes in the membrane permeability[2]. For example, our group has demonstrated a critical time window (~ 13 h) for NP delivery after brain injury in pre-clinical rodent moderate/severe TBI models[2]. NPs passively accumulate within the injury penumbra and the amount of NPs accumulation depends on temporal resolution of the BBB permeability post trauma[2].

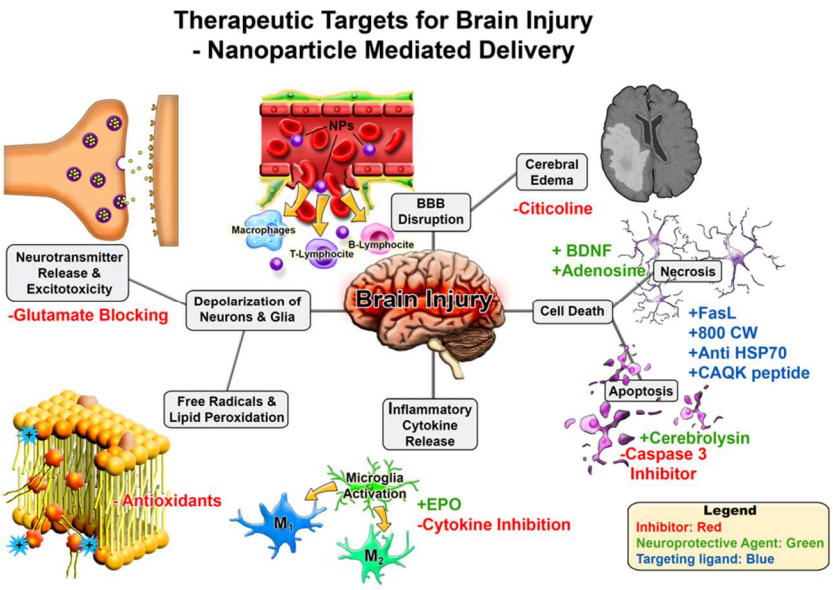

Figure 1.5 Therapeutic targets for brain injury for nanoparticle mediated drug delivery. Brain injury leads to a cascade of secondary damage events (denoted in grey boxes). These secondary injuries are potential targets for therapeutics where NP delivery may be useful. Potential interventions strategies are highlighted with red/green/blue font where inhibitors/blocking agents are in red, neuroprotective agents via pathway modulation in green, and targeting ligands in blue.

1.6.2 Active delivery

Although passive delivery may facilitate the transport of NPs through BBB, poor distribution of NPs in the brain remains a challenge[129]. Thus, active transport such as adsorptive-mediated and receptor-mediated transcytosis has been commonly explored in effort to enhance selective targeting and reach intracellular compartment after delivery. The adsorptive-mediated transcytosis mechanism is based on NP surface functionalization (conferring a positive charge) allowing electrostatic interaction with the BBB luminal surface (negatively charged) [92]. One strategy is to synthesize the NPs composed of positively charged constituents such as cationic cholesteryl hydrochloride[92]. An alternative strategy is to functionalize the NP's surface with cationic biomolecule such as cell-penetrating peptides (TAT peptide) and cationic proteins (albumin) [130]. For example, Lu et. al generated cationic albumin-conjugated PEGylated NPs for gene therapy of gliomas and NPs successfully crossed the BBB and arrived at the endothelial

cytoplasm, which then in turn induced apoptosis and delayed in tumor growth[130]. Caution should be noted for this strategy as research has shown that vesicular transport is actively down-regulated due to nonspecific exposure to cationic molecules thereby potentially inducing damage to the BBB[115].

More recent strategies for NP delivery across BBB is receptor-mediated transcytosis which is based on the presence of specific receptors on the luminal surface of cells.[92,125,131,132] Specifically, NP delivery is facilitated by displaying high affinity ligands on the NP surface to overexpressed BCEC receptors (i.e., transferrin (Tf) receptor, [133] low-density lipoprotein receptor, [134] insulin receptor, [132] or leptin receptor[135]) or common pathogenic targets (see review[136]). Upon ligand/receptor engagement, a clathrin-coated vesicle (diameter of 120 nm) forms from the plasma membrane initiating endocytosis[137]. The vesicle(s) then moved through BCEC cytoplasm and transported to the abluminal side of the cell[137]. The last step consists of exocytosis of said vesicle(s) at the abluminal side of the brain capillary endothelium[138]. Particularly, for BBB targeting the Tf receptor expressed on hepatocytes and endothelial cells of the BBB is of one the most extensively studied[92,131,132]. Wiley et al used gold NPs conjugated with Tf to probe receptor-mediated transcytosis mechanism via the transferrin receptor[133]. The study reported that accumulation of NPs in the brain parenchyma was directly dependent on the NP surface Tf concentration implying the tuning possibility of NPs avidity to the target receptors. However, caution should also be exercised when choosing the high affinity ligands for specific receptor, which strong bonding is not always efficient. For example, Cabezon et al reported anti-Tf antibody (8D3) enabled the transport of gold NPs (size of 20nm) via Tf-receptor mediated and independent clathrin-receptor pathway[139]. Results showed that although large amount of the NPs entered the BCECs, a small fraction of the NPs did not reach the brain parenchyma due to strong interaction between Tf receptor and anti-Tf antibody. Therefore, decreasing the affinity between antibody and receptor by utilizing low-affinity antibody[140] or single antibody fragment[141] might serve as a better strategy to complete the transcytosis of NPs.

Another receptor-mediated transcytosis mechanism is via lipoprotein receptors that are known to be highly expressed on endothelial brain microvessels and specifically recognize apolipoprotein E (apoE)[92,131,132]. Strategies to exploit this target have been reported by functionalizing the NPs with surfactants. Coating of NPs with surfactants such as polysorbate 80[142], Pluronic P85[143], and poloxamer 188 are known to preferentially adsorb apoE and display ability to cross the BBB via lipoprotein receptors[131,132,144-146]. For example, studies[147,148] used poly(butylcyanoacrylate) (PBCA) NPs loaded with drugs and coated with polysorbate 80 and showed significantly higher concentration of the drug in the brain. The PBCA NPs did not induce nonspecific BBB disruption but occurred due to apoE adsorption to facilitate BBB crossing[148].

Elucidating the transport mechanism is important in design and development of NPs for maximum efficiency of delivery to the target location. Passive and active mechanisms have been used for NP delivery to the brain across the BBB. Therapeutic targets for TBI for NP deliveries are summarized in Fig 1.5. Passive delivery of NPs via the leaky vasculature results in accumulation of large amount of NPs at the enhanced permeability region, however these pathway also might induce non-specific targeting[129]. Active delivery of NPs occurs via receptor-mediated transcytosis (such as transferrin and lipoprotein receptor) that relies on ligand-receptor affinity. Endogenous ligands, antibodies, peptides, and surfactants have been utilized in delivery of NPs across BBB to induce specific site targeting and reduce systemic side effects[131].

1.7 Objectives and Specific Aims

The pathology of TBI results in highly heterogeneous tissue damage including substantial blood-brain barrier (BBB) dysfunction immediately and delayed time point after injury. As the BBB breaks down, normally impermeable blood constituents may freely extravasate into the brain parenchymal space and may offer a unique opportunity to deliver drugs/nanoparticles that are normally excluded from the brain. Two broad types of TBI are focal and diffuse; for successful clinical translation, different models of TBI needs to be considered. However, there is a critical gap in the characterization of nanoparticle (NPs) and the investigation of the potential for delayed

NPs to characterize differences between sexes has not been previously tackled. Thus, the critical gap must be addressed to achieve effective theranostics for TBI that will aid in personalized delivery

Our *long-term goal* is to promote effective and personalized nanoparticle therapeutic interventions post-TBI. Our *short-term objectives* are 1) to optimize the key NP delivery parameters (NP size and time of injection) for maximal passive accumulation in focal and diffuse injury models of TBI, and 2) to determine the feasibility of delayed NP delivery and investigate sex dependence of NP accumulation. Our *central hypothesis* is that NPs will specifically accumulate within the injury penumbra, due to the compromised BBB and leaky vasculature following TBI.

We plan to attain the objective of this proposal through the following three specific aims:

Specific Aim 1: Temporal assessment of nanoparticle accumulation after experimental focal brain injury: Effect of particle size - controlled cortical impact. *Hypothesis 1a*: NPs will passively accumulate at the injury location after the injury due to the leaky vasculature. *Hypothesis 1b*: Higher NP accumulation will occur at immediate time points and smaller NPs will show prolonged accumulation as compared to larger sized NPs after focal brain injury.

Specific Aim 2: Temporal assessment of nanoparticle accumulation after experimental diffuse brain injury – fluid percussion and mild closed head injury. *Hypothesis 2*a: Passive accumulation of NPs at the injury location will occur at the specific injury region due to leaky vasculature after fluid percussion injury and mild closed head injury.

Specific Aim 3: Investigate NPs delivery: sub-acute time point and sex dependence after focal brain injury. *Hypothesis 3a*: NPs will accumulate at sub-acute time point due to secondary BBB breach. *Hypothesis 3b*: Accumulation of NPs will show sex dependence with males having higher NP accumulation compared to females at the sub-acute time point.

Taken together, we expect to characterize the NP accumulation after focal and diffuse brain injuries to further inform the size range of NPs and optimal injection time after injury. Moreover, we expect to achieve localized NP accumulation at the sub-acute time point and robust NP accumulation in females compared to males.

CHAPTER 2

TEMPORAL ASSESSMENT OF NANOPARTICLE ACCUMULATION AFTER EXPERIMENTAL BRAIN INJURY: EFFECT OF PARTICLE SIZE

Nanoparticle (NP) based therapeutic and theranostic agents have been developed for various diseases, yet application to neural disease/injury is restricted by the blood-brain-barrier (BBB). Traumatic brain injury (TBI) results in a host of pathological alterations, including transient breakdown of the BBB, thus opening a window for NP delivery to the injured brain tissue. This study focused on investigating the spatiotemporal accumulation of different sized NPs after TBI. Specifically, animal cohorts sustaining a controlled cortical impact injury received an intravenous injection of PEGylated NP cocktail (20, 40, 100, and 500 nm, each with a unique fluorophore) immediately (0 h), 2 h, 5 h, 12 h, or 23 h after injury. NPs were allowed to circulate for 1 h before perfusion and brain harvest. Confocal microscopy demonstrated peak NP accumulation within the injury penumbra 1 h post-injury. An inverse relationship was found between NP size and their continued accumulation within the penumbra. NP accumulation preferentially occurred in the primary motor and somatosensory areas of the injury penumbra as compared to the parietal association and visual area. Thus, we characterized the accumulation of particles up to 500 nm at different times acutely after injury, indicating the potential of NP-based TBI theranostics in the acute period after injury.

2.1 Introduction

Traumatic brain injury (TBI) is a leading cause of disability worldwide[8] with 1.7 million TBIs reported annually in the United States [9]. The pathology of TBI occurs from both immediate and delayed mechanisms resulting in highly heterogeneous tissue damage[17]. This pathology may include substantial blood-brain-barrier (BBB) dysfunction due to alterations in the capillary endothelial cells, specifically deregulation of tight junctions and/or vesicular transport [15]. As the BBB breaks down, normally impermeable blood constituents may now freely extravasate into the brain parenchymal space [21]. This transient, increased permeability within the injury penumbra

may offer a unique opportunity to deliver drugs that are normally excluded from the brain. In order to exploit this potential avenue for delivery after TBI, further characterization of the temporal profile of the “permeability window” as well as the size range for molecule/particle extravasation is necessary.

In laboratory settings, experimental animal brain trauma models provide insights into the events that occur during and after injury. One of the most commonly used models is the controlled cortical impact (CCI) model in the rodent; this model produces focal damage leading to major cortical damage directly in the zone of impact [27]. Previous CCI model studies with rats established the presence of a compromised BBB as indicated by the extravasation of horseradish peroxidase (HRP) [27] or Evans Blue (EB) [149,150] post-injury. Specifically, the BBB was compromised immediately after injury and remained significantly permeable for 5-7 days post-injury within the injury penumbra (with a second peak at ~3 days) [27,149]. Furthermore, Habgood et al. used weight-drop injury model to demonstrate that large molecular weight (MW) markers (HRP ~40 kDa) were permeable up to 24 h post-injury, as compared to smaller MW markers (biotin-dextran-amine, <10 kDa) that remain permeable as late as 4 days post-trauma [151]. Therefore, the BBB, post-injury, displays variable permeability based on the MW, with equivalent hydrodynamic diameter of about 3-6 nm [152,153]. These seminal studies provided evidence of BBB dysfunction after TBI [27,149,151]; however, the dynamic size range for particle extravasation greater than ~10 nm has not been previously elucidated.

Nanoparticles (NPs), particles ranging from 10-1000 nm in diameter [78], are utilized for various biomedical applications due to their pharmacological attributes. The unique physicochemical properties of NPs have shown promise in delivering a range of molecules, including water-insoluble drugs and large payloads, to desired sites in the body [154-157]. Specifically, surface modified NPs have been designed to achieve greater efficacy of therapeutic agents, prolonged pharmacological effects by improved drug protection, and reduced renal clearance compared to standard drug administration [158-160]. Moreover, contrast agents may be incorporated into NPs enabling visualization of the diseased site to diagnose and/or monitor

the *in vivo* efficacy of the therapeutics [154,161]. However, these remarkable attributes of NPs are commonly unattainable for neural applications due to BBB permeability limitations. We postulate the BBB disruption after TBI may afford a unique opportunity for NP delivery. Our hypothesis was recently supported by two independent studies demonstrating the feasibility and utility for intravenous NP delivery after TBI [128,162]. Yet, a systematic evaluation of the temporal window and the NP size range for NP delivery after TBI has not been previously performed. Therefore, the focus of this study was to establish the effect of NP size and time of NP injection after experimental TBI while maintaining a constant circulation time. As such, we investigated the accumulation of four different sized (20, 40, 100, and 500 nm) fluorescent polystyrene NPs at five time points acutely (up to 24 h) after TBI using the murine CCI model.

2.2 Methods

2.2.1 Materials

Carboxylated polystyrene NPs of different sizes were purchased from Life technologies (Carlsbad, CA, USA). Specifically, 20 nm (F8783), 40 nm (F8793), 100 nm (F8797) and 500 nm (F8813) NPs with dark red ($\lambda_{ex}/\lambda_{em}$=660/680), red ($\lambda_{ex}/\lambda_{em}$=580/605), blue ($\lambda_{ex}/\lambda_{em}$=350/440) and yellow-green ($\lambda_{ex}/\lambda_{em}$=505/515) fluorescence, respectively, were used. Methoxypolyethylene glycol amine 2000 (mPEGamine 2KDa) (06676), methoxypolyethylene glycol amine 750 (mPEGamine 750Da) (07966), n-[3-dimethylaminopropyl]-n-ethyl, n-[3-dimethylaminopropyl]-n-ethyl [EDC] (E1769), MES hemisodium buffer (M8902), N-Hydroxysuccinimide (NHS) (56405), and Peroxidase type II from horseradish (P8250-50KU) were purchased from Sigma Aldrich (St. Louis, MO, USA). ImmPACT DAB peroxidase (HRP) substrate (SK-4105) was purchased from Vector laboratories (Burlingame, CA, USA). Slide-A-Lyzer Cassettes (20K) (66003) were purchased from ThermoFisher scientific (Waltham, MA, USA). Fluorescent mounting media (Vectashield, Vector Labs, Burlingame, Ca, USA)

2.2.2 Nanoparticle PEG conjugation

Carboxylated NPs were PEGylated using EDC/NHS chemistry. Briefly, mPEGamine 750 Da was mixed with 20 nm NPs (NH_2:COOH at 2:1 mole excess) whereas mPEGamine 2 kDa

was mixed with 40 nm, 100 nm and 500 nm NPs; (NH_2:COOH at 5:1 mole excess). EDC/NHS (in MES buffer) was added to NP / PEG mixture (8 mM/4 mM for 20 nm and 200 mM/100 mM for other NPs) and HEPES buffer was added to obtain a final pH of 7.8 before incubating for 3 h at room temperature. Glycine (100 mM) was added to quench the reaction. Unbound PEG was removed via dialysis (20 kDa MW). PEGylated NPs were suspended in a 20 mM HEPES (pH 7.4). The concentration of each NP solution was determined with fluorescent standard curves generated from known concentrations of as-received Fluorospheres (FLUOstrar Omega fluorescence plate reader; BMG Labtech, Ortenberg, Germany). Yields of NPs ranged between 40-60 %. A concentration of 13.3 mg/ml for each NP was used for all *in vivo* studies.

2.2.3 Nanoparticle characterization

PEGylated NPs were visualized using transmission electron microscope (TEM). NPs in water were applied to 300-mesh, carbon coated copper grids for 60 s. After this, excess water was removed by blotting with filter paper before imaging using JEOL 1200EX TEM (Peabody, MA, USA), operated at 80 kV and images were collected with a CCD camera (Scientific Instruments and Accessories; Duluth, GA, USA). The hydrodynamic diameter and zeta potential of NPs in 20 mM HEPES (pH 7.4) were measured pre and post-PEGylation with a dynamic light scattering (DLS) device (Zetasizer Nano Malvern; Malvern, UK). For each NP, three measurements were made and the mean ± standard error of mean (s.e.m.) was reported.

2.2.4 Controlled cortical impact model

All animal studies were approved by Arizona State University's Institute of Animal Use and Care Committee (IACUC) and were performed in accordance with the relevant guidelines. Traumatic brain injury (TBI) was modeled using the well-established controlled cortical impact (CCI) injury model [56]. Briefly, adult C57Bl/6 mice (9-10 weeks old) were anesthetized with isoflurane (3 % induction, 1.5 % maintenance) and placed in stereotaxic frame. The frontoparietal cortex was exposed via 3 mm craniotomy and the impact tip was centered at -1.5 mm bregma and 1.5 mm lateral from midline. The impactor tip diameter was 2 mm, the impact velocity was 6.0 m/s and the depth of cortical deformation was 2 mm and 100 ms impact duration (Impact

ONE; Leica Microsystems). The skin was sutured and the animals were placed in a 37°C incubator until consciousness was regained. The naïve group did not undergo surgery.

2.2.5 Nanoparticle and horseradish peroxidase (HRP) injection

Retro-orbital injections of the venous sinus in the mouse were performed for intravenous delivery of the particles; this technique is an alternative to tail-vein injection [163]. Animals were anesthetized with isoflurane (3 %) and the NP cocktail (75 µl) of different sized NPs (50 mg/kg b.w.) was injected to the right eye, one hour before perfusion and sacrifice. HRP (83 mg/kg b.w.in 25 µl) was injected to the left eye ten mins before perfusion and sacrifice. Depending on the injury group, animals were sacrificed at 1 h, 3 h, 6 h, 13 h, and 24 h post injury. The NP circulation time of 1 h was held constant for each of the cohorts.

2.2.6 Tissue collection

According to the experimental groups – 1 h, 3 h, 6 h, 13 h and 24 h post-injury, animals were deeply anesthetized with lethal dose of sodium pentobarbital solution until a tail pinch produced no reflex movement. Animals were transcardially perfused with cold phosphate-buffered saline (PBS), followed by 4 % buffered paraformaldehyde solution. Brain tissue were collected and fixed overnight in 4 % buffered paraformaldehyde followed by immersion in 30 % sucrose solutions in 1X PBS for cryoprotection for 24 h. Samples were embedded within optimal cutting temperature (OCT) medium and frozen on dry ice. Samples were stored at -80°C until sectioned coronally at a 25 µm thickness with a cryostat.

2.2.7 Quantification of nanoparticle accumulation

Slides containing the frozen sections were incubated at room temperature for 20 mins in 1X PBS to rehydrate the tissue and remove OCT compound. Coverslips were mounted on the section after adding one drop of fluorescent mounting media (Vectashield). These sections were imaged using confocal microscopy (Leica TCS SP5 AOBS Spectral Confocal System, 20X magnification). Four region of interest (ROI) of the dimension 775 µm X 775 µm, were selected surrounding the injury penumbra (eight sections per animal, four animals per cohort) and two

ROIs at contralateral region (two sections per animal, four animals per cohort). Scanning settings for each NP: 20 nm, 40 nm, 100 nm and 500 nm were $\lambda_{ex}/\lambda_{em}$=633/700-758 nm (800 V gain); $\lambda_{ex}/\lambda_{em}$=561 nm/572-619 nm (645 V gain); $\lambda_{ex}/\lambda_{em}$=405 nm/420-465 nm (585 V gain), and $\lambda_{ex}/\lambda_{em}$=488 nm/507-535 nm (725 V gain), respectively. Configuration settings were maintained constant for all the images collected. For each ROI, Z stacking was performed and total Z width ranged from 20-25 µm with a slice thickness of 1 µm. The Z stacks images were converted to a single image by maximum projection tool using Leica software (LAS AF, Leica microsystems). The sum of four ipsilateral ROI for each section (eight sections per animal, four animals per cohort) were averaged and compared to the sum of the two contralateral ROI (two sections per animal, four animals per cohort). The maximum projected images were thresholded to remove background fluorescence using tissue sections from NP injected naïve brain and total intensity was calculated, using ImageJ software. The fluorescent intensity values were then converted to number of NPs based on an empirical method (See Appendix A Fig. A.2).

2.2.8 Quantification of HRP extravasation

The same tissue section used for NP analysis or their adjacent sections were incubated in PBS buffer for 20 mins. Freshly prepared DAB substrate solution (200 µl) was added and incubated for ten mins at room temperature. Slides were then washed in PBS buffer three times (two mins each) and coverslips were mounted after adding a drop of aqueous mounting media. Sections were imaged using color camera mounted microscope (Leica microscope) at 5X magnification and ROI dimension of 1.50 mm x 2.50 mm were used. ROI were selected surrounding the injury penumbra (eight sections per animal, four animals per cohort) and at contralateral region (two sections per animal, four animals per cohort). The ROI images were then analyzed using ImageJ software (National institute of health, Bethesda, MD, USA) to obtain total number of positive pixels.

2.2.9 Statistics

Statistical analyses were conducted in GraphPad Prism 5.0 (GraphPad Software, Inc., La Jolla CA). Comparison between zeta potential change of NPs post-PEGylation was done using

student's t-test. Analysis of total positive pixels in ipsilateral and contralateral region of interest for HRP and number of accumulated NP at different time points was conducted using ordinary two-way ANOVA. For HRP and each NP, comparison between ipsilateral ROI and its contralateral ROI was done by student's t-test. Comparison between ipsilaterlal ROI for HRP, and individual NPs, over time was conducted using Tukey's post hoc test. Spatial distribution of HRP extravasation and NP accumulation was done using ordinary two-way ANOVA, followed by Tukey's post hoc tests.

2.3 Results

2.3.1 Nanoparticle characterization

Four sizes of carboxylated polystyrene NPs (20 nm, 40 nm, 100 nm and 500 nm), each internally loaded with a distinct fluorescent dye with negligible overlap in signal were employed in the study (Fig. 2.1). The surface of carboxylated NPs was modified with amine-polyethylene glycol (PEG) [102,157] to reduce their zeta potential for improved NP stability and to prolong blood circulation time. The NPs were characterized via transmission electron microscope (TEM) and dynamic light scattering (DLS). PEGylation of NPs via amine/carboxyl EDC/NHS chemistry was confirmed through DLS based on a decrease in zeta potential and modest increase (~10 nm) in hydrodynamic diameter of the NPs (Fig. 2.1b and 2.1c, Table1; n = 3). A statistically significant decrease in zeta potential was observed for each NP after PEGylation ($p<0.05$; Table1, Fig. 2.1b). TEM images of NPs show monodispersed, spherical shaped particles for each population (Fig. 2.1d). To simplify nomenclature, the four NP groups employed in this study will be addressed by their nominal diameters, 20 nm, 40 nm, 100 nm, and 500 nm.

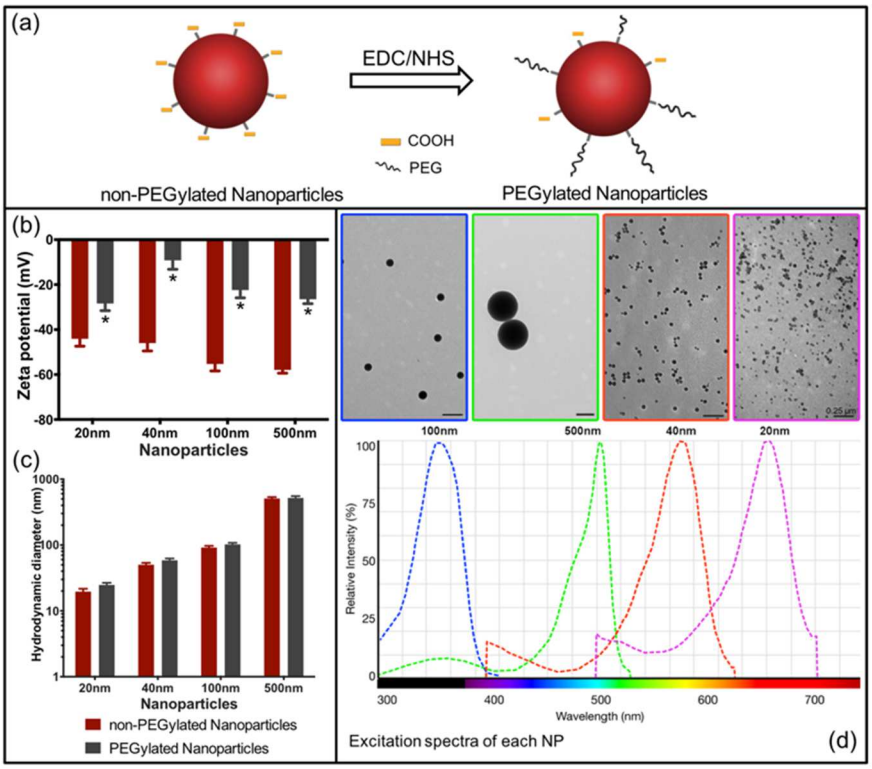

Figure 2.1 Nanoparticle characterization (a) Schematic of nanoparticle PEG conjugation using EDC/NHS chemistry. (b) Zeta potential of non-PEGylated and PEGylated nanoparticles, * $p<0.05$, t-test. (c) Hydrodynamic diameter of non-PEGylated and PEGylated nanoparticles. Error bars represent standard error of mean with n=3 per group. (d) TEM images of monodispersed nanoparticles (PEGylated) with their respective excitation fluorescent spectra [58]. Scale bar = 0.25 μm.

Nominal NP size (nm)	Hydrodynamic Diameter (nm)		Zeta Potential (mV)	
	non-PEGylated	PEGylated	non-PEGylated	PEGylated
20	19.6 ± 2.0	24.7 ± 2.0	-44.1 ± 3.3	-28.4 ± 3.2*
40	50.1 ± 3.5	58.4 ± 4.0	-46.0 ± 3.5	-9.2 ± 4.0*
100	91.5 ± 5.4	101.9 ± 6.0	-55.3 ± 3.1	-22.4 ± 3.5*
500	507.0 ± 27.5	517.6 ± 34.8	-57.9 ± 1.5	-26.5 ± 2.0*

Table 2.1 Nanoparticle characterization: Hydrodynamic diameter and zeta potential of non-PEGylated NP and PEGylated NP, mean ± standard error of mean (n = 3). * $p<0.05$, t-test. Measurements in 20 mM HEPES (pH 7.4).

2.3.2 In vivo study: Horseradish peroxidase (HRP) extravasation

A lateral CCI was imparted on the frontoparietal cortex generating a cortical lesion ipsilateral to the impact and leaving the contralateral hemisphere uninjured. An intravenous retro-orbital [163] HRP injection 10 min prior to sacrifice was included as a positive control to evaluate the blood brain barrier (BBB) integrity, as extravasation of HRP is a well-accepted indicator of breached BBB [27],[29,151,164] (Figure 2.1). Specifically, we observed extravasation of HRP in the primary and the adjacent injury region at 1 h post injury. However, the HRP extravasation was only localized to the primary injury site at and after 3 h post injury. Therefore, the quantification of HRP staining for 1 h cohort included both the primary and adjacent tissue region; analysis for the remaining cohorts focused only the primary injury site. Quantification of HRP extravasation to obtain the number of positive pixels using ImageJ software, demonstrated significant differences between ipsilateral and contralateral locations ($p=0.0002$) while a time dependent effect was not observed ($p=0.038$) using two-way ANOVA. Pair-wise analysis of extravasation of HRP specifically for each time point revealed a significant increase in HRP extravasation in the injury penumbra compared to contralateral tissue at all investigated time points (1 h, 3 h, 6 h, 13 h and 24 h) post injury ($p<0.05$; Fig. 2.2b). Comparing the ipsilateral HRP staining over time revealed a nearly 35% reduction in HRP staining at the 3 h, 6 h, 13 h, and 24 h time points compared to the maximal HRP staining at 1 h post-injury. This reduction was statistically significant for 13 h and 24 h cohorts ($p<0.05$) compared to 1 h cohort, thus demonstrating potential resolution of the BBB over time. Therefore, HRP extravasation confirmed the BBB dysfunction up to 24 h post-injury corroborating previous studies [27] (Fig. 2.2).

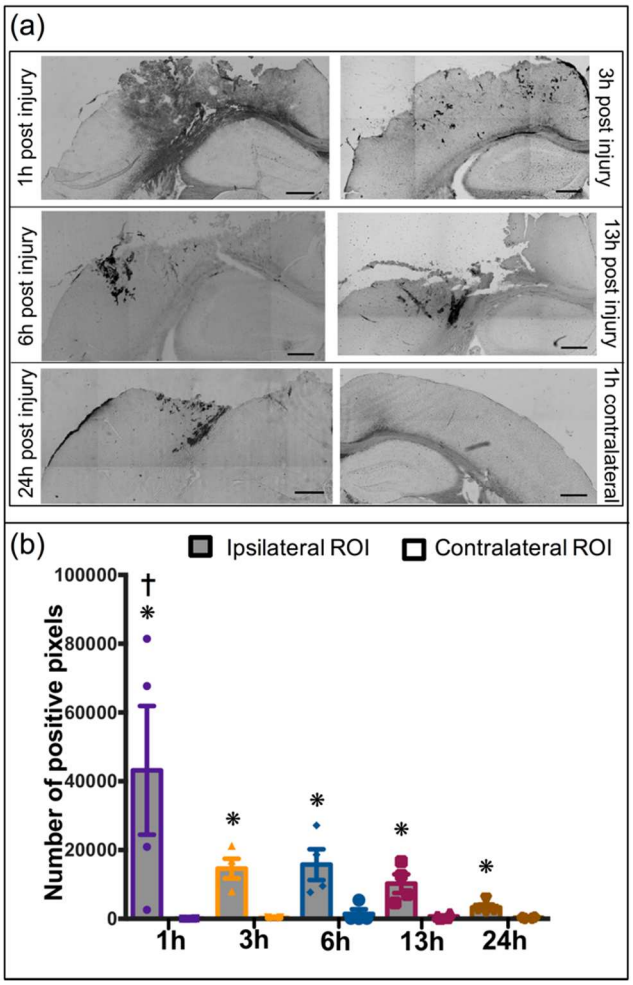

Figure 2.2 HRP Extravasation after TBI: (a) Representative images of extravasation of HRP injured region after 1 h, 3 h, 6 h, 13 h and 24 h post injury (a-e); contralateral region 1 h post injury (f). (b) Quantitative analysis of HRP extravasation over time. ∗ $p<0.05$ compared to their respective contralateral ROI, Student's t-test. † $p<0.05$ compared to 13 h and 24 h ipsilateral ROI, Tukey's *post-hoc* test. Error bars represents standard error of mean with n=4 per group. Scale bar = 500 μm.

2.3.2 *In vivo* study: Accumulation of nanoparticle within injury penumbra

We used a NP cocktail containing particles with diameters ranging from 20 nm to 500 nm, to determine the extent of NP accumulation acutely (up to 24 h) after brain injury with a constant

1 h circulation time. Specifically, we quantified the accumulation of each fluorescent NP within processed brain tissue sections spanning across the injury lesion (~-0.18 mm bregma to ~-3.28 mm bregma) via confocal microscopy (Fig. 3.3). Interestingly, we observed maximum accumulation of all NPs 1 h after injury, including the 500 nm particles. Additionally, the results indicated prolonged NP accumulation of 20 nm and 40 nm up to 13 h post injury within the injury penumbra where as significant accumulation of 100 nm and 500 nm NPs was found up to 6 h.

Two-way ANOVA results from our study revealed a significant difference between the ipsilateral and contralateral location for 20 nm ($p<0.0001$), 40 nm ($p<0.0001$), 100 nm ($p=0.0392$) and 500 nm ($p<0.0001$), (Fig. 2.4 (a-d)). Moreover, the analysis demonstrated a significant time dependent effect for 20 nm, 40 nm, 100 nm and 500 nm ($P=0.0001$), ($p<0.0001$), ($p=0.043$), ($p=0.0364$) (Fig. 2.4 (a-d)), respectively. To take a closer look at the effect of each of these variables individually, post-hoc pair-wise analyses of critical comparisons are described below.

2.3.2.1 Analysis of the BBB breach in injured and uninjured brain tissue

The first pairwise analysis focused on comparing NP accumulation within the ipsilateral injury penumbra to contralateral tissue at different time points (Fig. 2.4). Specifically, for 20 nm and 40 nm, ipsilateral accumulation markedly increased for all time points compared to contralateral tissue, except 24 h cohort (Fig. 2.4 a, b; $p < 0.05$). For 100 nm, statistically significant increase in NP accumulation on the ipsilateral side was only observed at 3h and 6 h post-injury (Fig. 2.4c; $p < 0.05$). Finally, the 500 nm NP accumulation was significantly greater for ipsilateral versus contralateral up to 6 h. Overall, 20 and 40 nm NPs significantly accumulated in the injury penumbra compared to the contralateral tissue up to 13h after injury while the time window was reduced by nearly half (6 h) for the 100 and 500 nm.

2.3.2.2 Analysis of the BBB breach within injured region across different time points -

The second critical pairwise analysis focused on comparing the temporal changes in NP accumulation within the ipsilateral injury penumbra across time points. For 20, 40 and 100 nm, there was a significant reduction in accumulation for 3 h, 6 h, 13 h and 24 h time points as

compared to 1 h post injury ($p<0.05$); less than 35 % of 1h NP accumulation was observed for other time points. (Fig. 2.4 a, b, c). Accumulation of the 500 nm NP was nearly 25 % of 1 h cohort for 3 h, 6 h, and 13 h post-injury and was significantly reduced ($p<0.05$; Fig. 2.4d). Interestingly, the mean NP accumulation for the 500 nm NP at 24 h exhibited similar accumulation as compared to the 1 h post injury; we noted that variance within this group was quite large as two of the four animals displayed high NP accumulation whereas the other two animals had modest NP accumulation. The overall trend for different sized NPs demonstrated maximum accumulation at 1h post-injury compared to other time points.

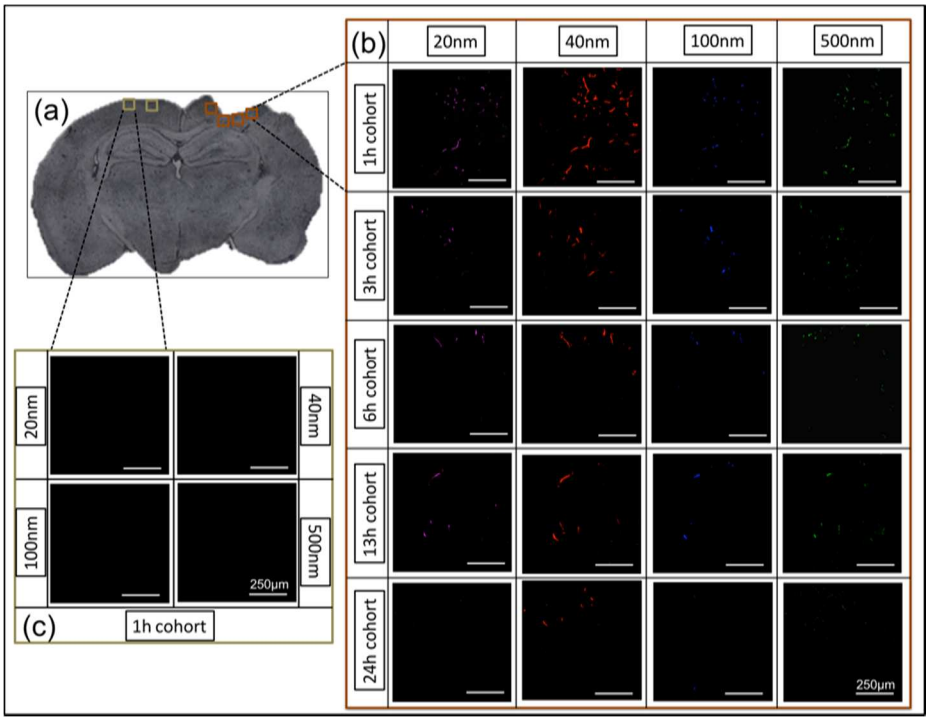

Figure 2.3 Accumulation of different size nanoparticles over time after injury. (a) Representative images of injured brain section (~-1.655 mm bregma, 25 µm thick). (b) Panel of 20X confocal images near the injury region on ipsilateral hemisphere (shown in (a)). Rows of the panel show time course and the columns show the different nanoparticle size. (c) Panel of 20X confocal images on contralateral hemisphere (shown in (a)), for each nanoparticle at 1 h post injury. Scale bar = 250 µm.

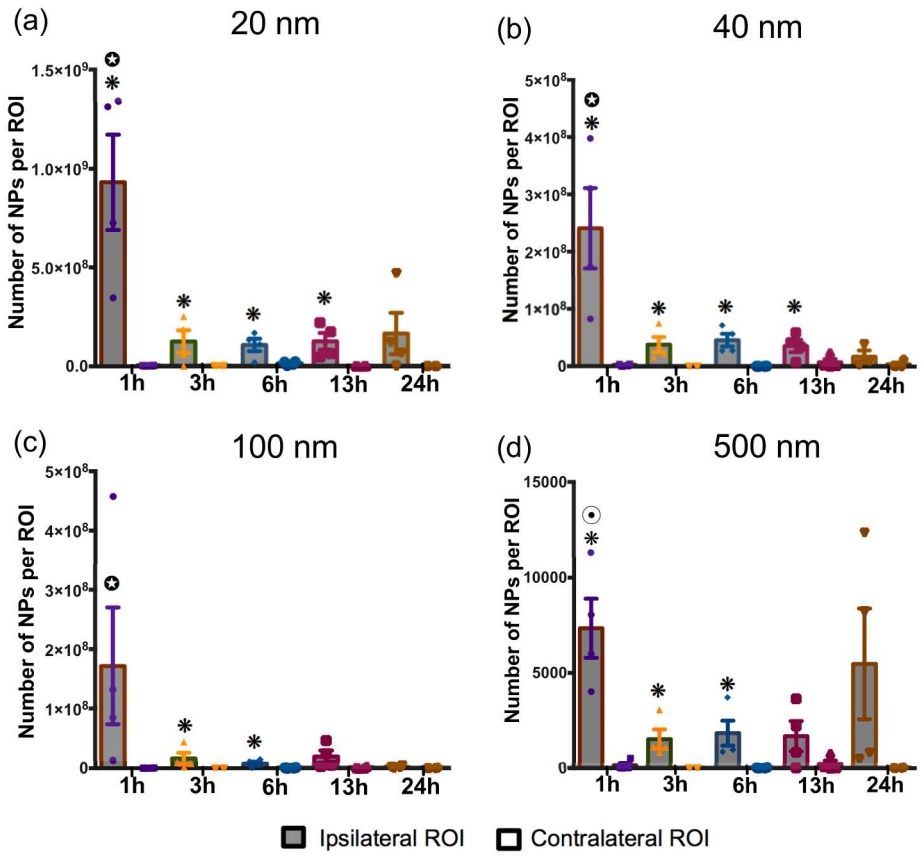

Figure 2.4 Nanoparticle accumulation after TBI. Accumulation of (a) 20 nm, (b) 40 nm, (c) 100 nm, (d) 500 nm nanoparticles at different time points after traumatic brain injury in mice. ✳ $p<0.05$ compared to their respective contralateral ROI, Student's t-test. ✪ $p<0.05$ compared to 3 h, 6 h, 13 h, and 24 h ipsilateral ROI, ⊙ $p<0.05$ compared to 3 h, 6 h, and 13 h ipsilateral ROI; Tukey's post-hoc test. Error bars represents standard error of mean with n=4 per group.

2.3.3 *In vivo* study: Spatial distribution of HRP and nanoparticles

The CCI impact to the frontoparietal cortex (-1.5 mm bregma, 1.5 mm lateral from midline) generates an injury lesion mainly to the cortex, which includes damage to the primary motor area (M1), primary somatosensory area, posterior parietal association area and anteriomedial visual cortex (V1). Interestingly, we observed selective distribution of HRP and NP accumulation based on the cortical region, a trend that held consistently with all post-injury time

point cohorts. In this regard, we examined a series of coronal sections across the injury lesion from anterior to posterior. We binned the tissue sections into three spatial sub-groups: anterior (~-0.18 mm bregma), middle (~-1.65 mm bregma) and posterior (~-3.28 mm bregma) (Fig. 2.5a). Our results demonstrated maximal accumulation of the NPs and HRP within the anterior and middle regions of the injury penumbra (statistically significant only at 1 h), as compared to that of posterior and contralateral regions (Fig. 2.5 and 2.6). Strikingly, the accumulation in the posterior region was similar to that of the contralateral region.

HRP extravasation significantly varied across the injury penumbra ($p=0.0003$) (Fig. 2.5 (b)). Further pairwise post-hoc analysis revealed a significant increase in extravasation for 1 h post-injury within the anterior and middle injury penumbra regions, compared to both posterior injury penumbra and contralateral tissue. Furthermore, HRP extravasation within the posterior injury penumbra was not significantly different than contralateral tissue.

Significant difference in accumulation was observed across the different regions of the brain for 20 nm, 40 nm, and 500 nm ($p=0.0002$), ($p<0.0001$), ($p=0.02$), respectively yet not significant for 100 nm ($p=0.10$), (Fig. 2.6). Tukey's post-hoc analysis of the 20 nm and 40 nm NPs demonstrated a significant increase in accumulation for the anterior injury region at 1 h compared to both the posterior injury region, and contralateral tissue ($p<0.05$) (Fig. 2.6 (a,b)). The accumulation of 20 nm, 40 nm, 100 nm and 500 nm NP within the core of the injury penumbra was significantly more than the posterior injury penumbra, and contralateral tissue at 1 h post injury ($p<0.05$) (Fig. 2.6 (a-d)). Interestingly, no significance was observed in NP accumulation between the posterior injury penumbra and the contralateral tissue regardless of the NP size.

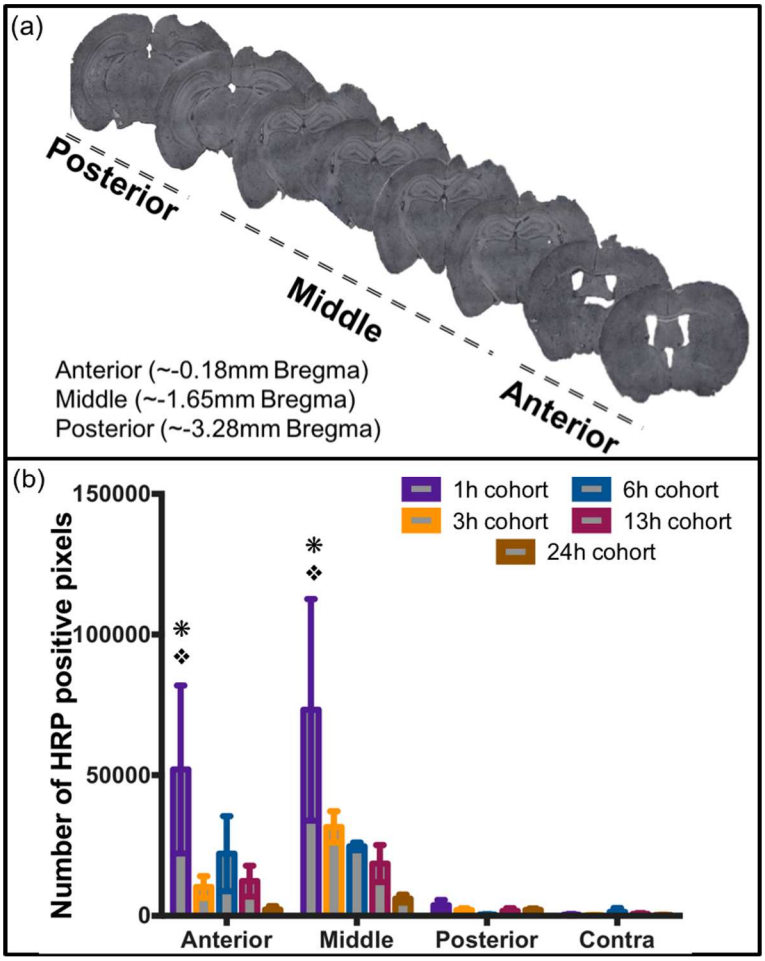

Figure 2.5 Spatial distribution analysis. (a) Representative brain images showing anterior, middle and posterior regions of the brain w.r.t. bregma. (b) Quantitative analysis of HRP extravasation at different anatomical regions and different time points after TBI. ⁕ $p<0.05$ compared to contralateral ROI (Contra), ❖ $p<0.05$ compared to posterior ROI (Posterior); Tukey's post-hoc test. Error bars represents standard error of mean with n=4 per group.

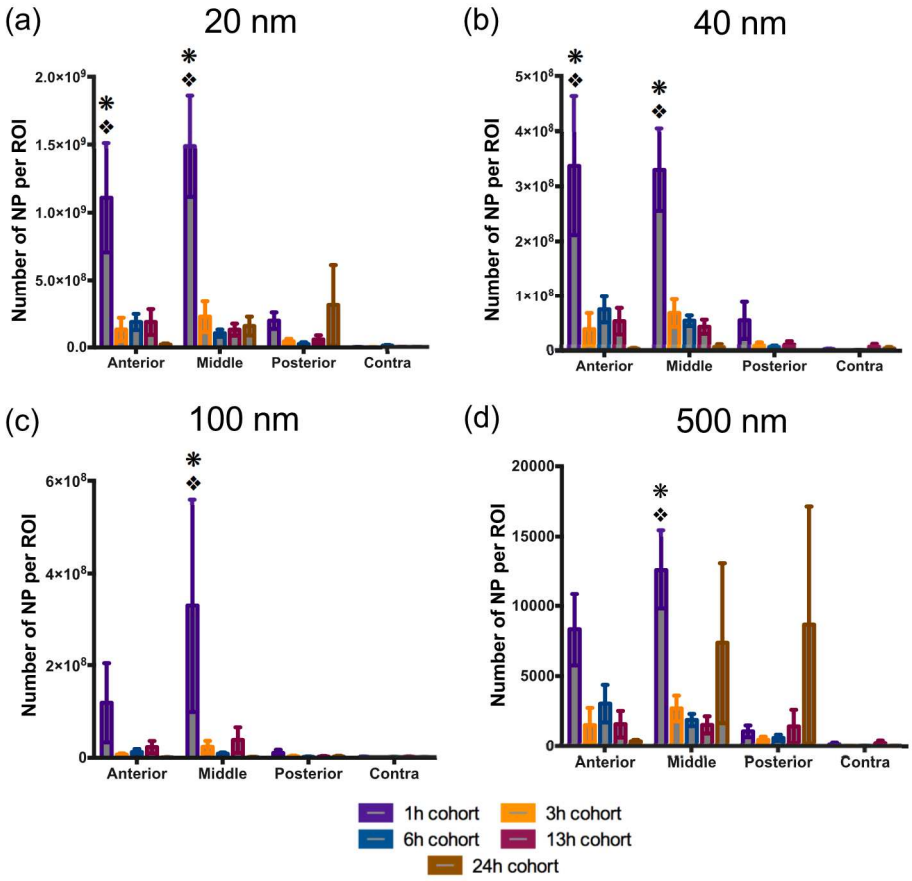

Figure 2.6. Spatial distribution of nanoparticle accumulation. Quantitative analysis of (a) 20 nm, (b) 40 nm, (c) 100 nm, (d) 500 nm nanoparticles at different anatomical regions and different time points. ✳ $p<0.05$ compared to contralateral ROI (contra), ❖ $p<0.05$ compared to posterior ROI (posterior); Tukey's post-hoc test. Error bars represents standard error of mean with n=4 per group.

2.4 Discussion and Conclusion

Theranostic delivery for the brain has been largely hindered by limitations of BBB permeability. However, short windows of BBB dysfunction or damage as a result of disease or injury pathology may provide an opportunity for delivery of contrast agents and poorly soluble drugs via NPs. To fully utilize the window of opportunity of BBB opening that occurs after TBI, we

need to further assess the spatiotemporal accumulation of NPs after injury. The study presented here directly addresses the critical knowledge gap to determine to effect of different size NP accumulation and the injection time points after experimental TBI, where the results provide key insights into NP behavior after TBI. Specifically, three key findings include: 1. NPs up to 500 nm may be delivered to TBI injured brain, 2. Maximal NP accumulation after occurs 1 h after TBI, 3. NP accumulation of 20 nm and 40 nm NPs occurred out to 13 h post-injury.

Systemic NP delivery depends on many parameters to ensure stability, prolonged blood circulation, and efficient delivery to the target tissue/organ. Specifically NP surface charge influences the physiochemical stability of NPs and the rate of particle elimination from circulation; previous studies have shown near neutral/slightly anionic NPs have reduced clearance by the reticuloendothelial system [112,165,166]. Functionalizing the surface of the NP with polymer polyethylene glycol (PEG) is most commonly used to minimize opsonization not only through steric hindrance but also charge shielding [102,157]. Since this study focused on evaluating size and time dependent NP accumulation after brain injury, we aimed to minimize the influence of NP parameters outside of size by PEGylating all of our NPs and obtained slightly anionic NPs for efficient systemic delivery.

Passive systemic NP delivery to the injured brain hinges on a damaged BBB and confirmation of a dysfunctional BBB was obtained with the HRP marker (~44 kDa with an estimated radius of ~3 nm[10]). We observed extravasation of HRP in the primary and the adjacent injury region at 1 h post-injury. However, for all subsequent cohorts, the HRP staining was localized to the primary injury site. A survey of the literature indicates some disagreement in utilizing HRP to classify the underlying mechanisms for BBB breakdown (i.e., injury induced rupture and/or paracellular permeability) [27,151,167] . As stated previously, the current study focused on evaluating NP accumulation ultimately for acute TBI theranostics. Therefore, it was necessary to correlate NP accumulation with BBB damage through HRP staining. One important observation is that while the incidence of HRP staining reduced over 24 h post injury, significant positive staining was observed out to 24 h after injury indicating the persistence of localized

dysfunctional BBB and opportunity for localized NP accumulation. These findings are critical in elucidating the optimal temporal delivery window for NPs (10 – 1000 nm) as the interest in using NPs for TBI has gained traction recently [128,162]. Specifically, two previous studies employed systemic NP delivery after TBI where the NPs ranged from 60 nm to 300 nm in diameter. These studies demonstrated feasibility for NPs to preferentially localize within the injury penumbra when delivered within 4 h post injury [128,162]. Yet, little is known about the impact of NP size and injection time to achieve effective delivery after TBI. We directly addressed this critical gap by evaluating a cocktail injection of different sized PEGylated NPs at different time points after injury while maintaining a consistent circulation time (1 h). The peak accumulation for all sized NPs was observed with injections immediately after injury (+1 h circulation time) mirroring the HRP extravasation results. Not surprisingly, we observed prolonged accumulation for two smallest NPs (20 nm and 40 nm) out to 13h post injury, whereas significant accumulation for the two largest NPs (100 nm and 500 nm) was seen only out to 6 h. Our report is the first to show the evidence of accumulation of up to 500 nm sized PEGylated NPs within the injury penumbra acutely after brain injury. This finding is supported by a NP study on cortical implants in mice where accumulation of up to 500 nm NPs near the implant region was observed at 4 weeks post-implant [168]. Overall, it is evident that our study not only corroborates previous reports, but more importantly expands our current knowledge regarding time and size dependent NP delivery after TBI.

We postulate that TBI pathology directly contributes to NP accumulation within the injury penumbra. TBI, particularly the CCI model, leads to physical rupture of the blood vessels, dysfunction of the BBB and permeable blood vasculature within the injury region [169,170]. A similar leaky vasculature phenomenon has been defined as the enhanced permeability and retention (EPR) effect in oncology literature [114,126,171-173]. Poorly structured and highly permeable vasculature contributes to increased passive accumulation of NPs within solid tumors [171,173,174]. Thus, the unique pathophysiological nature of the dysfunctional BBB and leaky vasculature after TBI, may lead to localized accumulation of NPs at the injured area due to a similar EPR effect. In the present study we observed localized areas of brain tissue containing

multiple sizes of NPs. In contrast, we did not observe significant NP accumulation in uninjured brain tissue as compared to injured tissue, suggesting localized leaky vessels near the injury site. Although the exact mechanism for the NP accumulation at the injury location was not probed, potential mechanisms include accumulation via mechanically-induced ruptured vessels or paracellular diffusion[21]. Future studies are warranted to better understand such mechanisms. Overall, the accumulation of different sized NPs occurred specifically within the primary injury site.

One interesting finding was preferential spatial accumulation within specific cortical regions within the injury penumbra. The CCI injury generated a cortical lesion encompassing the primary motor area (M1), somatosensory area, posterior parietal association area and anteriomedial visual cortex (V1) (from anterior to posterior). Remarkably, at 1 h post-injury significantly higher levels of both HRP and NPs were found within the more anteriorly located primary motor, and somatosensory area (M1) compared to posteriorly located parietal association and visual area (V1) of the brain. The specific mechanism that leads to lower accumulation of NPs in the posterior area is not clear. However, we postulate that the heterogeneous nature of the inherent cortical cerebral blood flow and injury-induced alterations in blood flow play key roles. Specifically, regional neural cellular density has been directly correlated with microvessel densities in murine models [175]. Such variations in microvascular density is directly linked to cortical blood flow [176,177] . Comparing the cortical regions encompassed in the injury penumbra, we found reports of reduced neural cell density within the parietal cortex [178]. Therefore, the inherently reduced cortical blood flow/microvascular density within the parietal cortex area may largely contribute to a low level of NP accumulation after TBI. Secondarily, TBI promotes localized alterations in the cerebral blood flow, depending on the size and location of contusions and hematomas [179] leading to abnormal blood supply to injured tissue. The blood supply to the motor, sensory and parietal cortex is supplied by the middle cerebral artery (MCA) [180], The CCI injury imparted over this region may damage the MCA or its branches resulting in rupture of anteriorly located blood vessels. This type of vascular damage may lead to two

phenomena potentially contributing to the regional distribution of NPs, 1. enhanced NP accumulation in anteriorly located blood vessels, and 2. hypoperfusion in downstream posteriorly located regions leading to reduced NP accumulation. Collectively, inherent variations in capillaries combined with injury-induced blood flow alterations may contribute to anteriorly dominate NP accumulation after CCI.

To maximize the NP size spectrum, each animal received an intravenous delivery of a NP cocktail containing four different sized NPs. Our analysis focused on direct comparison within each NP size and did not include cross NP size comparisons. Each NP injection contained an equal mass concentration yet varying number of NPs for each size group, thereby preventing direct comparison across NPs with high fidelity. Each NP group was loaded with a unique fluorophore with discrete fluorescent spectra. Therefore, accumulation of each NP within brain tissue at different time points post-injury was determined through an empirical conversion of total fluorescent intensity specific to each fluorophore to the total number of NPs (Appendix A Fig. A.2). Nonetheless, these limitations did not constrain the critical analysis within each NP size group where we revealed never before presented data on the dynamic size NP range delivery after TBI. The results of our study are integral for developing NP-based contrast agents or drug delivery. NPs for brain delivery applications [92] vary widely in composition ranging from amphiphilic monomers to lipids to more rigid polymer-based[181] [182]. Smaller NPs (<100 nm) have shown to have slower clearance, higher amount of encapsulated drug accumulation, efficient cellular uptake, and enhanced penetration of poorly permeable tissue, as compared to larger NPs (>200 nm) [174,183,184]. Previous studies have successfully used NPs (20 - 60 nm) as indicators of BBB damage in experimental stroke models [185,186] and as theranostic tools for imaging and drug delivery [174,184]. Results of our study can potentially be applied to devise multifunctional NPs with therapeutic drugs for brain injury such as superoxide dismutase[187], erythropoietin[52], statins [52] to be loaded into these NPs.

In conclusion, we established that PEGylated polystyrene nanoparticles of different sizes (20 nm, 40 nm, 100 nm and 500 nm) accumulate predominately near the injury region after CCI

injury in mice. Furthermore, maximal accumulation for all NP sizes was observed at 1 h post-injury. With a constant circulation time of 1 h across all cohorts, we identified an inverse relationship between the NP size and their accumulation at different time points post injury. The accumulation of NPs was not only influenced by the NP size and time after injury but also varied spatially within the brain tissue cortex. The anterior and middle regions of the injured tissue had maximal accumulation of NPs compared to the posterior region 1 h after brain injury. Detailed studies on biodistribution of each NP and their total accumulation per brain tissue are yet to be addressed. However, our current study provides the groundwork for NP delivery after TBI. Potential application of our study ranges from delivery of targeted contrast agents to therapeutics after TBI. Therefore, better understanding of NP accumulation will facilitate effective utilization of the BBB breakdown for TBI theranostics.

2.5 Acknowledgments

Authors would like to thank CLAS-Life Sciences Electron Microscope Lab and Bioimaging facility/Keck division (Arizona State University) for the use of transmission electron microscope and confocal laser scanning microscope, respectively. We thank Karthik Nambiar and David Lowry for the technical assistance in acquiring TEM images. We would also like to thank Dr. Dierdre Meldrum for the use of dynamic light scattering instrument. We would like to extend our thanks to Amanda Witten for assistance with the figure 2.1 and Appendix A figure A.1. This study was supported by the FLINN Foundation (SES, VDK, JL, PDA) and NIH (1DP2HD084067; SES).

CHAPTER 3

BLOOD-BRAIN-BARRIER DISRUPTION DICTATES NANOPARTICLE ACCUMULATION FOLLOWING EXPERIMENTAL BRAIN INJURY

Clinically, traumatic brain injury (TBI) results in a complex heterogeneous pathology that cannot be recapitulated in a single pre-clinical animal model. Therefore, we focused on evaluating the utility of nanoparticle (NP)-based therapeutics following three diffuse-TBI models: mild-closed-head injury (mCHI), repetitive-mCHI and midline-fluid percussion injury (FPI). We hypothesized that NP accumulation after diffuse TBI correlates directly with blood-brain-barrier permeability. Mice received PEGylated-NP cocktail (20-500nm) (intravenously) after single- or repetitive-(1 impact/day, 5 consecutive days) CHI (immediately) and midline-FPI (1h, 3h, and 6h). NPs circulated for 1h before perfusion/brain extraction. NP accumulation was analyzed using fluorescent microscopy in brain regions vulnerable to neuropathology. Minimal/no NP accumulation after mCHI/RmCHI was observed. In contrast, midline-FPI resulted in significant peak accumulation of up to 500nm NP at 3h post-injury compared to sham, 1h, and 6h groups in the cortex. Therefore, our study provides the groundwork for optimal NP-delivery based on NP-injection time and NP-size after mCHI/RmCHI and midline-FPI.

3.1 Introduction

Traumatic brain injury (TBI) is a leading cause of disability worldwide with 1.7 million TBIs reported annually with an annual estimated economic cost of $76.5 billion in the United States alone[9,14]. TBI occurs due to damage to the brain resulting from an external mechanical force, including rapid acceleration or deceleration, blast waves, crushing force, an impact or penetration by a projectile[12]. Broadly, TBI can be classified into focal injury, associated with cerebral contusion and hematoma, and diffuse brain injury, associated with multifocal and widespread microscopic pathology[188]. Over time, research has revealed TBI to be a complex disease process and not just a single pathophysiological event[11,15,21]. Upon sustaining a TBI the mechanical forces from impact inflict heterogeneous tissue damage, referred to as the primary

injury phase[11]. This insult initiates a myriad of pathophysiological and biochemical secondary injury signaling cascades, including hypo- or hyper-perfusion, edema, blood-brain-barrier (BBB) dysfunction and inflammation that evolves from minutes to days post-trauma[15].

The heterogeneous pathophysiology observed clinically following a TBI likely arises from the variations in the mode of the impact such as the location, type, and severity, as well as other factors including age, sex, and genetics[50]. Pre-clinical animal models have been developed in the laboratory to effectively study and evaluate TBI pathology using a reproducible injury event while also controlling for above factors[51,55]. However, a single injury model may not fully recapitulate all the facets of the secondary injury that are observed in human TBI[51]. The most commonly used focal injury model is the controlled cortical impact (CCI), which produces a focal lesion, axonal injury, and necrosis[56]. Pre-clinical models of diffuse brain injury include mild closed head injury (mCHI), repetitive mild CHI (RmCHI) and midline fluid percussion injury (FPI). The RmCHI model produces early deficits in motor coordination and locomotor hyperactivity with increased astrocytic reactivity[64]. Midline FPI produces a diffuse injury and results in neurological and physiological alterations[61,189]. Clearly, RmCHI and FPI provide clinically-relevant, albeit different, injury phenotypes with distinct cellular alterations. Taken together, preclinical parameters such as injury phenotype is essential to successfully shepherd therapeutic approaches to clinical trials. Therefore, therapeutic strategies need to be evaluated in multiple TBI models while considering opportunities for different optimal therapeutic windows for each injury phenotype. However, a critical gap exists in understanding if/when BBB opening may occur after diffuse TBI, which can facilitate nanoparticle (NP) delivery.

The BBB dysfunction after injury may lead to extravasation of blood components into the brain parenchyma. Studies in different TBI animal models have demonstrated acute and delayed BBB disruption followed by restoration as evidenced by extravasation of endogenous serum immunoglobulins (IgG) [167,190] and/or intravenously injected small molecule tracers, including Evans Blue[191] and horseradish peroxidase (HRP) [167,190]. For example, Tanno *et. al.* established the transient BBB breakdown occurred after FPI (lateral) and the time course for re-establishment of the BBB varied based on the regions of the brain and proximity to the injury

hub[167]. Similarly, Schmidt *et. al.* [190] demonstrated that BBB disruption displayed regional differences following FPI (midline) with prominent HRP leakage in the cerebral cortex (proximal to injury hub) and corpus callosum[190]. In contrast to RmCHI, a recent study reported no positive IgG immune-reactivity at 7 days after final impact and thus potentially no BBB breakdown[64]. Yet, these results raise the question regarding the state of the BBB at acute time points after RmCHI. Collectively, these seminal studies support the notion that TBI compromises the BBB resulting in the extravasation of blood constituents into the normally impermeable brain parenchymal space.

BBB breakdown/permeability offers a unique opportunity to deliver drugs/nanoparticles that are normally excluded from the brain[1,17,75,129]. Previously, we and others demonstrated the feasibility of delivering NPs to brain lesions after a focal brain injury via the disrupted BBB[2,128,162]. The NP delivery to the brain through the transient BBB opening after focal TBI was dependent on the size of the particle, with smaller particles having prolonged permeability compared to larger particles[2,151]. However, the utility of NPs to deliver diagnostic/therapeutic agents in other injury phenotypes such as diffuse brain injury is largely unknown. Therefore, in this study, we assessed NP-size dependent accumulation in three different diffuse brain injury models: mild closed head injury (mCHI), repetitive mild CHI (RmCHI) and midline fluid percussion injury (FPI). We hypothesized that NP accumulation in diffuse injury models would correlate directly with blood-brain barrier permeability.

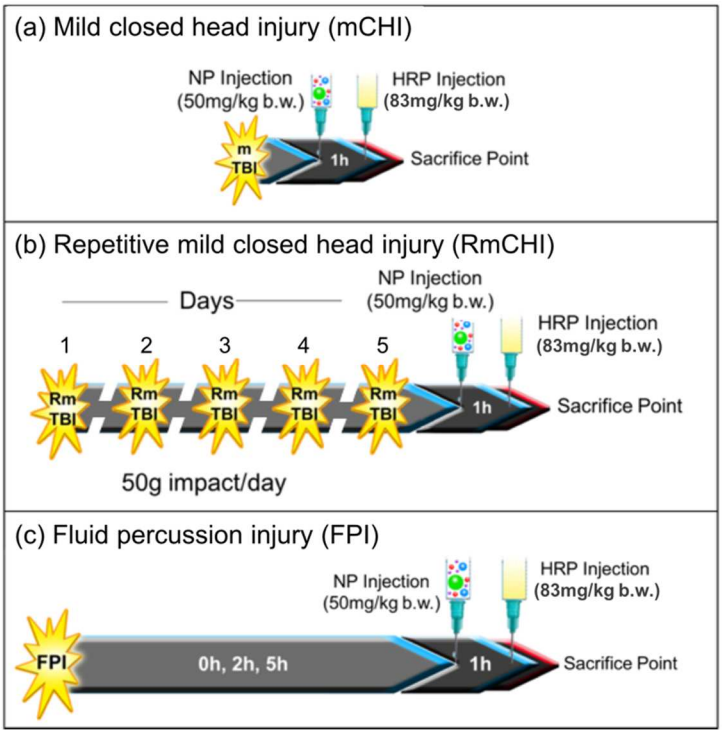

Figure 3.1 In vivo experimental study design: Cocktail of different size nanoparticles was intravenously injected (a) immediately after mild closed head injury (mCHI), (b) immediately after the fifth impact of a repetitive mild RmCHI, and (c) immediately, 2 h and 5 h after fluid percussion injury (FPI). Animals were killed one hour after NP injection. The positive control permeability marker, horseradish peroxidase (HRP), was injected intravenously, 10 min before brain collection.

3.2 Materials and Methods

3.2.1 Materials

Carboxylated polystyrene NPs of different sizes were purchased from Life Technologies (Carlsbad, CA, USA). Specifically, the materials (with catalog numbers) used were 20 nm (F8783), 40 nm (F8793), 100 nm (F8797) and 500 nm (F8813) NPs with dark red ($\lambda_{ex}/\lambda_{em}$=660 nm/680 nm), red ($\lambda_{ex}/\lambda_{em}$=580 nm/605 nm), blue ($\lambda_{ex}/\lambda_{em}$=350 nm/440 nm) and yellow-green ($\lambda_{ex}/\lambda_{em}$=505 nm/515 nm) fluorescence, respectively. Methoxypolyethylene glycol amine 2000 (mPEGamine 2KDa) (06676), methoxypolyethylene glycol amine 750 (mPEGamine 750Da) (07966), n-[3-dimethylaminopropyl]-n-ethyl, n-[3-dimethylaminopropyl]-n-ethyl [EDC] (E1769),

MES hemisodium buffer (M8902), N-Hydroxysuccinimide (NHS) (56405), and Peroxidase type II from horseradish (P8250-50KU) were purchased from Sigma Aldrich (St. Louis, MO, USA). ImmPACT DAB peroxidase (HRP) substrate (SK-4105) was purchased from Vector laboratories (Burlingame, CA, USA). Slide-A-Lyzer Cassettes (20K) (66003) and Kimwipes (06-666) were purchased from ThermoFisher scientific (Waltham, MA, USA). Vectashield antifade mounting medium (H-1000) from Vector Labs (Burlingame, Ca, USA) and Anti-mouse IgG antibody 488 (ab150105) from Abcam (Cambridge, UK) were purchased.

3.2.2 Nanoparticle PEG conjugation

Carboxylated NPs of different sizes, 20nm, 40nm, 100nm, and 500nm were PEGylated using EDC/NHS chemistry. See Appendix B for details.

3.2.3 Animals

Male C57BL/6 mice (20-24g) (Envigo, Inc., Indianapolis, IN) were used for all experiments (n=3 per group). Animal care was approved by the Institutional Animal Care and Use Committees at the University of Arizona (Tucson, AZ). Each study has been approved by an institutional review committee and the procedures followed are in accordance with institutional guidelines and humane treatment of the animals. See Appendix B for details.

(1) Closed head injury (CHI)

Mice were subjected to mild CHI or repetitive mCHI using the protocol previously described[63,64]. Briefly, mice were lightly sedated via isoflurane inhalation and placed on Kimwipe secured to a Plexiglas stage. External anatomical landmarks (such as ear canals, eyes) were used to carefully position the animal to center under the vertical aluminum guide tube. The impact weights (9mm diameter) with the desired mass (100g or 50g) was positioned at the top of aluminum tube and was allowed to fall freely down (865mm) the aluminum guide tube on to the head of the mouse. A cushion sponge was located below the Kimwipe stage to receive the falling mouse. Animals received a single impact of either 100g or 50g (n=6, pooled across the different weights, animals that displayed hematoma/skull fracture were excluded from the study). The RmCHI cohort (n=3) received 50g impact, 1 per day for 5 consecutive days.

(2) Midline Fluid Percussion Injury (FPI)

For injury induction 24h post-surgery for craniotomy (Appendix B), mice were re-anesthetized with 5% isoflurane delivered for three minutes. The cap was removed from the injury-hub assembly and the dura was visually inspected through the hub to make sure it was intact with no debris. The hub was then filled with normal saline and attached to an extension tube connected to the male end of the fluid percussion device (Custom Design and Fabrication, Virginia Commonwealth University, Richmond, VA). An injury pressure of 1.1-1.2atm was administered by releasing the pendulum onto the fluid-filled cylinder. Sham-injured mice underwent the same procedure except the pendulum was not released. Mice were monitored for the presence of a forearm fencing response and righting reflex times were recorded for the injured mice as indicators of injury severity[192]. The righting reflex time is the total time from the initial impact until the mouse spontaneously rights itself from a supine position. The fencing response is a tonic posturing characterized by extension and flexion of the forearms that has been validated as an overt indicator of injury severity[192].
Furthermore, naïve animals (no impact/injury) were injected with the cocktail of nanoparticles (20, 40, 100 and 500nm) and were perfused one hour post-injury.

3.2.4 Nanoparticle (NP) and horseradish peroxidase (HRP) injection – mCHI/RmCHI

Retro-orbital injections of the venous sinus in the mouse were performed for intravenous delivery of the NPs and HRP, an alternative technique to tail-vein injection[163]. Animals were anesthetized with isoflurane (3%) and the NP cocktail (75µl) of 20 and 40nm NPs for mCHI/RmCHI (at a dose of 50mg/kg b.w.) was injected to the right eye, one hour before perfusion. HRP (83mg/kg b.w. in 25µl) was injected behind the left eye ten minutes before perfusion. Animals were killed at 1h after mCHI/RmCHI. The NP circulation time of 1h was held constant for each of the cohorts. Schematics show the experimental timeline for mCHI (Figure 3.1a) and RmCHI (Figure 3.1b).

3.2.5 Nanoparticle (NP) and horseradish peroxidase (HRP) injection – midline FPI

Retro-orbital injections of the venous sinus in the mouse were performed for intravenous delivery of the NPs and HRP, an alternative technique to tail-vein injection[163]. Animals were

anesthetized with isoflurane (3%) and the NP cocktail (75µl) of 20, 40, 100 and 500nm NPs for the midline FPI study (at a dose of 50mg/kg b.w.) was injected to the right eye, one hour before perfusion. HRP (83mg/kg b.w. in 25µl) was injected behind the left eye ten minutes before perfusion. Depending on the cohort group, animals were killed at 1 h, 3 h, and 6 h after midline FPI. The NP circulation time of 1 h was held constant for each of the cohorts. A schematic shows the experimental timeline for midline FPI (Figure 3.1c).

3.2.6 Tissue collection

According to the injury groups, mCHI/RmCHI animals (1h after final impact) animals were deeply anesthetized with isoflurane overdose. For the FPI study, animals (1h, 3h, and 6h post-injury) were deeply anesthetized with lethal dose of sodium pentobarbital solution until a tail/toe pinch produced no reflex movement. Animals were transcardially perfused with cold phosphate-buffered saline (PBS), followed by 4% buffered paraformaldehyde solution. Brain tissue was collected and fixed overnight in 4% buffered paraformaldehyde followed by immersion in 30% sucrose solutions in 1X PBS for cryoprotection for 24h. Samples were embedded in optimal cutting temperature (OCT) medium and frozen on dry ice. Samples were stored at -80°C until sectioned coronally at a 25µm thickness with a cryostat.

3.2.6 Analysis of HRP and NP accumulation after mCHI/RmCHI and FPI

Tissue sections were incubated in PBS buffer for 20mins at room temperature prior to use. For HRP analysis, freshly prepared DAB substrate solution (200µl) was added to the tissue and incubated for ten mins at room temperature. Slides were then washed in PBS buffer three times (two mins each) and coversliped after adding a drop of aqueous mounting media. Sections were imaged using Slide Scanner (PathScan Enabler IV, Meyer Instruments, TX, USA). See Appendix B for details.

For NP analysis, slides containing the frozen sections were incubated at room temperature for 20mins in 1X PBS to rehydrate the tissue and remove OCT compound. Slides were coverslipped after adding one drop of fluorescent mounting media (Vectashield). The whole brain sections were imaged with conventional epifluorescent/confocal microscopy at 10X/20X objective, respectively. See Appendix B for details.

3.2.7 Immunohistochemical analysis for mCHI/RmCHI

The sections were incubated with a solution made up of anti-mouse IgG secondary antibody 488 (1:200) with 2% goat serum and 0.1% Triton X-100 for 2h at room temperature in the dark. The sections were rinsed with PBS (4 times, 5 min each). A conventional epifluorescent microscope (Leica DMI6000 B, Leica Microsystems, Wetzlar, Germany) was used to image the stained sections. See Appendix B for details.

3.2.8 Statistics

Statistical analyses were conducted in GraphPad Prism 5.0 (GraphPad Software, Inc., La Jolla CA). For the midline FPI study, the analysis of HRP/NP percent area in the regions of interest between the injured and sham groups at different time points was conducted using an ordinary two-way analysis of variance (ANOVA). Specifically, to compare the HRP/NP percent area between the injury and the sham group at each time point, Bonferroni's post-hoc test was conducted. Tukey's post-hoc test was conducted for pairwise comparison of HRP/NP percent area for each group (injury and sham) at different time points. For correlation analysis of HRP and NP, Pearson correlation test was conducted. The statistical values (P-value, F-value, and degree of freedom) are included in Appendix B sections. The P-values are reported in the results section.

3.3 Results

3.3.1 Absence of HRP after mCHI/RmCHI

Our previous study using the CCI model of focal TBI, the highest level of HRP extravasation was observed within 1h following impact[2]. Therefore, we evaluated this time point in the mCHI model and observed minimal to no HRP accumulation (50 g and 100 g impact; Figure 3.2) suggesting an intact BBB acutely after mCHI (~50 mins after CHI). Furthermore, we did not observe any HRP staining within 1h following the fifth impact in the RmCHI model (one per day for five consecutive days). Representative images of HRP staining after mCHI after single 50g (Figure 3.2a), and 100g (Figure 3.2b), and multiple impacts (50g, 5X; Figure 3.2c) were comparable to naïve brain tissue (Figure 3.2d). Furthermore, to investigate if evidence of BBB breach was not captured by the exogenous HRP tracer, we immunostained for endogenous IgG.

We observed positive IgG staining at 1h post-impact after single and multiple (5X) impacts (images in Appendix B), suggesting that the BBB may have opened transiently prior to the HRP tracer injections.

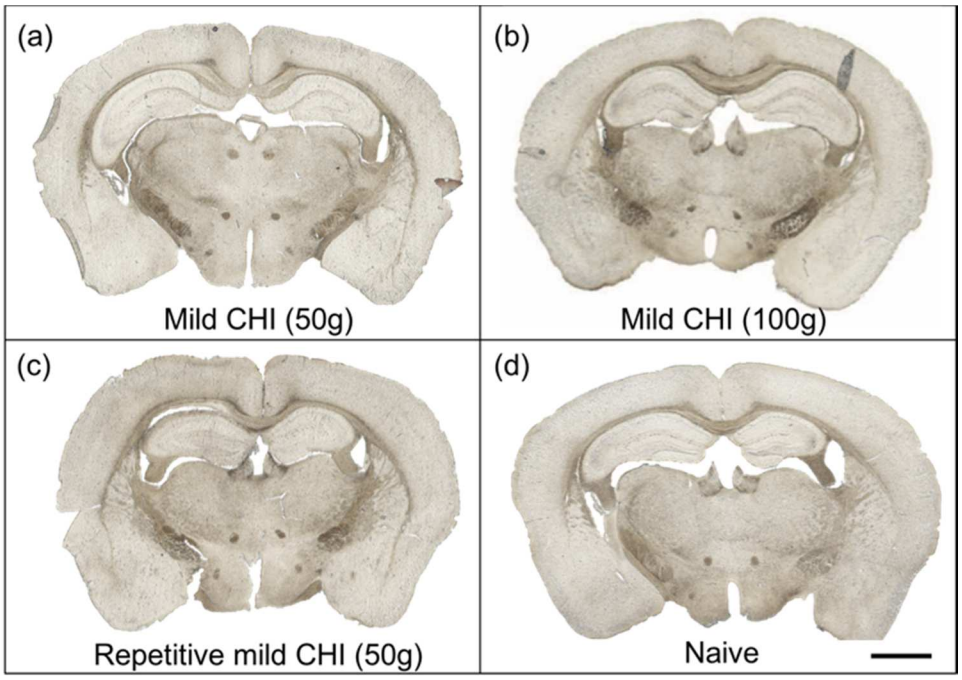

Figure 3.2 Representative images of HRP extravasation after mCHI and repetitive mCHI (a) single impact mCHI (50g), (b) single impact mCHI (100g), (c) multiple impacts (5X) RmCHI (50g), (d) control (naïve). HRP circulated for 10mins prior to tissue collection at 1 h post-injury. Scale bar = 1500µm

3.3.2 Positive HRP extravasation after midline FPI

Representative images of HRP staining pattern of each FPI cohort at different time-points are shown in Figure 3. The two-way ANOVA identified a significant difference between the two groups (injured and sham) for both cortex ($p=0.0002$) and corpus callosum ($p=0.025$) (See Table B2 for full statistical data, (Appendix B)). Also, a significant time-dependent effect for both cortex ($p=0.0067$) and corpus callosum ($p=0.0117$) was observed. In the cortex, Bonferroni's post hoc test comparing the injury and sham groups demonstrated a significant difference in the 3h cohort

(p=0.0001). Comparing the cortex of the injured groups at different time points, using Tukey's post-hoc test, revealed HRP staining at the 3h time point was three-fold greater than the 1h (p=0.0018) and 6h time point (p=0.007; Figure 3.3ii). In the corpus callosum, there was minimal to no HRP extravasation at 1h and 6h post-injury (Figure 3.3iii). However, a peak accumulation at 3h post-injury was observed (about 15-fold increase) compared to the sham group (Bonferroni's post hoc, p=0.0024) in the corpus callosum. Moreover, Tukey's post-hoc test demonstrated a peak accumulation at 3h post-injury (about 15-fold increase) compared to the 1h (p=0.0021; Figure 3.3ii) and 6h (p=0.0021; Figure 3.3iii). Therefore, HRP extravasation confirmed the BBB dysfunction at 3h after FPI in the cortex and corpus callosum.

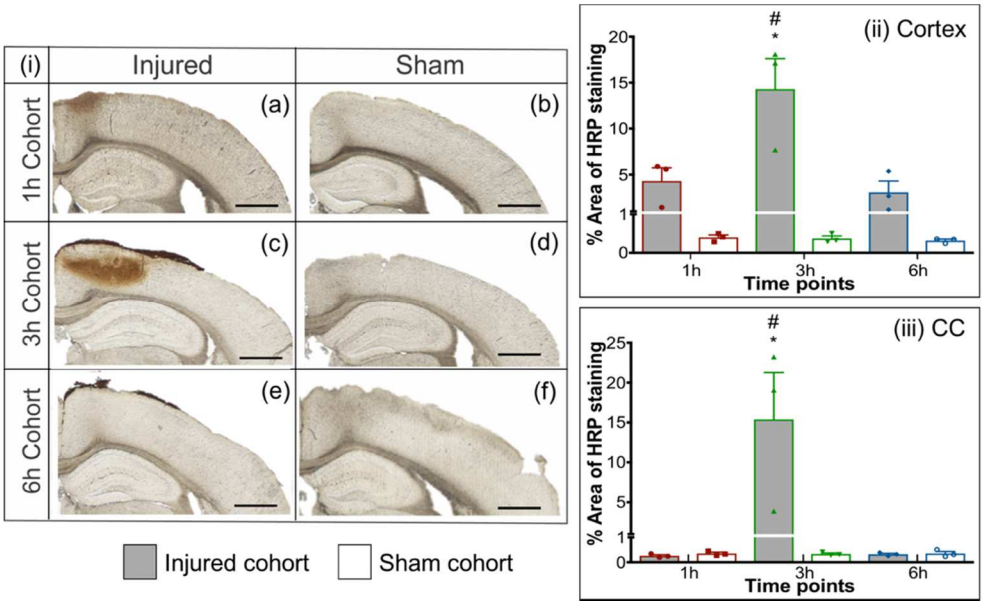

Figure 3.3 Extravasation of HRP after FPI Representative images of HRP extravasation after FPI with injured and sham groups of 1h (a-b), 3h (c-d), 6h (e-f). HRP was injected ten mins before sacrifice. Quantification of HRP extravasation after FPI. (ii) Cortex, (iii) Corpus callosum. *p<0.05 compared to respective sham group, two-way ANOVA, Bonferroni's post-hoc test. #p<0.05 compared to 1h and 6h injured cohort, two-way ANOVA, Tukey's post-hoc test. Error bars represent standard error of mean with n=3. Scale bars = 200μm.

3.3.3 Accumulation of NP after diffuse injury

To determine the extent of NP accumulation after acute TBI, we intravenously injected NP cocktail after mCHI/RmCHI (only 20nm and 40nm) and FPI (20, 40, 100 and 500nm) and with a constant circulation time of 1h.

3.3.3.1 Absence of NP Accumulation after mCHI/RmCHI:

For the mCHI study, there was no fluorescent signal observed in any of the tissue sections after either single impact or multiple impacts (figures in Appendix B).

3.3.3.2 Presence of NP Accumulation after midline FPI:

We quantified the accumulation of each fluorescent NP via confocal microscopy for the midline FPI model (Figure 4-6). In the cortex, there was a significant effect between the injury and sham group for 20nm (two-way ANOVA, $p = 0.0002$), 40nm ($p = 0.0006$), 100nm ($p = 0.0071$), and 500nm ($p = 0.0003$). Moreover, the analysis demonstrated a significant time-dependent effect for 20nm ($p = 0.0002$), 40nm ($p = 0.0006$), 100nm ($p = 0.0069$), and 500nm ($p = 0.0013$) (Figure 3.5a-d). To examine the effect of each of these variables individually, post-hoc pair-wise analyses of critical comparisons are described below.

Analysis of the NP accumulation in midline FPI injured and sham brain tissue:

The first pairwise analysis focused on comparing NP accumulation in the injured and sham group across time points in the two ROIs (cortex and corpus callosum). Specifically, in the cortex, Bonferroni's post-hoc test displayed significant difference in 20 nm ($p<0.0001$), 40 nm ($p<0.0001$), 100 nm ($p<0.0021$) and 500 nm ($p<0.0001$) NPs accumulation at 3h post-injury as compared to their respective sham groups (Figure 3.5(a-d)). No significant difference was observed at 1h and 6h post-injury compared to their respective sham groups for any NP. Furthermore, in the corpus callosum ROI, there was no significant difference between the injured and the sham group for all NP sizes. Overall, all the NPs displayed significant accumulation at 3h post-FPI compared to the sham group in the cortex.

Analysis of the NP accumulation in midline FPI injured group across different time points:

The second critical comparison focused on the NP accumulation within the injured group across different time points in the two ROIs: cortex and corpus callosum. In the cortex, for all the NP sizes, 20, 40, 100 and 500 nm, Tukey's post-hoc test demonstrated a significant increase at 3h post-injury for 20 nm ($p<0.0001$), 40 nm ($p\leq0.0001$), 100 nm ($p=0.002$) and 500 nm ($p\leq0.001$) compared to both 1h and 6h cohorts ($p < 0.05$). The peak increase of accumulation in the cortex at 3h post-injury was at least twice that at 1h and 6h for each NP size (Figure 3.5a-d). In the corpus callosum, although there was no significant difference among the NP accumulation (20, 40, 100 and 500 nm) across time points, there was a trend with increased accumulation at 3h post-FPI compared to that at 1h and 6h (Figure 3.6a-d).

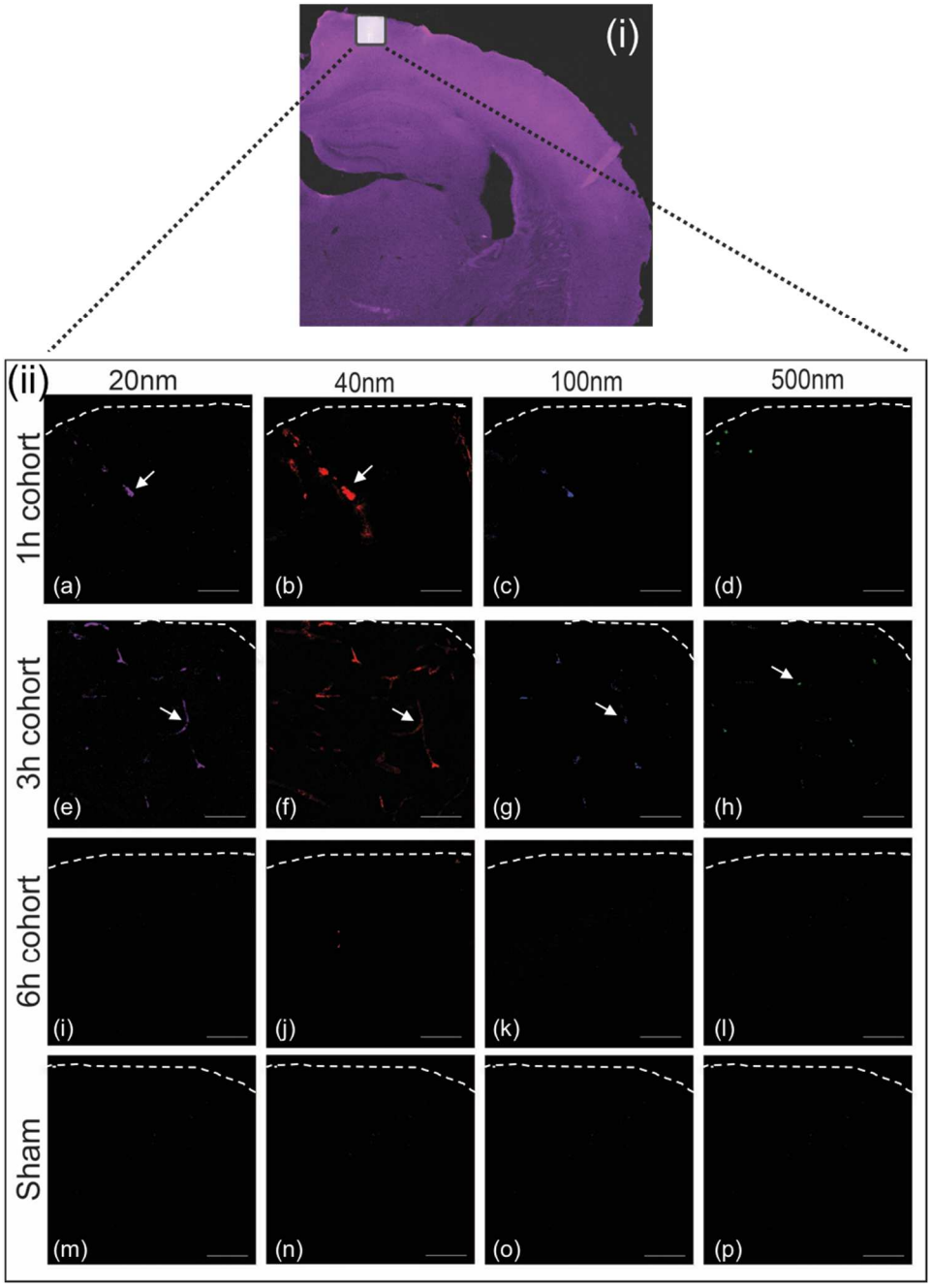

Figure 3.4 Accumulation of different size nanoparticles over time after FPI. (i) Representative image of whole brain scan and white box highlights the approximate location of the higher magnification cortical region. (ii) Representative images of NP accumulation at 1 h (a-d), 3 h (e-h), 6 h (i- l), and sham (control) (m-p). Columns display different size of NP

accumulation over different time points post-midline-FPI. NPs were injected 1h before sacrifice. Scale bar = 100 μm.

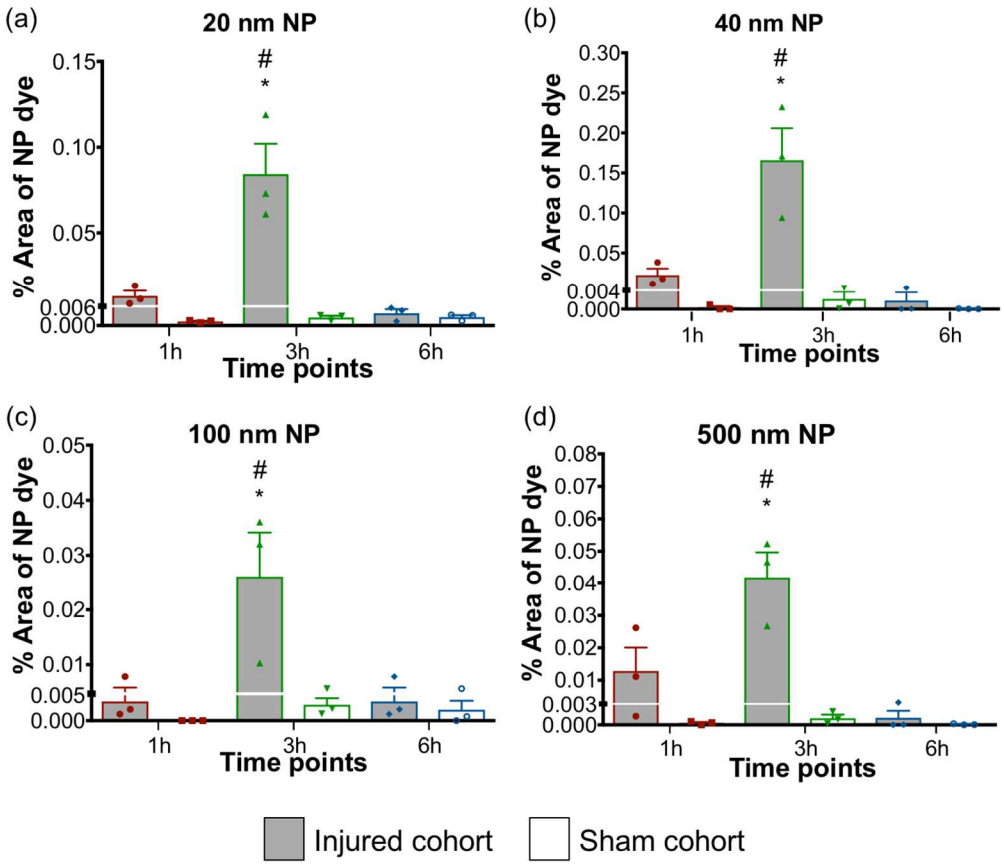

Figure 3.5 Nanoparticle accumulation after FPI in cortex. Accumulation of 20nm, 40nm, 100nm and 500nm nanoparticles at different time points (1h, 3h, and 6h) after FPI. NPs were injected 1h before sacrifice. *p<0.05 compared to respective sham group, two-way ANOVA,

Bonferroni's post-hoc test. #p<0.05 compared to 1h and 6h injured cohort, two-way ANOVA, Tukey's post-hoc test. Error bars represent standard error of mean with n=3 animals per group.

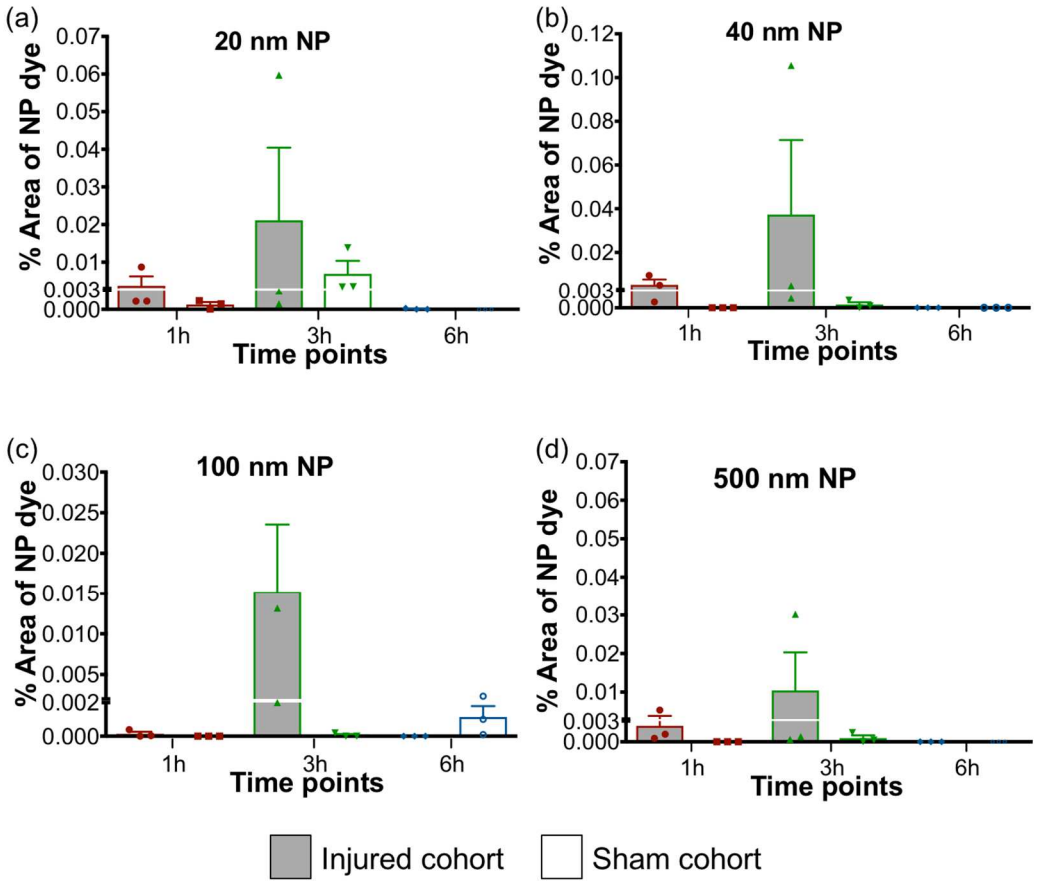

Figure 3.6 Nanoparticle accumulation after midline-FPI in corpus callosum. Accumulation of 20nm, 40nm, 100nm and 500nm nanoparticles at different time points (1h, 3h, and 6h) after FPI. NPs were injected 1h before sacrifice. Two-way ANOVA statistical test was conducted. Error bars represents standard error of mean with n = 3 animals per group.

Correlation of HRP and NP accumulation after midline-FPI

To further validate our hypothesis that NP accumulation directly depends on blood brain barrier permeability, we evaluated the relationship between HRP and NP staining with Pearson correlation coefficient. For the cortex ROI, in figure 3.7, each scatter plot represents corresponding data points of the percent area of HRP staining versus percent area of NPs across all the time periods. The results (Figure 3.7) show a significant correlation between the HRP staining and 20nm ($p = 0.0005$), 40nm ($p < 0.0001$), 100nm ($p < 0.0001$) and 500nm ($p = 0.0002$). Moreover, the Pearson correlation coefficient for: 20nm ($r = 0.9147$), 40nm ($r = 0.9574$), 100nm ($r = 0.9608$), and 500nm ($r = 0.9388$) indicates a robust correlation between HRP and the NPs. Particularly, HRP staining was maximally observed at 3h post-injury and those animals/brain tissue displayed peak NP accumulation (20nm, 40nm, 100nm and 500nm). Furthermore, the same analysis was performed for the corpus callosum, but no correlation was identified due to limited NP accumulation.

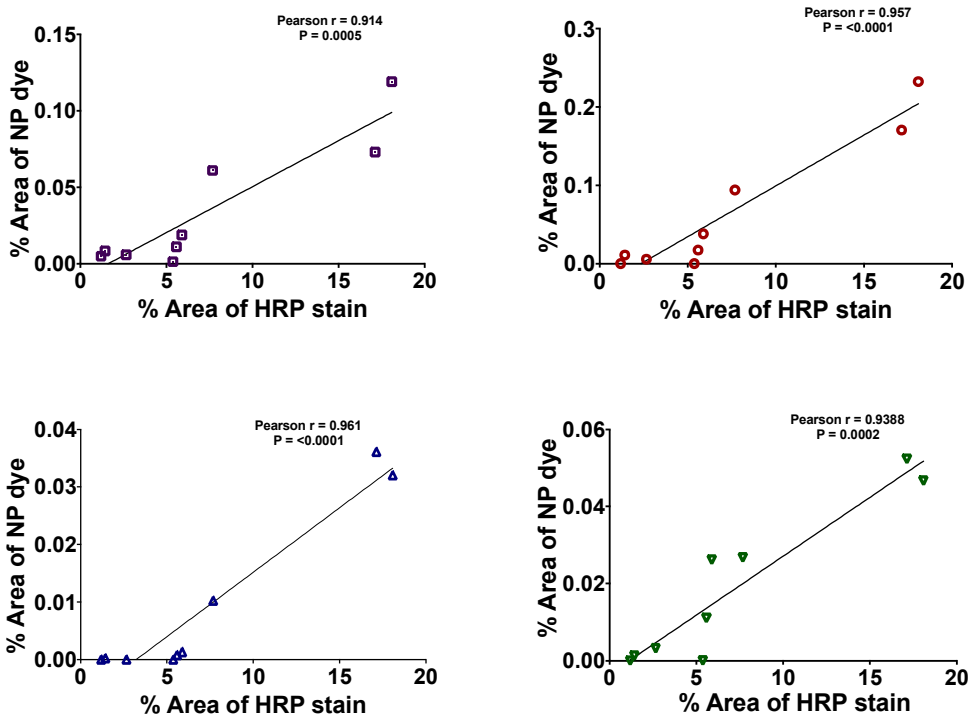

Figure 3.7 Correlation of HRP and NP accumulation after midline-FPI in cortex. The x-axis shows the percentage of the HRP stain (data from Figure 3) and the y-axis shows the percentage

of NP accumulation (data from Figures 4-6) of (a) 20nm (r = 0.9147), (b) 40nm (r = 0.9574), (c) 100nm (r = 0.9608), and (d) 500nm (r = 0.9388). Pearson correlation coefficient (r) was close to 1, indicating a robust correlation between HRP and the NPs.

3.4 Discussion & Conclusions

Research on NP delivery after brain injury has gained traction over the last couple of years[193-197]. TBI may lead to a transient breach in the BBB that can be capitalized to passively deliver NPs. Previously, using experimental focal injury (controlled cortical impact) our group has demonstrated the feasibility of NP delivery up to 500 nm in size with a peak NP accumulation at 1 h post-TBI[2]. Yet, there is a critical gap in understanding the relationship between BBB opening and models of diffuse TBI for NP delivery. Here in this study, we used three models of diffuse brain injury (mild CHI, repetitive mild CHI and midline-fluid percussion injury (FPI)) to evaluate the effect of different size NP accumulation at acute time points after injury. We reported four key findings: 1) mCHI and RmCHI did not show any NP accumulation 1 h after final impact; 2) NPs up to 500 nm can be delivered to injured brain sustaining a diffuse TBI by midline-FPI model; 3) maximal accumulation occurred 3 h post-FPI for all NP sizes (20, 40, 100 and 500 nm); and 4) significant correlation was observed between HRP staining and NP accumulation in the cortex after midline-FPI.

RmCHI is common in sports-related TBIs and war combat morbodities[198,199], with the potential for long-term consequences, including chronic traumatic encephalopathy[200]. Evaluation and management of RmCHI remain a challenge due to the diffuse and microscopic pathology, where NP delivery for diagnostic and therapeutic approaches may provide a new strategy to improve detection of mCHI and clinical management. In this study, we intravenously injected 20 and 40nm NPs immediately following impact in mCHI and RmCHI with one-hour circulation time; HRP (BBB integrity marker) was injected ten minutes prior to sacrifice. We did not observe any HRP or NP accumulation at 1h after single impact mCHI nor after 5 consecutive impacts in the rmCHI model. We acknowledge that probing BBB integrity via this approach

captures a single snapshot of the dynamically complex response after impact. Therefore, we further probed BBB integrity via immunohistochemistry for endogenous IgG within the parenchyma. IgG is not present in healthy brain tissue, but it may get trapped due to a transient BBB breakdown. Intriguingly, we observed IgG staining in the hippocampus in both single and multiple impact groups compared to staining in the naïve group (Appendix B). The presence of endogenous IgG and the absence of any exogenous HRP (injected 50mins post-impact) suggests one of two possibilities. One, a transient BBB breach occurs immediately after and/or during both single and multiple impacts but sealed prior to the injection of HRP (i.e. within 50mins). Alternatively, the presence of IgG could possibly be due to active transport across the endothelial cells via deregulated endocytosis pathway such as transcytosis[201]. Furthermore, the absence of any NP accumulation after immediate injection suggests that the BBB permeability was size dependent, where the 20nm NPs may have been too large for extravasation as compared to the smaller sized IgG (estimated radius of 5nm[152]).

In contrast to the mCHI study, the midline-FPI study showed both HRP and NP accumulation after injury. We observed extravasation of the HRP (~44kDa with an estimated radius of ~3 nm[152]) in the cortex (proximal to injury hub) at 1h, 3h, and 6h post-injury. Significant HRP staining at 3h post-injury was also noted in the corpus callosum. Previous rat FPI (midline-and lateral-) models reported similar observations of HRP extravasation at 1h with a marked reduction at 6h post-injury in the cerebral cortex and corpus callosum[167,190]. One key objective of this study was to establish the feasibility of NP delivery after diffuse brain injury to then further develop NP-based therapeutic and diagnostics. Demonstrating the time course of BBB disruption after diffuse brain injury was the first step in achieving this objective. In addition, although mCHI did not show any NP accumulation at 1h post-injury, studies to assess NP accumulation at different time points is warranted.

In the recent years, the interest for NP application for TBI has been increasing[2,128,197,202,203]. For example, Bailey *et al* used cerium oxide NPs (~10 nm) as an antioxidant agent in the lateral FPI model[203]. Although this study demonstrated the feasibility of

NP delivery following diffuse brain injury, little is known about the impact of NP size and optimal time window for effective delivery after TBI. We directly addressed this critical gap by evaluating a cocktail injection of different size PEGylated NPs at different time points after injury while maintaining a constant circulation time of 1 h. Furthermore, systemic NP delivery parameters such as size, charge and surface modification may influence the physiochemical stability and the rate of NP elimination from the circulation[109,114]. Since the focus of this study was to evaluate the size and time-dependent NP accumulation after diffuse brain injury, the NPs were PEGylated to obtain slightly negatively charged NPs for efficient systemic delivery and to minimize the influence of parameters outside of size. Maximal accumulation for all size NPs was observed at 3h post-injury in the cortex (Figure 4). Our study is the first to report accumulation up to 500 nm PEGylated NPs following midline-FPI. This finding supports our previous study using the focal brain injury model, controlled cortical impact (CCI), where we reported accumulation of ~500nm NPs near the injured cortex out to 12h post-injury[2]. Taking our data one step further, we identified a direct correlation of the BBB integrity as measured through HRP staining with NP accumulation (Figure 6). Collectively, our results add to our current understanding regarding the size and time-dependent NP delivery after diffuse TBI. Insight into such parameters is critical for determining the optimal delivery window for NPs following TBI.

An interesting finding from our study in the midline-FPI cohort was the peak accumulation of the NPs at 3h post-injury compared to 1h and 6h group. Acutely after FPI, regional cerebral blood flow reportedly decreases[204] contributing to distressed endothelial cells and ultimately vasogenic and cytotoxic edema[21]. This reduced cerebral blood flow may impede intravenously administered molecules to reach the injured area(s) of the brain[205]. Furthermore, Lin and co-workers established a positive correlation between the BBB permeability and cerebral microvascular perfusion acutely after FPI in rat models[205]. Immediately and 1h post-injury, ischemic centers were prominent in the injured cortex indicating compromised capillary perfusion [205]. However, by 4h post-injury, the blood vessels were significantly more perfused compared

to immediate time point[205]. Therefore, such altered blood vessels/perfusion phenomena that occur post-injury further supports our observation of peak NP accumulation at 3h.

Another interesting finding from our study is the differential spatial NP accumulation within the brain regions (cortex and corpus callosum). The midline-FPI resulted in the leaky vasculature in the cortex and the corpus callosum as visualized by HRP extravasation. Additionally, the NP accumulation was significant compared to the sham groups only in the cortex and not in the corpus callosum. Regional differences may be attributed to the variations in BBB structure in the cerebral cortex and white matter[206]. Previous studies have reported not only a lower capillary density[207] but also tighter barrier due to higher astrocytes and tight junction expressions in the corpus callosum compared to cortical regions [206]. Thus, the heterogeneity in the BBB structure could play a role in the absence of NP accumulation in the corpus callosum compared to the cortex.

In conclusion, we established that PEGylated polystyrene NPs (20 and 40nm) failed to accumulate in the brain tissue after mCHI and RmCHI. In contrast, the FPI cohorts displayed NP accumulation of up to 500nm in size. With a constant circulation time of 1h, we observed a significant peak accumulation at 3h post-FPI compared to 1h and 6h post-FPI. The NP accumulation was not only influenced by the NP injection time, but also on the spatial location in the brain tissue. There was significant NP accumulation only in the cortex and not in the BBB breached corpus callosum. Our current study provides the groundwork for the feasibility of NP delivery in terms of NP injection time and NP size after mCHI and FPI. Prospective application of our study ranges from contrast agents to therapeutic drug delivery after TBI and is grounded on an improved understanding of the BBB breakdown post-injury.

3.5 Acknowledgments

Authors would like to thank Dr. Jason Newbern for technical assistance-confocal microscopy. Authors would like to thank Amanda Witten for the artistic rendering-graphical abstract and figure 1. We would like to thank Kyle Offenbacher for drawing the ROIs-FPI analysis.

Authors would like to thank funding sources NIH NICHD (1DP2HD084067; SES), and Flinn Foundation (1976; VDK, SES, JL, PDA).

CHAPTER 4

EXTENDED THERAPEUTIC WINDOW AND SEX DEPENDENCE OF BLOOD BRAIN BARRIER DISRUPTION FOR NANOPARTICLE DELIVERY AFTER EXPERIMENTAL FOCAL BRAIN INJURY

4.1 Introduction

Traumatic brain injury (TBI) is an acquired injury to the brain that occurs from sudden trauma to the head[14]. It is a leading cause of disability worldwide with about 1.7 million TBIs reported in the United States annually[8,9]. Brain injury is characterized by structural failure and neurologic dysfunction begins at the time of initial impact and lasts from hours to weeks[18,19]. The immediate primary injury occurs due to the external impact and is considered untreatable, but preventable. The primary injury results in the secondary injury, a cascade of neural and vascular events, including inflammation, excitotoxicity, hypoxia, edema, and blood-brain-barrier (BBB) disruption[18,19]. The secondary process develops over hours and days allowing a time window for intervention. However, therapeutic intervention strategies to improve outcomes of TBI have not been clinically successful[69,71]. One of the major limitations for effective neuro-therapeutics is the delivery across the normally tightly and selectively regulated BBB[125]. The consequences of BBB breach after brain injury is known to be detrimental, yet the breach may provide a transient window for delivery of drugs that normally would not cross this barrier[1,15,27,128].

Nanoparticles (NPs) are particles ranging from 1 to 1000nm in size[73,77,78] and can be systemically administered. NPs can be used to deliver a variety of different therapeutics/materials such as drugs (hydrophobic and hydrophilic), proteins, vaccines, macromolecules and genes[68,72,74]. NP delivery through the microcirculation is a viable approach for facilitating drug delivery to the brain since the diameter of the smallest capillaries is ~5-6um[81]. The US Food and Drug Administration (FDA) has approved over two-dozen NP systems for clinic[85]. A major advantage of the NPs is their small size and mobility to access a wide range of cells for both extracellular and intracellular delivery[68,74,87,208]. Another advantage of NPs is the potentially

tailored interaction with biological systems at the molecular and supramolecular level to induce desired physiological response[1,68,74,87]. The potential benefits of nanotechnologies for brain injuries[1] may eventually offer opportunities to address current clinical limitations. However, there is a critical gap in understanding the influence of BBB dysfunction for effective NP delivery after TBI.

A well-established preclinical model of focal TBI is the controlled cortical impact (CCI) injury. This model recapitulates the human TBI characteristics such as edema, haemorrhage, contusion, inflammation and blood-brain barrier (BBB) disruption[2,30,56,149,150,209]. Seminal studies for BBB breakdown have used tracer molecules such as Evans Blue after CCI to establish a biphasic opening[149,210]. The first peak of the BBB breach is at 4-6 hours and the second peak at ~3days post-TBI[149,210]. Our group has previously established in CCI that 20-40 nm NPs readily accumulated within the injury penumbra out to 13h post-TBI[2]. However, the feasibility of NP delivery after 24h post-TBI remains largely unknown. Therefore, we sought to profile the sub-acute time course of this possible window by examining acute (3h and 24h), sub-acute (3d and 7d) post-injury.

Another important factor that can influence BBB dysfunction after TBI and thus subsequent NP delivery is the sex. Sex is known to play a role in the morbidity and mortality after TBI yet mechanisms for such sex-based differences are not well elucidated[211,212]. Sexual dimorphism has been reported for many brain structures and functions such as cognition[36,41,213,214]. For example, studies report higher global cerebral blood flow rate in females than males during resting state in humans[36,41,213] Although there have been an established differences in female and male clinical outcomes[36,213,215-220], preclinical studies in TBI/BBB dysfunction for the past three decades [149,151,167,190,221,222] have routinely been conducted using only male animals to minimize intrinsic biological variability[223]. A recent study in mice found that TBI leads to a more aggressive neuroinflammatory response in males compared to females during the acute and sub-acute post-injury phases[49]. Specifically, the study found significantly higher cortical microglia/macrophage activation and pro-inflammatory cytokine expression in males at 1d and 3d post-TBI compared to females[49]. Furthermore,

studies using male animals have suggested that the delayed (~3d) BBB breakdown after TBI is associated with neuroinflammatory response[2,30,56,149,150,209],[210]. However, sex differences in BBB disruption at the delayed time point (~3d) after TBI has not been studied. As an extension of this BBB disruption, sex differences in passive NP delivery via BBB disruption following TBI is unknown.

Taken together, there is a serious gap in understanding (1) the feasibility of NP delivery at sub-acute time point post-TBI and (2) depicting sex differences in NP accumulation after TBI. Therefore, our hypothesis is twofold, (1) NP accumulation will occur at 3 days post-injury owing to the biphasic opening of the BBB, and (2) Robust NP accumulation in males compared to females at sub-acute time points due to varying neuroinflammatory response that may influence BBB breakdown.

4.2 Materials and Methods

4.2.1 Materials

Carboxylated polystyrene NPs of different sizes were purchased from Life Technologies (Carlsbad, CA, USA). Specifically, the materials (with catalog numbers) used were 40 nm (F8793) NP with red ($\lambda_{ex}/\lambda_{em}$=580 nm/605 nm) fluorescence. Methoxypolyethylene glycol amine 2000 (mPEGamine 2 KDa) (06676), n-[3-dimethylaminopropyl]-n-ethyl, n-[3-dimethylaminopropyl]-n-ethyl [EDC] (E1769), MES hemisodium buffer (M8902), N-Hydroxysuccinimide (NHS) (56405), and Peroxidase type II from horseradish (P8250-50KU) were purchased from Sigma Aldrich (St. Louis, MO, USA). ImmPACT DAB peroxidase (HRP) substrate (SK-4105) was purchased from Vector laboratories (Burlingame, CA, USA). Slide-A-Lyzer Cassettes (20 K) (66003) were purchased from ThermoFisher scientific (Waltham, MA, USA). Vectashield antifade mounting medium (H-1000) from Vector Labs (Burlingame, Ca, USA) were purchased.

4.2.2 Nanoparticle PEG conjugation

As presented in our previous study[2], carboxylated NPs were PEGylated using EDC/NHS chemistry. Briefly, mPEGamine 2 kDa was mixed with 40 nm (NH_2:COOH at 5:1 mole excess). EDC/NHS (in MES buffer) was added to NP / PEG mixture (200 mM/100 mM) and

HEPES buffer was added to obtain a final pH of 7.8 before incubating for 3 h at room temperature. Glycine (100 mM) was added to quench the reaction. Unbound PEG was removed via dialysis (20 kDa MW). PEGylated NPs were suspended in a 20 mM HEPES (pH 7.4). The concentration of NP solution was determined with fluorescent standard curves generated from known concentrations of as-received Fluorospheres (FLUOstar Omega fluorescence plate reader; BMG Labtech, Ortenberg, Germany). Yields of NPs ranged between 40-60 %. A concentration of 12.5 mg/ml for each NP was used for all *in vivo* studies.

4.2.3 Nanoparticle characterization

The hydrodynamic diameter of NPs in 20 mM HEPES (pH 7.4) was measured pre- and post-PEGylation with a dynamic light scattering (DLS) device. Three measurements were made and the mean ± standard the error of mean (s.e.m.) was reported.

4.2.4 Animals

Female and male C57BL/6 mice (20-24 g) were used for the first set of experiments (n=4 per group). Female and male transgenic CX3CR1-EGFP mice were used for two-photon microscopy experiments (n=3 per group). Mice were housed in a 14 h light/10 h dark cycle at a constant temperature (23°C ± 2° C) with food and water available *ad libitum*. Female mice of random cycling were used to better reflect clinical applicability. Animal studies using C57BL/6 mice were approved by Arizona State University's Institute of Animal Use and Care Committee (IACUC) and were performed in accordance with the relevant guidelines. The two-photon microscopy study using transgenic animals was approved by the Institutional Animal Care and Use Committee at the University of Arizona (Tucson, AZ).

4.2.5 Controlled cortical impact model

Traumatic brain injury (TBI) was modeled using the well-established controlled cortical impact (CCI) injury model[56]. Briefly, anesthetized (isoflurane) adult (C57Bl/6 wild-type or transgenic CX3CR1-EGFP) mice (females and males; n=4) were mounted onto the stereotaxic frame. The frontoparietal cortex was exposed via 3 mm (for wild-type) and 4 mm (for transgenic) craniotomy and the impact tip was centered on the craniectomy. The impactor tip diameter was 2 mm, the impact velocity was 6.0 m/s and the depth of cortical deformation was 2 mm and 100 ms

impact duration (Impact ONE; Leica Microsystems). The skin was sutured and the animals were placed in a 37°C incubator until consciousness was regained. The naïve group did not undergo surgery.

4.2.6 Nanoparticle (NP) and horseradish peroxidase (HRP) injection

Retro-orbital injections of the venous sinus in the mouse was performed for intravenous delivery of the NPs and HRP, an alternative technique to tail-vein injection[163] were performed for intravenous delivery of the NPs and HRP. Animals were anesthetized with isoflurane (3 %) and the NP (dosage: 31.25 mg/kg b.w., volume:50 µL) of 40 nm NPs was retro-orbitally injected near the right eye, three hours before perfusion. HRP (83 mg/kg b.w.in 25 µL) was injected behind the left eye ten minutes before perfusion. Depending on the cohort group, animals were killed at 3 h, 1 d, and 3 d after CCI. The NP circulation time of 3 h was held constant for each of the cohorts. The summary of the experimental timeline is depicted in Figure 4.1.

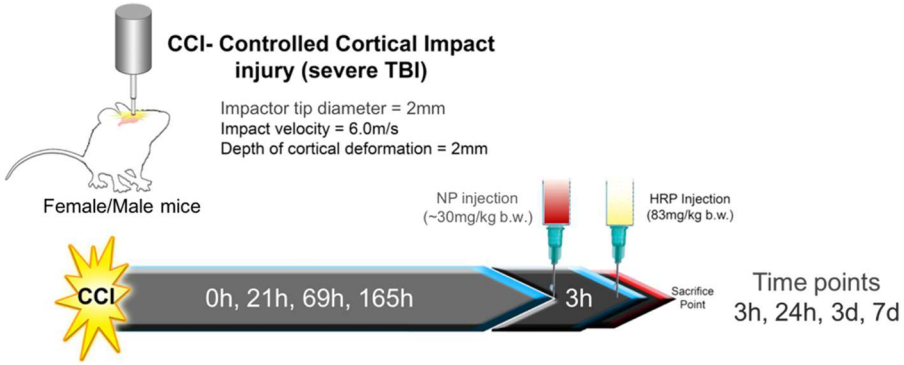

Figure 4.1: In vivo experimental study design: Nanoparticle (40 nm) was intravenously injected in CCI induced female and male mice 3h before sacrifice at 3h, 24h, 3d and 7d post-injury. The positive control BBB permeability marker, horseradish peroxidase (HRP) was injected 10 mins before sacrifice.

4.2.7 Tissue collection

According to the time point of the cohort, C57Bl/6 mice were deeply anesthetized with lethal dose of sodium pentobarbital solution until a tail/toe pinch produced no reflex movement. Animals were transcardially perfused with cold phosphate-buffered saline (PBS), followed by 4 %

buffered paraformaldehyde solution. Brain tissue was collected and fixed overnight in 4 % buffered paraformaldehyde followed by immersion in 30 % sucrose solutions in 1X PBS for cryoprotection for 24 h. Samples were embedded in optimal cutting temperature (OCT) medium and frozen by placing in a glass container with methybutane kept on dry ice. Samples were stored at -80°C until sectioned coronally at a 20 µm thickness with a cryostat.

4.2.8 Quantification of HRP extravasation

The tissue section was incubated in PBS buffer for 20 mins at room temperature prior to use. The tissue sampling regions were ~-1.65 mm Bregma (three sections per animal, n=2 for 3h cohort and n=4 for all other time points). For HRP analysis, freshly prepared DAB substrate solution (200 µl) was added to the tissue and incubated for ten mins at room temperature. Slides were then washed in deionized water three times (two mins each) and coverslips were mounted after adding a drop of aqueous mounting media. Sections were imaged using Slide Scanner (PathScan Enabler IV, Meyer Instruments, TX, USA). The ROI images were then analyzed using ImageJ software (National institute of health, Bethesda, MD, USA) to obtain total number of positive pixels.

4.2.9 Quantification of NP accumulation

For NP analysis, slides containing the frozen sections were incubated at room temperature for 20 mins in 1X PBS to rehydrate the tissue and remove OCT compound. Coverslips were mounted on the section after adding one drop of fluorescent mounting media (Vectashield). The tissue sampling regions were ~-1.65 mm Bregma and ipsilateral cortex (four sections per animal; n=3 for 3h cohort and n=4 for all other time points) and contralateral cortex (two sections per animal; n=3 for 3h cohort and n=4 for all other time points) were imaged with conventional epifluorescent microscopy at 10X objective.

4.2.10 Two-photon microscopy surgery and cranial window placement

Transgenic mice (female and male) underwent the CCI injury induction as described above. Based on the imaging time points (immediately after injury or at 1, or 3 days post-injury), anesthetized animals received intravenous nanoparticle injections (50 mg/kg b.w. 50 µL; retro-orbital). Following the injection, cranial window was placed for imaging. The cranial window

protocol is modified from a previously published protocol[224,225]. Briefly, the craniectomy/injury region was cleaned using saline and gelfoam soaked in saline was applied to stop any bleeding (if any). The region around the craniectomy was dried using cotton swab. After ensuring no bleeding, 5 mm diameter glass coverslip was gently placed on the brain tissue, centered at -2 mm bregma and 2 mm lateral midline. The glass coverslip was sealed using dental cement to secure it and to create a well for the water-immersion objective. On cohort of control, naïve animals were used to establish baseline nanoparticle extravasation across the BBB. These control animals were anesthetized, injected with nanoparticles, then subjected to craniectomy (4mm), and cranial window placement according to the aforementioned protocol. For imaging, animals were under anesthesia and were mounted on a microscope adaptable animal holding frame. Animals were placed on the mount using ear bars to stabilize their heads for imaging. Animals were imaged for a maximum of 3 hours under anesthesia (isoflurane). After two-photon imaging was completed, while animals are still under anesthesia, horseradish peroxidase (83mg/kg of b.w. maximum injection volume of 50 µL) was injected via retro-orbital ten mins before sacrifice. Animals were perfused using the protocol explained above. The detailed two-photon experimental set-up is illustrated in Figure 4.2.

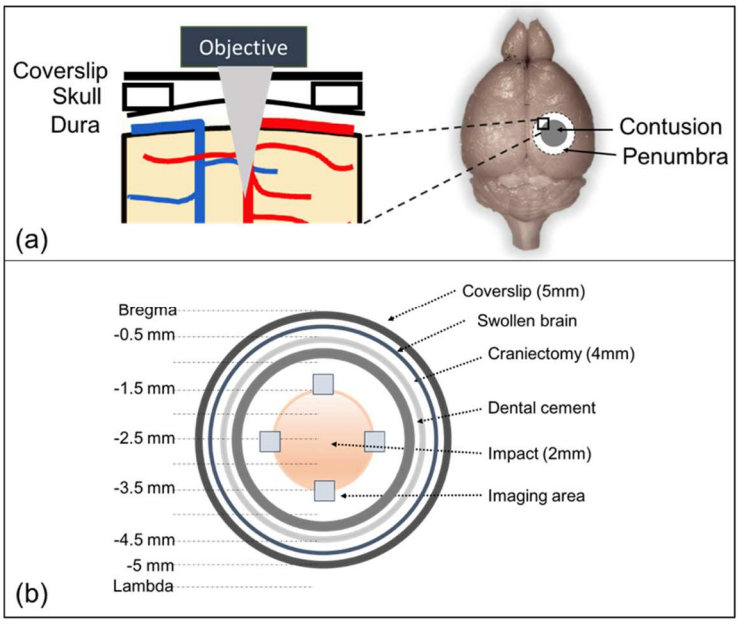

Figure 4.2: The experimental setup for two-photon microscopy imaging. (a) Sagittal view of the entire setup. (b) Cross sectional view of the location of imaging region with respect to the contusion and penumbra region. Transgenic (CX3CR1-EGFP) female and male mice were used for this study. After a craniectomy (4 mm) and impact (2 mm), a glass coverslip of 5 mm was placed on top of the swollen brain tissue and was secured with dental cement. A water-immersion objective lens was used and the anesthetized animal was secured on stereotaxic stage for two-photon imaging.

4.2.11 Two-photon microscopy NP extravasation measurement *in vivo*:

Two-photon microscope from Olympus (number) was used to image NP extravasation after TBI in anesthetized transgenic female and male mice. After placing the cranial window, water immersion 25X objective lens (NA=1.05) was used to image NPs filled in the cerebral microvessels and diffuse NP signal displaying the NP extravasation outside of the blood vessels. 12 bit images of 512 X 512 pixels (0.509 X 0.509 mm in x-y plane) were obtained. We used galvano scanner with one-way scan direction and sampling speed of 4.0 us/pixel. The excitation wavelength of 920 nm was used for red channel and green channel with ~15% laser transmissivity.

4.2.12 Statistics

Statistical analyses were conducted in GraphPad Prism 5.0 (GraphPad Software, Inc., La Jolla CA). Analysis of total positive pixels in ipsilateral and contralateral region for HRP and number of accumulated NP at different time points was conducted using ordinary two-way ANOVA. Furthermore, two sets of pairwise analysis were conducted using Bonferroni's multiple comparison tests. The first pairwise analysis was for the hemispheres - ipsilateral and contralateral. The second pairwise analysis was conducted for the sex - female and male cohorts.

4.3 Results

4.3.1 Horseradish peroxidase (HRP) extravasation

Controlled cortical impact (CCI) was used to induce focal TBI in mice. The impact to the

frontoparietal cortex generates a cortical lesion ipsilateral to the impact and leaving the contralateral hemisphere uninjured. The BBB integrity was evaluated using a well-established BBB permeability marker, horseradish peroxidase (HRP) [29,167,226]. For each cohort, HRP was injected 10 mins prior to sacrifice. Representative images of the ipsilateral and contralateral hemispheres are shown in Figure 4.3. The extravasation of HRP at all the time points was restricted to the primary injury region.

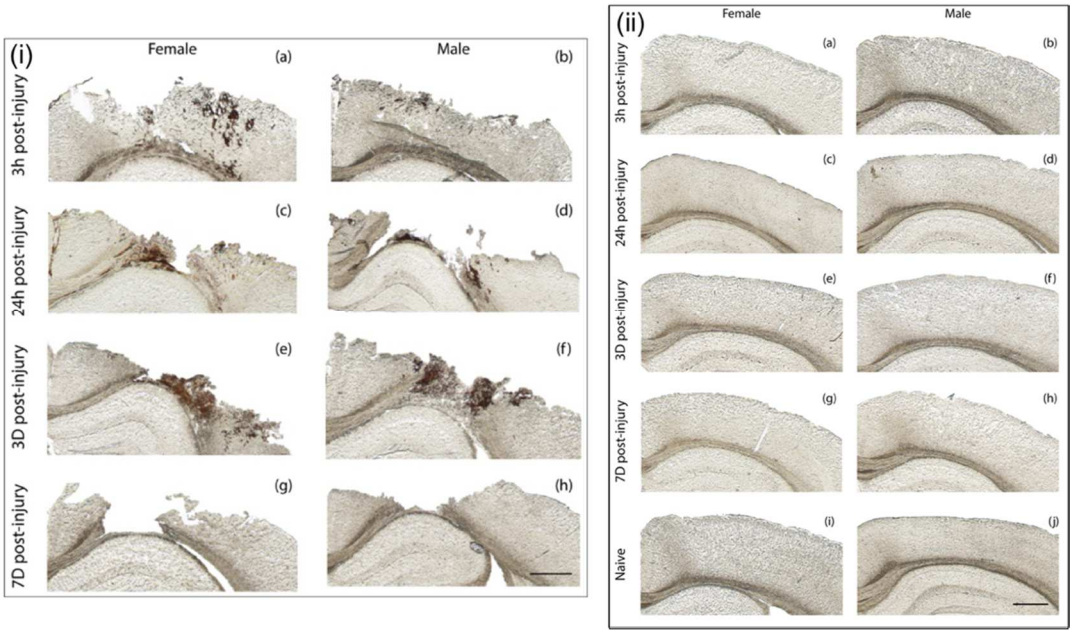

Figure 4.3: Representative images of HRP staining after TBI: (i) Ipsilateral hemisphere: HRP extravasation at 3h ((a)-(b)), 24h ((c)-(d)), 3d ((e)-(f)) and 7d ((g)-(h)) post-CCI. (ii) Contralateral hemisphere: HRP staining at 3h ((a)-(b)), 24h ((c)-(d)), 3d ((e)-(f)), 7d ((g)-(h)) post-CCI and naïve ((i)-(j)). The first column for each panel shows the HRP response in female cohort and the second column in males. Scale bar=1mm.

4.3.2 Quantification of HRP stain: Analysis of HRP extravasation across different time points

We found that both female, Figure 4.4(a) and males cohorts, Figure 4.4(b) displayed significantly higher HRP stain at 3h, 24h, and 3d post-injury compared to their respective contralateral hemispheres and to the 7d ipsilateral hemisphere. In contrast to the females, males

displayed significantly higher (~150% increase) HRP stain at 3h and 3d ipsilateral compared to 24h ipsilateral hemisphere shown in Figure 4.4(b).

Female cohort:

Among the female cohort the HRP extravasation was significantly dependent on hemisphere ($p<0.0001$) and time points ($p=0.001$), Figure 4.4(a). Significant difference at 3h ($p=0.0002$), 24h ($p<0.00001$), 3d ($p=0.0003$) and no significance for 7d ($p>0.999$) was observed compared to their respective contralateral hemisphere. Furthermore, there was significantly higher HRP extravasation in the female group at 3h ($p<0.0001$), 24h ($p<0.0001$) and 3d ($p=0.0005$) ipsilateral hemisphere compared to that of 7d. No significance was observed between 3h, 24h and 3d ipsilateral hemispheres ($p>0.33$).

Male cohort:

HRP extravasation in male mice was significantly dependent on hemisphere ($p<0.0001$) and time points ($p<0.0001$), Figure 4.4(b). Significant difference at 3h ($p<0.0001$), 24h ($p=0.0148$), 3d ($p<0.0001$) and no significance for 7d ($p>0.999$) was observed compared to their respective contralateral hemisphere. We report that HRP extravasation was significantly (more than ~200%) higher at 3h ($p<0.0001$) compared to 24h and 7d ipsilateral hemisphere. At 24h post-injury, HRP extravasation was only different from 7d ($p<0.0001$) and not any other time point. The second wave of HRP extravasation peak was seen in 3d post-injury, that was significantly (more than ~150%) higher compared to 24h ($p<0.0001$) and 7d ($p=0.0178$).

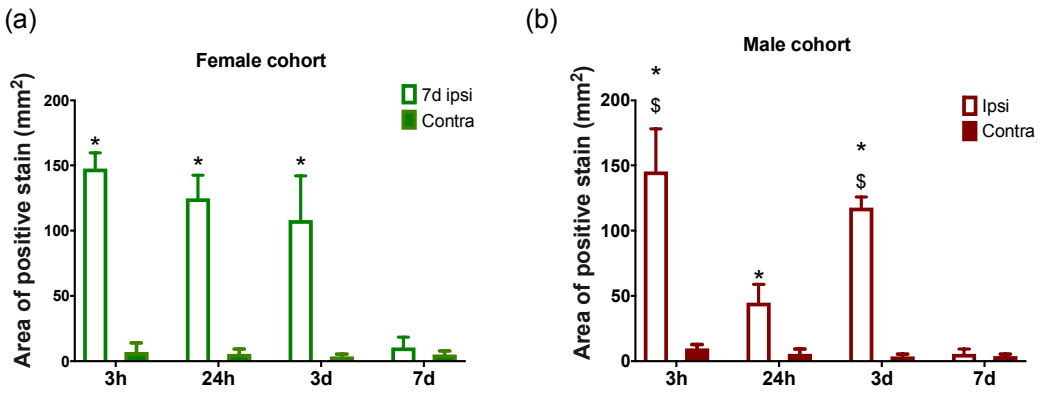

Figure 4.4: Quantification of HRP stain across different time points: Extravasation of HRP in female cohort (a) and male cohort (b) at different time points post-injury. *p<0.05 compared to their respective contralateral hemisphere and 7d ipsilateral hemisphere, two-way ANOVA, Bonferroni's multiple comparisons. $p<0.05 compared to the 24h male ipsilateral hemisphere, two-way ANOVA, Tukey's multiple comparisons. Error bars represent standard error of mean. n=2, for 3h cohort and n=4, for all other time points.

4.3.2 Quantification of HRP stain: Analysis of HRP extravasation between female and male cohort

We analyzed the sex difference in HRP extravasation via the BBB breach at different time points after TBI. We found a significant difference between ipsilateral and contralateral for both female and male cohorts at 3h post-injury. However, there were no sex differences in HRP stain at 3h post-injury. At 24h post-injury, the females displayed significantly higher HRP extravasation compared to their contralateral, whereas the males were not. We found sex difference at 24h post-injury where the females displayed significant (~180%) higher HRP stain compared to their male counterpart. At 3d post-injury, we found significantly higher HRP extravasation in the ipsilateral hemispheres for both female and male cohorts but no sex difference.

3h post-injury: The HRP extravasation at 3h post-injury displayed significant difference (p=0.002) between the hemispheres, Figure 4.5(a). Specifically, significantly increase HRP stain was seen in the ipsilateral compared to contralateral in females (p=0.011) and male (p=0.014). There was no significance for sex difference.

24h post-injury: HRP extravasation at 24h post-injury displayed significant difference between the hemispheres (p<0.0001) and sex (p=0.004), Figure 4.5(b). We report a significant difference for female cohort (p<0.0001) but not for males (p=0.082). Furthermore, there was significantly (~180%) increase HRP stain in the female ipsilateral hemisphere compared to that of males (p=0.001).

3d post-injury: The HRP stain at 3d post-injury displayed a significant difference between the hemispheres ($p<0.0001$), Figure 4.5(c). The ipsilateral hemisphere displayed higher HRP stain compared to contralateral for the female cohort ($p=0.003$) and for males ($p=0.001$). There was no significance for sex difference.

7d post-injury: Analysis for HRP extravasation at 7d post-injury did not show any significance for the hemispheres nor for sex, Figure 4.5(d).

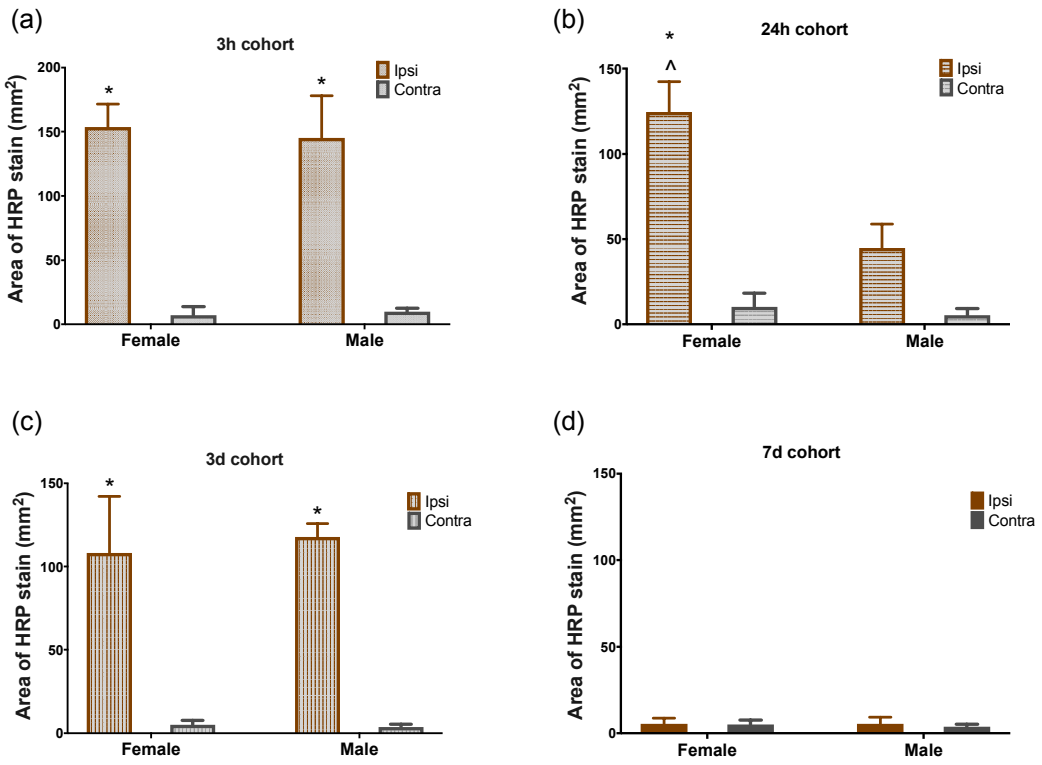

Figure 4.5: Quantification of HRP stain between female and males post-injury: Extravasation of HRP at 3h (a), 24h (b), 3d (c) and 7d (d) post-injury. *$p<0.05$ compared to their respective contralateral hemisphere, two-way ANOVA, Bonferroni's multiple comparisons. ^$p<0.05$ compared to the male ipsilateral hemisphere, two-way ANOVA, Bonferroni's multiple comparisons. Error bars represent standard error of mean. n=2, for 3h cohort and n=4, for all other time points.

4.3.3 Nanoparticle accumulation after CCI

For each cohort, PEGylated polystyrene NP (40 nm, 48.2±11 nm) was injected 3 hours prior to sacrifice. NP accumulation was quantified at the middle region of the injury (~-1.65 mm bregma) via epifluorescent microscopy. Representative images of the ipsilateral and contralateral hemispheres are shown in Fig 4.6 and Fig 4.7, respectively. Interestingly, we observed significant peak NP accumulating at 3h followed by a smaller peak at 24h and 3d post-injury within the injury penumbra whereas no significant accumulation at 7d post-injury.

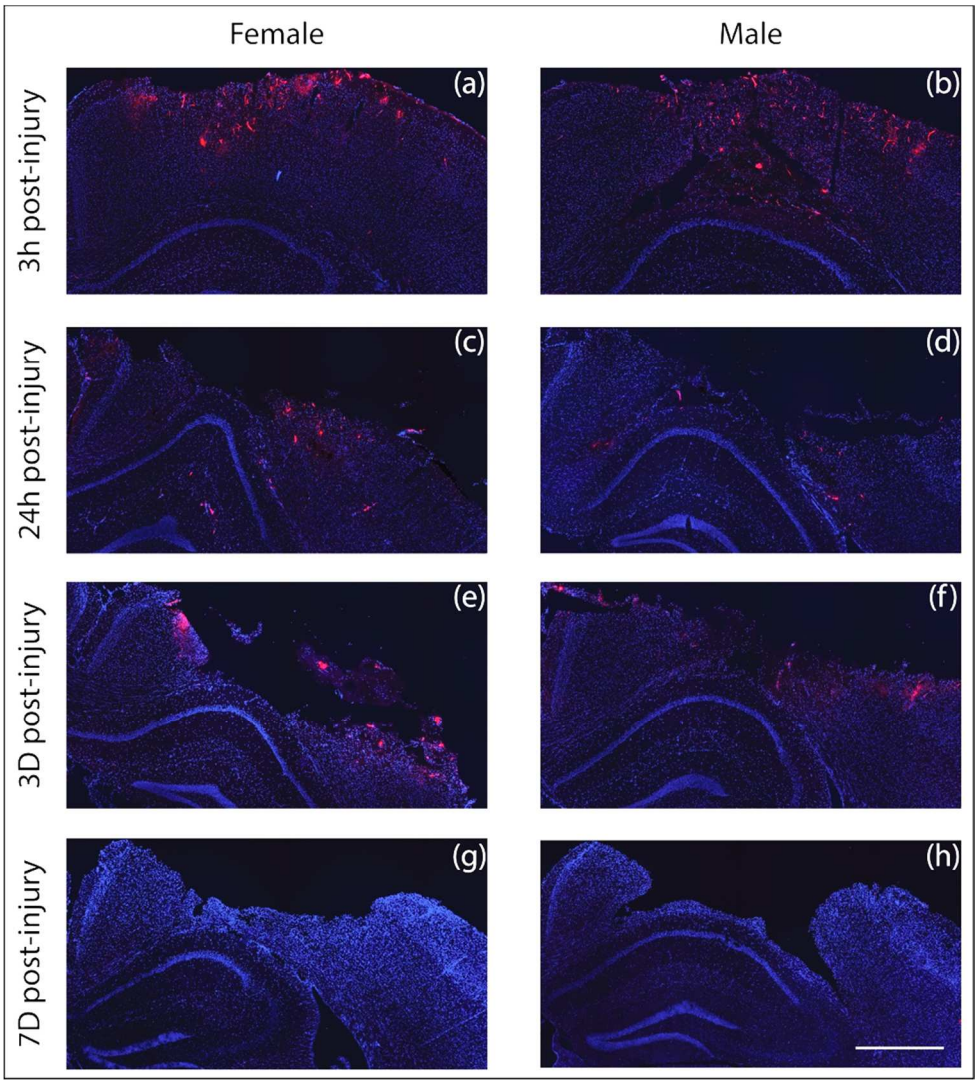

Figure 4.6: NP accumulation after TBI in ipsilateral hemisphere: Representative images of NP extravasation at 3h ((a)-(b)), 24h ((c)-(d)), 3d ((e)-(f)) and 7 days ((g)-(h)) post-CCI. The first

column shows the HRP response in female cohort and the second column in males. Scale bar=750μm.

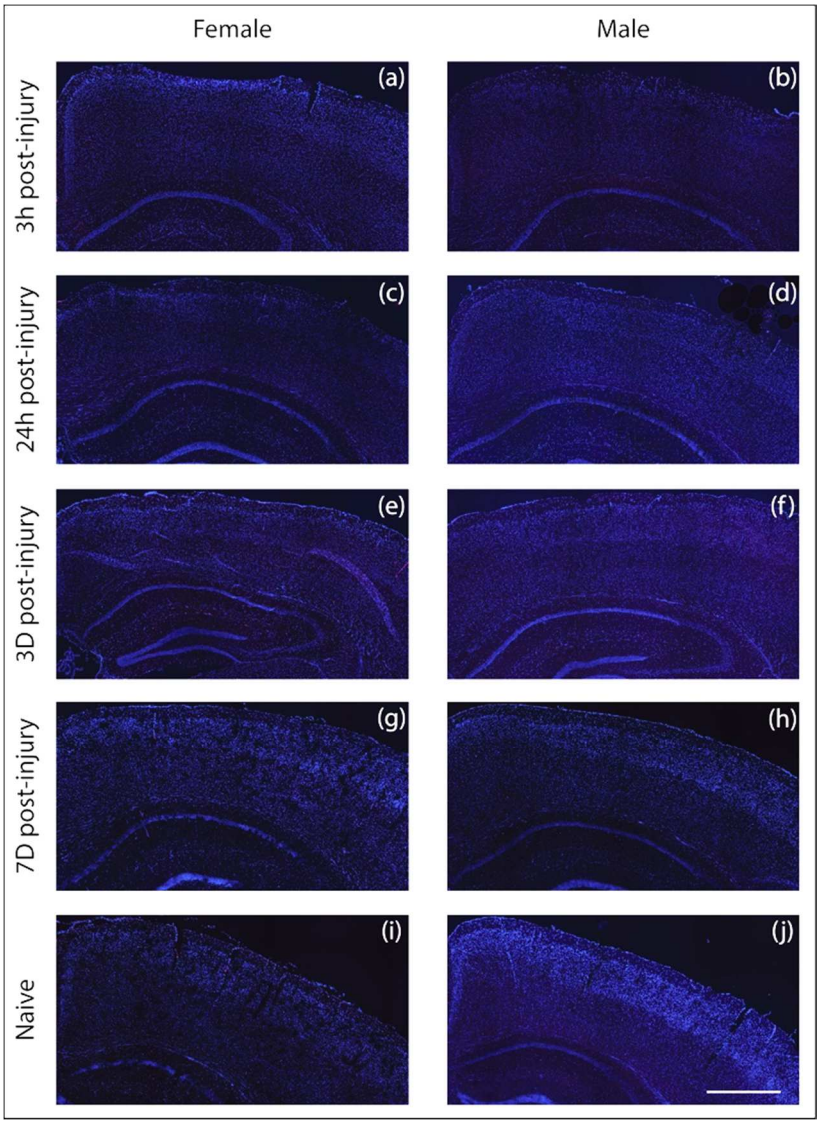

Figure 4.7: NP accumulation after TBI in contralateral hemisphere: Representative images of NP accumulation at 3h ((a)-(b)), 24h ((c)-(d)), 3d ((e)-(f)), 7 days ((g)-(h)) post-CCI and naïve ((i)-(j)). The first column shows the HRP response in female cohort and the second column in males. Scale bar=750μm.

4.3.4 Nanoparticle accumulation after CCI: Analysis of NP accumulation across different time points

Overall, in female cohorts, we found significantly higher NP accumulation at 3h, 24h, and 3d post-injury compared to their respective contralateral hemispheres and to the 7d ipsilateral hemisphere. No significant NP accumulation was observed at 7d. In contrast, the male cohorts showed significantly higher NP accumulation at 3h, and 3d post-injury compared to contralateral hemispheres and to the 7d ipsilateral hemisphere. At 24h post-injury, males did not show significant NP accumulation compared to contralateral. Moreover, 3h male cohorts displayed significantly higher NP accumulation compared to the 24h ipsilateral hemisphere.

Female cohort:

NP accumulation in female mice across different time points showed significance in the hemisphere ($p<0.0001$) and time points ($p<0.0001$), Figure 4.8(a). We report significantly higher NP accumulation at 3h ($p<0.0001$), 24h (0.00007), 3d ($p=0.0032$) and not significant for 7d ($p>0.999$) compared to their respective contralateral hemispheres. Furthermore, there was significantly higher NP accumulation in the female 3h ipsilateral hemisphere ($p<0.0001$, more than 160% increase) compared to that of 24h, 3d, and 7d. There was also a significant difference in 24h ($p=0.0009$) and 3d ($p=0.0026$) ipsilateral hemisphere compared to 7d. No significance was observed between 24h ipsilateral compared to that of 3d ($p=0.9702$).

Male cohort:

NP accumulation in male mice was significantly dependent on hemisphere ($p<0.0001$) and time points ($p<0.0001$), Figure 4.8(b). We report a significantly increased NP accumulation at 3h ($p<0.0001$), 3d ($p=0.0084$) and not significant for 24h ($p=0.0684$) and 7d ($p>0.999$) compared to their respective contralateral hemisphere. Furthermore, there was significantly higher NP accumulation in the male 3h (more than 500% increase) ($p<0.0001$) compared to 24h, 3d and 7d in the ipsilateral. There was also significant difference in 3d ($p=0.0082$) ipsilateral hemisphere compared to 7d. No significance was observed between 24h ipsilateral compared to that of 3d ($p=0.7743$) and 7d ($p=0.0672$).

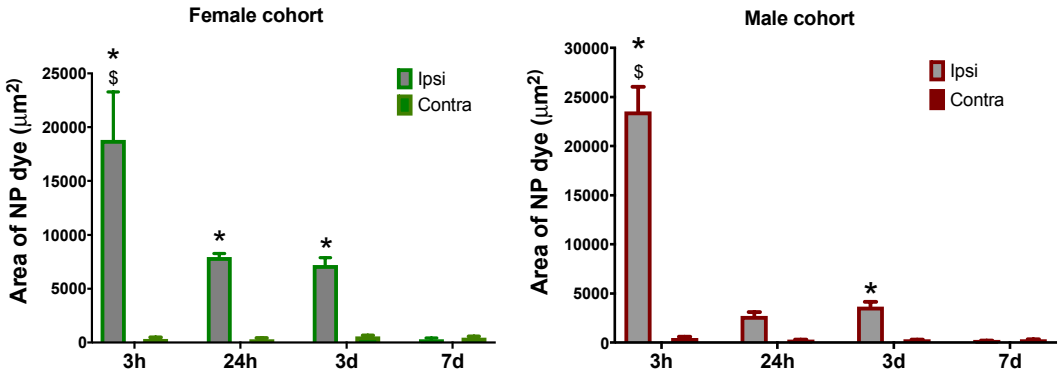

Figure 4.8: NP accumulation across different time points after injury: Accumulation of NP in the female cohort (a) and male cohort (b) at different time points post-injury. *p<0.05 compared to their respective contralateral hemisphere and 7d ipsilateral, two-way ANOVA, Bonferroni's multiple comparisons. $p<0.05 compared to the 24h male ipsilateral hemisphere, two-way ANOVA, Tukey's multiple comparisons. Error bars represent standard error of mean. n=3, for 3h cohort and n=4, for all other time points.

4.3.5 Nanoparticle accumulation after CCI: Analysis of NP accumulation between female and male cohort

To summarize our findings (Figure 4.9), we found a significant difference in NP accumulation between ipsilateral and contralateral for both female and male cohorts at 3h post-injury. However, there were no sex differences in NP accumulation at 3h post-injury. At 24h and 3d post-injury, the females and males displayed significantly higher NP accumulation compared to their contralateral. Interestingly, found sex dependence in the extent of NP accumulation at both 24h and 3d post-injury was observed where the females displayed significant ~170% and ~95% higher, respectively, compared to their male counterpart. At 7d post-injury, we found no significance in NP accumulation for hemispheres/sex.

3h post-injury: NP accumulation at 3h post-injury displayed significant difference ($p<0.001$) between the hemispheres Figure 4.9(a). Particularly, NP accumulation in the ipsilateral hemisphere was significantly increased for female ($p=0.0002$) and male ($p<0.0001$) compared to

their respective contralateral tissue. The sex of the animal did not play a significant role on NP accumulation at 3h post-injury.

24h post-injury: NP accumulation at 24h post-injury displayed a significant difference between the hemispheres ($p<0.0001$) and sex ($p=0.0001$) Figure 4.9(b). We report a significant difference between the ipsilateral and contralateral hemisphere for the female cohort ($p<0.0001$) and for males ($p=0.002$). Furthermore, there was significantly (~170%) higher NP accumulation in the female ipsilateral hemisphere compared to that of males ($p<0.0001$).

3d post-injury: At 3d post-injury, NP accumulation displayed a significant difference between the hemispheres ($p<0.0001$) and the sex ($p=0.0007$) Figure 4.9(c). There was a significant difference between the ipsilateral and contralateral hemisphere for the female cohort ($p=0.003$) and for males ($p=0.001$). Furthermore, there was significantly (~95%) higher NP accumulation in the female ipsilateral hemisphere compared to that of males ($p=0.0001$).

7d post-injury: NP accumulation at 7d post-injury did not show any significance for the hemispheres ($p=0.175$) nor for sex ($p=0.35$) Figure 4.9(d).

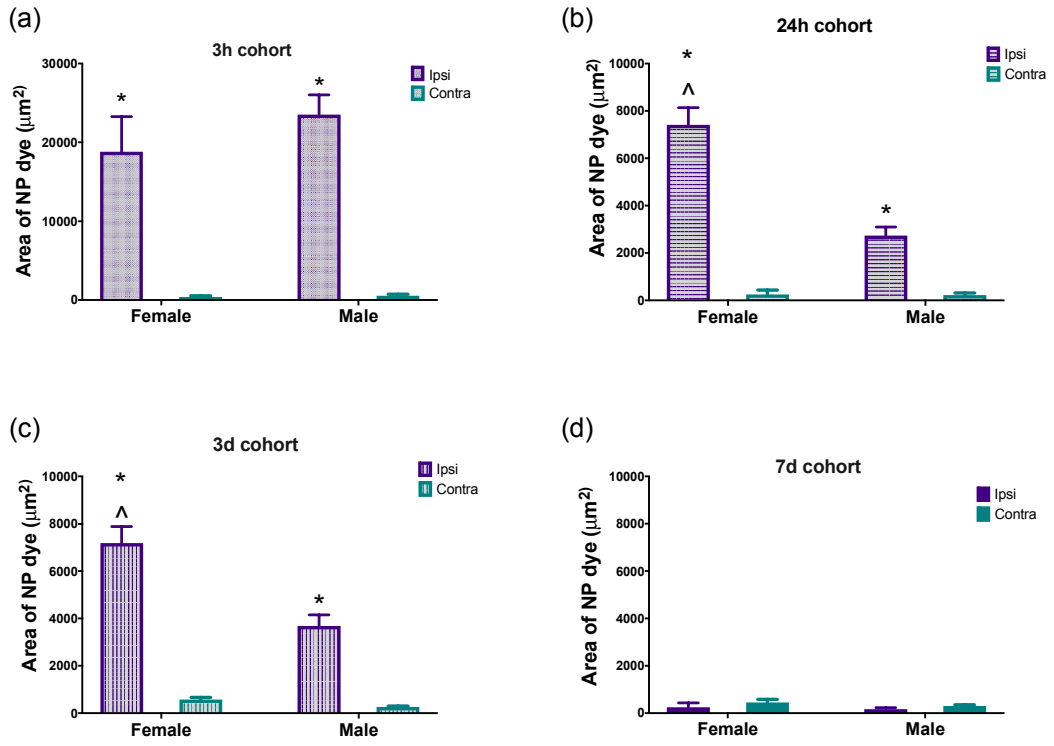

Figure 4.9: Quantification of NP accumulation between female and male post-injury: Accumulation of 40 nm NP at 3h (a), 24h (b), 3d (c) and 7d (d) post-injury. *p<0.05 compared to their respective contralateral hemisphere, two-way ANOVA, Bonferroni's multiple comparisons. ^p<0.05 compared to the male ipsilateral hemisphere, two-way ANOVA, Bonferroni's multiple comparison. Error bars represent standard error of mean. n=3, for 3h cohort and n=4, for all other time points.

4.3.6 Two-photon microscopy imaging

We used two-photon microscopy to confirm our findings of NP accumulation outside of the vasculature and in the brain parenchyma. In Figure 4.10, the images show NP (in red) and the microglia (green) residing in the brain parenchyma. In the naïve animals, we observed intact large and small blood vessels (no NP extravasation) and in close proximity to healthy ramified microglia. In both female and male mice, at 3h, 24h, and 3d there was diffused signal around the blood vessels demonstrating NP extravasation in the brain parenchyma. At 24h and 3d post-injury we observed activated microglial with amoeboid morphology.

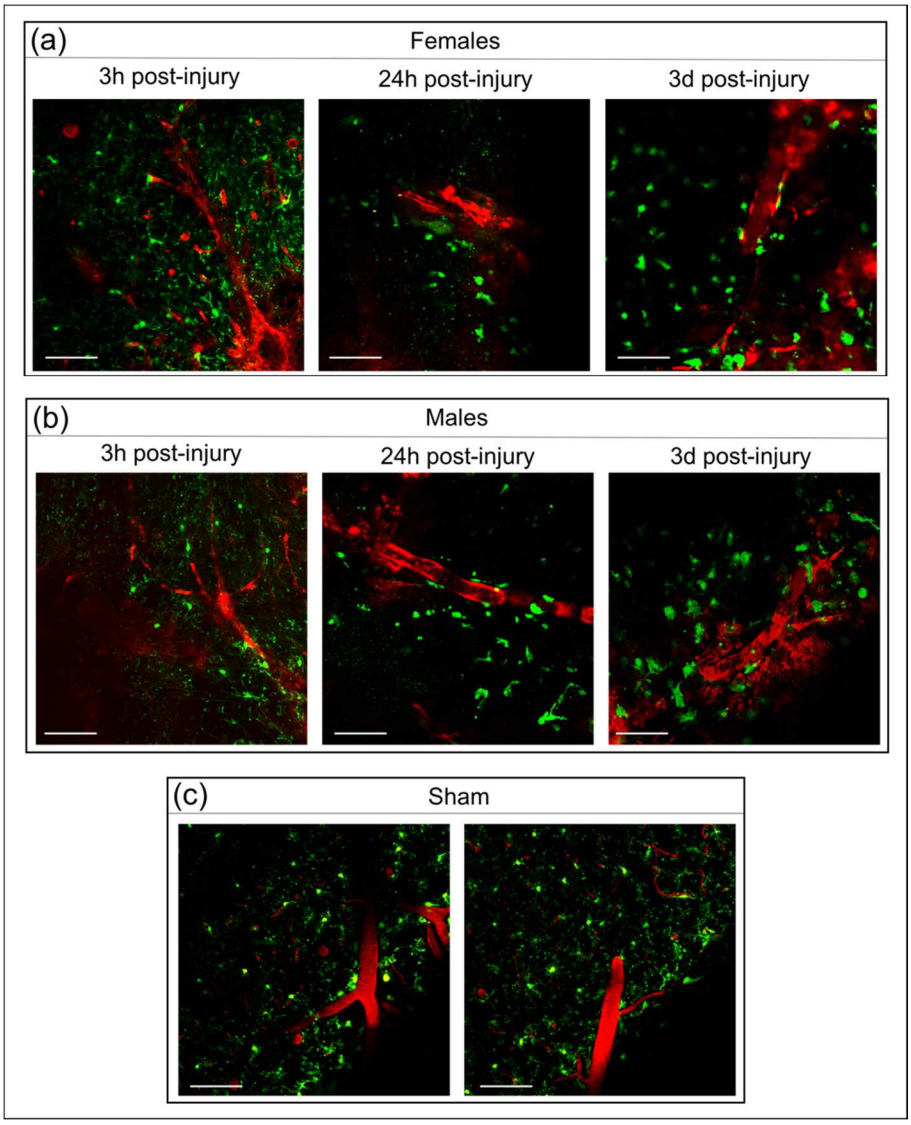

Figure 4.10: Two-photon microscopy in vivo imaging of CCI induced transgenic animals. A water-immersion objective lens was used and the anesthetized animal was secured on stereotaxic stage for two-photon imaging. Animals were injected with 40 nm NPs 3h before imaging. NPs are in red and CX3CR1 microglia in green. Representative images of NP extravasation in (a) females and (b) males at 3h, 24h and 3d post-CCI. Representative images of the male sham group are displayed in (c). Scale bar=100um.

There are ongoing analyses to further validate our two-photon microscopy data. The amount of NP extravasation into the brain parenchyma will be quantified by analyzing the intensity of diffused signal around the vasculature. The quantification will be completed for each sex and at different time points post-injury. We will use the sham group as a control to compare the extent of NP extravasation. Overall, these studies provide support regarding the NP accumulation and extravasation into the parenchyma space and help improve our understanding of the NP delivery via BBB breakdown.

4.4 Discussion & Conclusions

The blood-brain barrier (BBB) is a unique property of the brain that regulates molecular transport from the bloodstream to the brain, which restricts certain molecules in the bloodstream from penetrating the brain parenchyma. Previous reports have suggested that sex of the animal may play an important role in BBB disruption in neurological diseases[40,44]. Although the BBB disruption after TBI is detrimental, such opening may provide an opportunity for delivery of drugs and therapeutics via NPs. To fully utilize the window of opportunity of BBB opening after TBI, a complete assessment the temporal resolution and the sex dependence for NP accumulation via the BBB was warranted. In this study, we directly address the critical gap using focal TBI mouse model and PEGylated polystyrene NPs. The key insights include: (1) significant NP accumulation occurred at 3h, 24h and 3d post-injury after focal brain injury regardless of the sex, (2) contrary to our hypothesis, NP accumulation was significantly higher in female mice at 24h and 3d post-injury compared to age-matched male counterparts.

Horseradish peroxidase (HRP) is a large molecule tracer for BBB dysfunction. After focal brain injury, we observed significant HRP extravasation at 3h, 24h and 3d post-injury, indicating a breach in BBB at these time points. Specifically, males had significantly increased HRP at 3h and 3d compared to 24h. This observation is supported by previous seminal studies showing a biphasic BBB disruption after CCI, with the first peak at the acute time point (~4h) and the second peak at 3d[149,227]. Majority of the animal studies in TBI and BBB distribution have used male animals[149,151,167,190,221,222]. To the best of our knowledge, this is first report showing that

the temporal progression and the degree of BBB disruption after TBI is sex-dependent. Specifically, we found that female mice did not show a biphasic trend similar to that reported and observed in males. We establish that the females had a consistent and significant HRP extravasation at 3h, 24h and 3d compared to the respective contralateral hemisphere and did not show decrease in BBB opening at 24h (as seen in males). Moreover, the degree of BBB opening, in terms of the extent of HRP extravasation exhibited significantly higher (~50%) HRP stain at 24h post-injury in females compared to males.

NP accumulation displayed a peak accumulation at 3h post-injury in both sexes. The acute (3h) BBB disruption can largely be associated with the mechanical disruption of the vessels due to the primary impact. CCI consistently produces major cortical damage including tearing of the dura, parenchyma and severe vascular disruption directly at the site of impact[27,150]. No difference in HRP or NP accumulation at 3h post-injury was observed, leading to the notion that this acute BBB breakdown is largely associated with the mechanical disruption. Later time points at 24h and 3d post-injury, there was not only significant NP accumulation in both females and males but contrary to our hypothesis, we observed sex dependence in the extent of NP accumulation. Specifically, at 24h and 3d, the females displayed a robust NP accumulation (~40% more) significantly higher than male counterpart. Our current findings are largely consistent with our previous report[2], where we found peak accumulation at 1h and reduced over time post-CCI. It should be noted that the NP accumulation is critically dependent on the circulation time. A variance in NP accumulation is at 24h post-injury was observed between our current study (significant NP accumulation at 24h in males) and the previous one (no significance at 24h). The longer circulation time in this study (3h vs 1h) may have contributed to the significance observed at 24h. The longer circulation time in this study was selected to accommodate the two-photon microscopy study. Taken together, we demonstrated the feasibility of NP delivery to the injured brain region at 3h, 24h and 3d post TBI.

The NP accumulation at 3d correlated with the BBB disruption and the extent of HRP stain. This BBB disruption at the delayed time point is mainly associated with the secondary injury that follows the primary injury, although the mechanism(s) have not been clearly

elucidated[15,21]. Evidence suggests increased paracellular permeability due to disruption of tight junction complexes and integrity of the basement membrane as a dominant mechanism[15,21],[15,31]. Tight junction protein complexes situated between endothelial cells control BBB permeability by limiting paracellular diffusion; key tight junction proteins include junctional adhesion molecules, occludin and claudins[32]. Oxidative stress due to ROS and free radical production after brain trauma alter the critical organization of tight junctions proteins at the BBB resulting in increased paracellular leakage[15,33]. Additionally, the disruption of vasculature and brain tissue caused by the primary impact, triggers the coagulation cascade and causes oxidative stress with increased production of proinflammatory mediators[15,228]. These pathophysiological processes lead to activation of the glial cells and alter their interaction with the cerebrovascular endothelial cells and may contribute to BBB dysfunction[15,21],[34,35].

The key finding of our study is the sex dependence in the time course and the extent of NP accumulation at 24h and 3d post-CCI that was contrary to our proposed hypothesis. We observed that the females showed NP accumulation with comparable peaks at both 24h and 3d. In contrast, the males displayed modest NP accumulation at 24h with a subsequent increased peak at 3d post-CCI. Moreover, the extent of NP accumulation at 24h and 3d was significantly higher in females compared to males. Our observation is contrary to our hypothesis of expecting a higher level of BBB dysfunction and thus NP accumulation in males compared to females. However, robust BBB permeability in females compared to males reflects the findings of previous BBB breakdown studies in the epileptic mouse model[40,44]. We have ongoing studies to investigate the neuroinflammatory response for microglia/macrophage and astrocyte response after injury. These studies will provide more insights into the role of sex differences in neuroinflammation and if there is any pertinent role of neuroinflammation directly influencing BBB breakdown at different time points post-injury.

Many studies have reported sex differences in brain structure and metabolism. For instance, females have higher cerebral blood flow compared to males[36] and sex differences in brain metabolism have been reported where females have higher whole brain glucose metabolic rates compared to males[229]. Literature suggests sexual dimorphisms of the

brain[212,214,230],[37,38,215,231] or sex hormones[48,232,233] or in combination could play a role in regulations of such sex differences. One hypothesis for robust NP accumulation in females as compared to males is due to the potential neuroanatomical sex differences and variable physiological response after injury. Many of animal and human studies have demonstrated normal sexual dimorphisms of the brain such as cerebrum is larger in male than females and females show higher cell packing density in some regions of the brain[37,38,215,231]. Studies in corpus callosum have shown that female mean axonal diameters are smaller and thinner than that of males in rats[234,235] and humans[236]. A recent *in vitro* study by Dolle and group[230] showed that female axonal injury was accompanied by higher calcium influx and thus more susceptible to injury compared to male axons. These studies demonstrated that the female and males may have a different physiological response to injury due to variations in the neuroanatomy. Therefore, it is plausible that females might show an overall greater structural and physiological damage after trauma leading to a robust BBB breakdown compared to the males.

Another or combinatory hypothesis is that sex hormones such as estrogen may influence the regulation of BBB. The delivery of exogenous estrogen is known to be neuroprotective and to reduce BBB breakdown[237-240], yet these positive outcomes significantly depend on the plasma estradiol level[241] after brain injury. Harukuni and group[241] show the deleterious outcome of estrogen at normal physiologic range presenting a shift from the neuroprotective role (via exogenous estrogen) to possible pro-excitatory effect after brain injury. Additionally, estrogen is known to enhance nitric oxide (NO) production by endothelial NO synthase (eNOS) [232]. Previous studies have established that NO can modulate the BBB permeability[242,243] and the effect of NO on BBB permeability is sex dependent[244,245]. Therefore, the normal estrogen level in female mice (random estrous cycle) could lead to pro-excitatory effect and enhanced NO leading to higher BBB permeability compared to the male cohort. Taken together, female mice may have a variable neuroanatomical structure with greater physiological damage and/or the estrous cycle could lead to pro-excitatory effect and modulation of neurotransmitters such as NO contributing to increased BBB permeability post-injury with robust NP accumulation compared to males.

In conclusion, in this work, we have demonstrated that female mice exhibit a robust NP accumulation at the sub-acute time point after moderate-severe TBI compared to male mice, primarily due to sex differences in BBB permeability. However, at 7d post-injury, both females and males did not display any BBB breach. Future studies to elucidate the underlying hormonal and sex-related differences for variable BBB permeability are warranted. The BBB permeability after TBI is a complex phenomenon and the delineation of the time course of permeability become extremely important. As such, the BBB permeability at acute and sub-acute time points in females and males will provide the opportunity to more accurately tailor time-dependent therapeutics via NPs.

4.5 Acknowledgements

This work was funded by the Flinn Foundation (SES, VDK, JL, PDA) and NIH (1DP2HD084067). Authors would like to thank Dr. Shenfeng Qiu, UofA-COM, for assistance with the two-photon microscopy and providing the stereotaxic frame/animal mount for imaging. Authors would like to thank Jordan Todd and Kyle Offenbacher for their assistance with the animal handling. We would like to thank Katherine R. Giordano for breeding/maintaining the transgenic animal colonies. Also, we would like to thank Chen Wu for assistance with animals for two-photon microscopy and perfusions.

CHAPTER 5

CONCLUSIONS & FUTURE DIRECTIONS

5.1 Summary of Findings

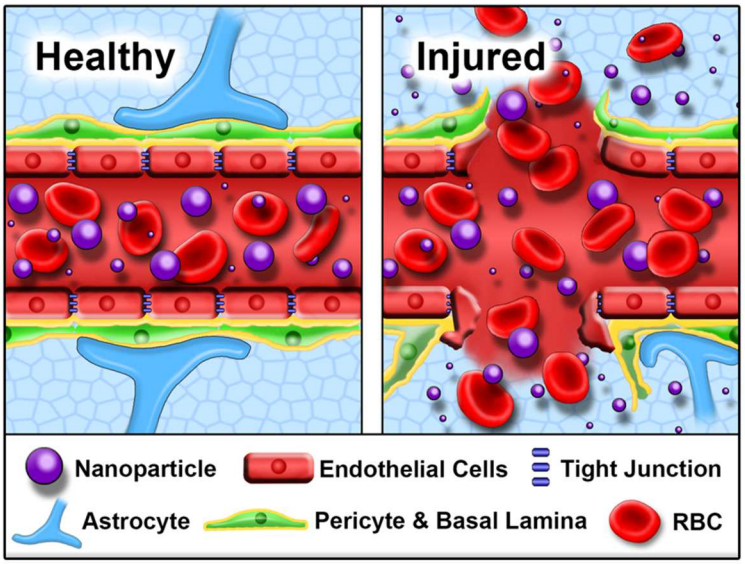

Figure 5.1 A graphical illustration of nanoparticle accumulation/extravasation after brain trauma. Different sizes of nanoparticles can be delivered to the brain tissue after injury in case of blood-brain-barrier breach after injury.

5.1.1 Aim 1: Temporal assessment of nanoparticle accumulation after experimental focal brain injury: Effect of particle size - controlled cortical impact (CCI).

We determined that nanoparticles (NPs) passively accumulate within the injury penumbra following focal brain injury due to the leaky vasculature. Polystyrene PEGyated NPs of different sizes (20 nm, 40 nm, 100 nm, and 500 nm) accumulate near the injury region after CCI injury in mice. Furthermore, maximal accumulation for all NPs was observed at 1 h post-injury. We identified an inverse relationship between the NP size and their accumulation at different time points post-injury. The smaller NPs, 20 nm and 40 nm, had prolonged accumulation (until 13 h) post-injury compared to larger NPs, 100 nm and 500 nm, had significant accumulation until 6 h post-injury. NP accumulation was not only influenced by the NP size and time after injury but also

varied spatially within the brain tissue cortex. The anterior and middle regions of the injured tissue had a maximal accumulation of NPs compared to the posterior region 1h after brain injury.

5.1.2 Aim 2: Blood-brain barrier disruption dictates nanoparticle accumulation following experimental diffuse brain injury – fluid percussion and mild closed head injury.

We determined that passive accumulation of NPs at the cortex (proximal to injury hub) due to BBB breach only in the fluid percussion injury (FPI). We report that mild closed head injury (mCHI) and repetitive mCHI did not show any NP accumulation 1h post-final impact. Furthermore, in FPI study we observed 20nm, 40nm, 100nm and 500nm NPs accumulate in the primary somatosensory and primary and secondary motor cortex sustaining a diffuse TBI. Moreover, maximal NP accumulation occurred at 3h post-FPI for all NP sizes. We determined that there was a significant correlation between blood-brain barrier permeability marker (HRP) staining and NP accumulation in the cortex after midline-FPI.

5.1.3 Aim 3: Investigate NPs delivery: sub-acute time point and sex dependence after focal brain injury.

To fully utilize the window of opportunity of BBB opening after TBI, thorough assessment of the temporal resolution and the sex dependence for NP accumulation via the BBB is necessary. In this study, we directly address this critical gap using focal TBI mouse model and PEGylated polystyrene NPs. The key insights include: (1) Significant NP accumulation occurred at 3h, 24h and 3d post-injury after focal brain injury in both female and male cohorts. (2) NP accumulation was significantly higher in female mice at 24h and 3d post-injury compared to age-matched male counterparts.

5.2 Discussion and Future Studies

Effective diagnostic and therapeutic options available for brain injuries are limited by the complex brain injury. Brain trauma may lead to BBB opening and provide opportunities for therapeutic delivery via NPs. The approaches for therapeutic interventions via NP delivery are aimed at salvaging the pericontusional/penumbra region for possible neuroprotection and

neurovascular unit preservation. However, a systemic evaluation of the BBB therapeutic window for the NP strategies in multiple TBI animal models and considering both the sexes had not been previously performed. Indeed, we found striking differences in the dynamics of the NP accumulation across different TBI models and sexes. In focal injury model, we clearly demonstrated that higher levels of NP accumulation occurred immediately after injury and smaller NPs showed prolonged accumulation as compared to larger NPs. The second model we investigated was mild closed head injury model (mCHI) and we did not observe any HRP or NP accumulation at 1h after single impact mCHI or after 5 consecutive impacts in the repetitive mCHI model. In contrast, the midline-FPI cohort displayed a peak accumulation of the NPs at 3h post-injury compared to 1h and 6h group. Furthermore, we report significantly increased NP accumulation at 3h, 24h and 3d in both females and males after focal brain injury. Interestingly, we observed significantly higher NP accumulation in females compared to males at 24h and 3d post-CCI. In sum, we have demonstrated that the dynamics of NP delivery depends on the injury phenotype and sex predominantly attributed to BBB breach.

In this study, we have demonstrated the key factors that contribute to successful NP delivery after brain injury. These factors are (1) NP design/size (ranging from 20 -500nm). (2) NP delivery time with respect to BBB breakdown, (3) mechanism of injury: focal/diffuse and injury phenotype, and (4) sex (female vs male). Due to the breadth of these study, we have yet to probe additional parameters that contribute to the NP delivery. These include NP design characteristics, such as PEG density, NP biodistribution, mechanism of NP accumulation in the injured region, and mechanism of sexual dimorphism/sex hormones in NP delivery after TBI. Therefore, future studies will need to explore these parameters/mechanisms for better understanding and utilization of NP delivery following TBI.

To study the dynamics of NP delivery, we used a PEG-modified surface with a spherical shape and slightly anionic NP with varying sizes. For systemic NP delivery system to achieve the desired benefits, the residence time in the bloodstream must be long enough for the NP to reach or recognize its site of action[72,74,92,110,159]. Key parameters identified to help evade

clearance mechanisms include surface modification, charge, shape, and size[88]. Since the first two studies aimed at evaluating the size and time-dependent NP accumulation after brain injury, we minimized the influence of NP parameters outside of size by PEGylating the NPs. PEGylated NPs of different sizes (20nm, 40nm, 100nm and 500nm) showed significantly reduced zeta potential and had slightly negative charge within the range of -9 to -28mV. PEGylation of the NP is known to improve blood circulation time by reducing blood clearance[92,110,117,246]. Optimal PEG coating in terms of thickness and density reduces protein adsorption and phagocytic uptake for long circulating NPs in the blood[246,247]. Moreover, previous report[248] demonstrate that NPs with a dense PEG density can penetrate brain extracellular space compared to uncoated NPs. Therefore, the precise PEG coating densities are required to be confirmed by future studies.

Therapeutic NP delivery to the brain under normal physiological conditions is largely hindered by the BBB permeability. However, a short transient window of BBB dysfunction or damage as a result of TBI pathology may provide a window of opportunity for delivery. Previous preclinical studies using molecular tracers such as Evans blue and horseradish peroxidase (estimated hydrodynamic diameter of <10nm) showed that the BBB was compromised acutely and sub-acutely post-injury that eventually resolves. Yet, the dynamic size range for NP extravasation greater than 10nm was not previously investigated. Therefore, we hypothesized that NPs (10-1000nm) will passively accumulate at the injury location after brain injury due to BBB disruption at acute and sub-acute time points post-TBI. Moreover, human TBI is a heterogeneous event and a single injury model may not fully recapitulate all the facets of the secondary injury that are observed in human TBI[51]. Besides, previous studies[49,249] indicate the role of sex difference might affect BBB breakdown after TBI and yet there have been no studies exploring this aspect. To address these limitations, we investigated the NP delivery in three different animal models of TBI and different sexes. We found that the dynamics of NP delivery was different depending on the animal model being investigated, yet, NP accumulation largely correlated with BBB disruption as evidenced by concomitant correlation with small molecule extravasation. Furthermore, females and males at 24h and 3d time points post-focal

injury showed stark differences in the amount of NP accumulation and directly correlated with the extent of BBB disruption in each sex.

In focal brain injury, we report up to 500nm size NP significantly accumulate in the injured region. Also, we found that smaller size NPs, 20nm and 40nm showed prolonged accumulation until 13h post-injury compared to larger size NPs. For the diffuse TBI (FPI) study we observed accumulation of NPs up to 500nm and did not observe any differences based on the NP size with respect to time post-injury. In the current study, we used different size of NPs (20nm, 40nm, 100nm, and 500nm) each loaded with a unique fluorescent dye such that we could inject them together and yet image them separately. As such, this approach resulted in an inability to directly compare the amount of NP dye/number of NP accumulation after injury. Therefore, future studies can be designed to address this limitation that will help inform NP size/design strategies for an improved delivery system. Moreover, we found NPs up to 500nm in size can be delivered to the brain due to BBB disruption after both focal and diffuse (FPI) injury. Although up to 500nm NPs can be intravenously delivered to the BBB breached regions, it must be noted that the extracellular space (ECS) of the brain parenchyma does impose a restriction for free penetration/diffusion through the ECS[248]. A Previous study established that the ECS is restricted by NP size and surface coating[248]. They report that densely PEG coated NP of about 100nm in size can rapidly penetrate the brain tissue compared to uncoated and/or larger size NPs[248]. Overall, these factors are critical in designing the NPs for a value-added delivery system.

Focal and diffuse brain injuries lead to a different injury phenotype due to different mechanism of injury. The acute BBB breakdown is known to be primarily caused by the mechanism of the injury and the mechanical threshold for BBB disruption may overlap with the thresholds for tissue injuries[250,251]. In focal brain injury such as CCI that produces a focal cortical mechanical injury resulting in cortical tissue damage leading to contusion[56,252]. Consequently, the location of the acute BBB breakdown region observed in our study corresponds to those gross region of cortical tissue pathologies[27,56,149,252]. The mechanical

force at the time of impact exceeds the mechanical threshold for tissue and BBB integrity leading to the damage/disruption. The BBB breakdown at the sub-acute time points after CCI occurs due to the downstream pathophysiological alterations to the BBB and overlaps with the gross cortical tissue pathology. In diffuse TBI such as midline FPI is known to produce rapid secondary axotomy within the cortex and thalamus without cell death[61,253,254]. In our study we observed BBB breakdown only in the cortical tissue specifically the primary somatosensory and motor cortex, suggesting that the physical forces required to damage axons in the cortical tissue may also lead to BBB disruption. In contrast, the mild CHI is known to produce mild astrocyte reactivity in the cortex and hippocampus[64]. However, we did not observe any BBB breach in the cortex/hippocampus or any other brain regions implying that the mechanical threshold for astrocyte damage may be lower than that of the BBB damage. Taken together, a better understanding of the BBB disruption may serve as an assessment tool presenting the regions that endured the highest deformations after brain injury. Such improved understanding can help direct non-invasive diagnosis via neuroimaging techniques and potential pharmacological interventions.

The BBB breach directly contributes to NP accumulation within the injury penumbra. Such leaky vasculature phenomenon has been defined as the enhanced permeability and retention (EPR) effect which contributes to increased passive NP accumulation[114,126,171-173]·[171,173,174]. However, the exact mechanism for EPR effect at the injury location is not clearly known. EPR effect can occur due to mechanical damage to the cerebral vessels and/or paracellular transport through BBB breach leading to passive NP accumulation. The acute (~3h) BBB breakdown after focal injury could primarily be caused by the mechanism of the injury leading to physical damage to the BBB unit leading to vascular disruption[149]. The BBB breach at sub-acute (24h and 3d) time point after focal injury and at 3h post diffuse injury (FPI) is mainly associated with the known mediators of BBB disruption leading to paracellular transport[149]. The mechanism of passage of substances between endothelial cells is called paracellular transport and tight junctions play a critical role in maintaining the balance of the transport to support a

healthy BBB[110]. TBI pathology may lead to BBB dysfunction due to factors such as glutamate, reactive oxygen species, matrix metalloproteinases (MMPs), pro-inflammatory cytokines such as TNF alpha and IL-1beta and vascular endothelial growth factor A (VEGFA)[21]. These factors lead to disruption and/or down regulation of tight junctions and basal lamina proteins thus causing BBB breach[21]. Overall, the pathology contributes to persistent gaps between endothelial cells facilitating paracellular diffusion of the NPs through the BBB[168,255,256]. As such, understanding the mechanism for passive NP delivery via BBB will help improve the strategies for optimizing the delivery time and achieving effective theranostics.

In focal injury, the NP accumulation at acute time points could be associated largely with the physical damage to the BBB leading to leaky vasculature. We found significant NP accumulation at 1h post-focal injury near the injured cortical region. Moreover, at sub-acute time points, we found that the extent of BBB disruption was dependent on the sex. Specifically, we found female mice exhibited significantly larger extent of BBB disruption displayed by the tracer molecule extravasation compared to males at 24h post-injury. The amount of NP accumulation correlated well with the extent of BBB breakdown demonstrating the NP accumulation directly correlates with the BBB disruption. Although the exact mechanism for the sex difference in the extent of BBB disruption is not clearly know, we postulate that it could be due to the role of sexual dimorphism of the brain and/or sex hormones.

Sex is considered to be an important factor for TBI yet there is no definite conclusion about the exact role of sex/sex hormones in outcome after TBI. In clinical settings, studies show gender associated morbidity in terms of the mortality and complication rates after TBI[257-260],[219,261,262]. Specifically, concussion studies showed sex differences not only in the injury outcome but also in the structural brain alterations[263-265]. In sports-related concussion, females demonstrated a higher risk, performed worse on neurocognitive tests, presented greater post-concussive symptoms severity and longer periods of recovery compared to males[263-265]. Moreover, a recent repetitive concussion study demonstrated sex differences in structural brain alterations including the internal capsule and corona radiate of the right hemisphere[220].

Furthermore, in pre-clinical settings, several studies indicate that the brain's response to injury is sex dependent[48,49,212,237,266-271] however there is no conclusive elucidation of whether the observed differences stem from distinct developmental mechanisms and/or are singularly hormone-dependent[219]. For example, studies have investigated the role of microglia[49,212,266] and signaling events such as cell death and/or inflammation exhibiting sexual dimorphism in injured brain[219,267-270]. Additionally, studies have demonstrated positive outcome after brain injury due to endogenous estrogen and/or following estrogen treatment[48,237,271], as such, a few studies show contradicting evidence[241,272]. Overall, the role of sexual dimorphism of the brain and/or sex hormones in neuroinflammation/outcome needs to be clearly investigated to critically understand the role of sex in BBB permeability to design sex-dependent NP theranostics.

Sex differences in NP delivery: The role of sex is not only important in the outcome of TBI but is also an important aspect in pharmacokinetic and pharmacodynamics research[273,274]. The physiological changes during menstrual cycle with fluctuation in hormonal level such as estrogen and progesterone as well as plasma protein levels have been reported[273]. Specifically, variations in the plasma constituents may affect NP/plasma protein interactions resulting in altered pharmacodynamics in females compared to males[273,275]. Sex dependence on NP delivery has only recently been considered with few peer-reviewed publications. Notably, with either inhalation or oral delivery of gold NPs, biodistribution analysis demonstrated a two-fold higher NP accumulation in the kidneys of female rats compared to males [276,277]. Yet, no such study has been completed for intravenous delivery of NPs and is warranted. In sum, these studies indicate that sex may play an important role in the biodistribution of the NPs after delivery thereby further influencing NP delivery following TBI.

Limitations of NP toxicity: Although the use of NPs therapeutics for brain injury represents a major innovative pharmacological strategy, limitations do exist for NPs [86,92] such as the particle-particle aggregation due to their small size and large surface area that make the physical handling of NPs difficult in liquid and dry forms[72]. Moreover, little is known about the behavior of

NPs and their interactions with the human brain. Clinical and animal studies investigating the toxic effects of NPs on CNS are limited. Recent *in vivo* toxicity studies of NPs in animal models have indicated toxicity for some NPs (such as quantum dots and carbon nanotubes), but reported limited negative effects for others (such as silica coated magnetic NPs, liposomes, and iron oxides)[86,92]. Neurotoxicity of NPs can occur not only due to the NP core structure but also because their surface functionalization (peptides/antibodies for active delivery) that can alter the biological response[86,92]. Surface functionalization using surfactants/peptides may assist in NP delivery via BBB permeability, yet in doing so may increase the risk to induce non-specific permeability of toxic substances[86,92]. Also, neurotoxicity may arise from NPs functionalized with cationized proteins[86,92]. Nevertheless, some NPs have passed rigorous toxicity testing for regulatory approvals and have been successfully used in the clinic[86,92]. Further investigation of the influence of the composition, size, and surface properties of NP for safe NP applications will aid in translation from preclinical to clinical applications.

The therapeutic intervention strategies to improve outcomes of TBI have not been successful in the clinic[69,71]. One of the main limitations of clinical failure is efficacy due to drug clearance, inactivation and degradation[52,69,70]. A plethora of literature shows that nanoparticles can be used to improve efficacy[174,183,184]. Previous studies have successfully used NPs (20 - 60 nm) as indicators of BBB damage in experimental stroke models[185,186]. Studies in ischemic and TBI models showed significantly improved delivery of therapeutics when encapsulated in NPs (~300 nm) compared to bolus injection[194,278]. Moreover, NPs can be developed utilizing the material properties to create systems such as active polymer emulsions[128] and antioxidants[202]. The studies demonstrated that using therapeutic NPs (~50 – 100 nm)[128,202] in CCI model led to improved outcome in rodent models. Furthermore, small NPs such as cerium oxide (~10nm) have shown to improve cognitive functions after FPI by reducing oxidative damage[203]. These reports provide support to our study that NPs can be used for diagnostic/therapeutics delivery after brain injury. As such, our current study lays the

groundwork for understanding the temporal window for NP delivery via BBB in different injury models and sexes.

Nevertheless, as briefly discussed earlier, several areas for future work should be considered, including elucidating the mechanism of NP accumulation and the role of sexual dimorphism/sex hormones in BBB disruption. A few of these approaches are discussed below.

5.1.1 Detailed nanoparticle characterization

The circulation time for our study was kept consistent for either 1h or 3h depending on the study design. However, based on the short circulation time and previous reports[248,279] of successful PEGylated polystyrene NPs usage, we did not conduct PEG density characterization and stability testing. Future studies need to characterize the PEG density using technique such as H^1 nuclear magnetic resonance (NMR)[280]. The NP stability can be probed in the presence of proteins by dynamic light scattering studies[280]. Therefore, these studies will inform about the NP stability and PEG coating density that is important for stealthiness and effective diffusion in the extracellular matrix in the brain parenchyma. Overall, these factors are important design considerations for effective NP delivery strategies for brain injury.

5.1.2 Mechanisms of NP accumulation

TBI may lead to dysfunction of the BBB and permeable blood vasculature within the injury region[167,169,170,190] and leads EPR effect and hence the NP accumulation. However, we have not directly surveyed the mechanism of NP accumulation. EPR effect can occur due to mechanical damage to the cerebral vessels and/or paracellular transport through BBB breach leading to passive NP accumulation. Therefore, future studies will need to explore the mechanism of NP accumulation and probe the expression of putative factors of BBB breakdown such as proinflammatory cytokines, MMP9, VEGFA[21,281]. Techniques such as immunohistochemical (IHC), fluorescent in situ hybridization (FISH), western blot analysis and gelatin zymography can be used. Particularly, (a) IHC staining for blood vessels/endothelial cells, tight junction protein such as occludin, glutamate and VEGFA (b) FISH analysis for mRNA expression of

proinflammatory cytokines. (c) Western blot analysis for expression of tight junction protein such as occludin, claudin-5 and ZO-1 (d) Gelatin zymography for upregulation of preform MMP9 activity. (e) Changes in vascular permeability by MMP inhibition. Moreover, PEG coated gold NPs can be used to study the paracellular NP transport though BBB and brain tissue sections analyzed using transmission electron microscopy. From these studies, we intend to learn the expressions levels (increase or decrease) of BBB breakdown factors and can be correlated with the extent of BBB breakdown. Moreover, these studies will provide direct evidence of NP transport via BBB. Consequently, these studies will help us identify the key contributors for BBB breakdown and thus transport mechanism of NP delivery.

5.1.3 Nanoparticle uptake and cellular co-localization

In this study we assessed the delivery of NPs to the brain at different time points after brain injury. In order to evaluate the temporal window for NP delivery we maintained a short circulation time of 1h or 3h, depending on the experimental design. Even with 3h circulation time we observed limited NP uptake by macrophages/microglia as examined by two-photon microscopy studies. Our study has not evaluated a longer (> 3h) circulation time and more information regarding the amount of macrophage /microglia uptake and/ or cell penetration in brain parenchyma can be obtained by increasing the blood circulation time. Future *in vivo* studies with longer NP circulation time and histological analysis of NP co-localization with macrophage, microglial and astrocytes will be beneficial. These analyses will provide the necessary information for understanding the cellular NP uptake and co-localization and eventually aid in developing improved NP strategies for brain injuries.

5.1.4 Elucidating the role of sexual dimorphism/sex hormones on NP accumulation via BBB disruption after TBI

The sub-acute BBB breakdown is largely known to be associated with the secondary injury after TBI. The factors that influence the BBB breakdown such as the role of sex has not been investigated and here we demonstrated that the females had a robust sustained BBB breakdown compared to their male counterparts. However, the nature of these differences

between sexes is not clearly understood. Studies have shown sexual dimorphism in the neuroanatomy that could result in variable structural damage and physiology[215,230] after injury. Moreover, sex hormones are known have an important role in the central nervous system functions and disorders, leading to modulation of neurotransmitters such as nitric oxide contributing to increased BBB permeability[232,249]. Therefore, future studies need to investigate the role of sex on BBB breakdown/NP accumulation after TBI using intact females (non-ovariectomized, proestrous), intact females (non-ovariectomized, nonproestrous), ovariectomized females, orchidectomized males and intact males. Comparison of intact females: proestrous (higher estrogen level and lower progestrone) and intact female: non-proestrous (lower estrogen and higher progesterone) level will inform about the effect of different female sex hormones (estrogen vs progestrone). Comparison of orchidectomized males and intact males will inform about the effect of testosterone/male sex hormone. Moreover, comparison of ovariectomized females with orchidectomized males will inform about the sexual dimorphism and variability in the physiological response after brain injury. Therefore, from these studies we expect to learn about the effect of sex hormone and/or sexual dimorphism for NP delivery via BBB breach after brain injury.

Furthermore, to understand the implications of neuroinflammatory response, there is ongoing IHC analysis for microglia and astrocytes. This study is carried out to determine the levels of glial cell expressions across different time points and sexes. As such, this study will better inform us about the sex differences in our experiments in terms of neuroinflammation post-TBI. We can then analyze if the neuroinflammatory response could have any direct/indirect relationship with the BBB breakdown/NP accumulation.

5.1.5 Active NP delivery strategies

The studies presented in this thesis focused on investigating the feasibility of NP delivery after experimental brain injury. The passive delivery of NPs via the leaky vasculature/paracellular transport results in accumulation of large amount of NPs at the enhanced permeability region; however, these pathway also might induce non-specific targeting[129]. Therefore, building on the

current work future studies can expand the focus to active targeting for NP delivery. Active delivery of NPs occurs via receptor-mediated transcytosis (such as transferrin and lipoprotein receptor) that relies on ligand-receptor affinity. Nanobodies such as ligands, antibodies, peptides, and surfactants have been utilized in delivery of NPs across BBB to induce specific site targeting and reduce systemic side effects[1,131].

5.1.6 Biodistribution and neurotoxicity

Although the use of NPs therapeutics for brain injury represents a major innovative pharmacological strategy, valid concerns about NP biodistribution and toxicity remain.[86,92] Therefore, future studies need to analysis and track the amount of NP/drug concentrations in all major tissues after administration over a period of time until the elimination. Furthermore, little is known about the behavior of NPs and their interactions with the human brain with limited clinical and animal studies investigating the toxic effects of NPs on CNS. Neurotoxicity of NPs can occur due to the NP core and the surface functionalization. Nevertheless, some NPs have passed rigorous toxicity testing for regulatory approvals and have been successfully used in the clinic.[86,92] Therefore, critical investigation of the influence of the composition, size, and surface properties of NP for safe NP applications will aid in translation from pre-clinical to clinical applications.

Considering the discussed limitations, this study significantly impacted the TBI-NP field by contributing to the knowledge of delivery window via BBB breach. For successful clinical translation, therapeutic strategies need to be evaluated in multiple TBI animal models and both sexes while considering opportunities for different optimal therapeutic windows for each injury phenotype. As such, we found striking differences in the dynamics of the NP accumulation across different TBI models and sexes. Thus, the results from this project will enhance the TBI-NP field by stimulating researchers to explore strategies to advance NP delivery for improved TBI outcome.

REFERENCES

[1] V.N. Bharadwaj, D.T. Nguyen, V.D. Kodibagkar, S.E. Stabenfeldt, Nanoparticle-Based Therapeutics for Brain Injury, Adv. Healthcare Mater. 7 (2018). doi:10.1002/adhm.201700668.

[2] V.N. Bharadwaj, J. Lifshitz, P.D. Adelson, V.D. Kodibagkar, S.E. Stabenfeldt, Temporal assessment of nanoparticle accumulation after experimental brain injury: Effect of particle size, Sci. Rep. 6 (2016) 29988. doi:10.1038/srep29988.

[3] P.K. Dash, J. Zhao, G. Hergenroeder, A.N. Moore, Biomarkers for the diagnosis, prognosis, and evaluation of treatment efficacy for traumatic brain injury, Neurotherapeutics. 7 (2010) 100–114. doi:10.1016/j.nurt.2009.10.019.

[4] S.J. Kim, G.J. Moon, O.Y. Bang, Biomarkers for stroke, J Stroke. 15 (2013) 27–37. doi:10.5853/jos.2013.15.1.27.

[5] S.G. Kanekar, T. Zacharia, R. Roller, Imaging of stroke: Part 2, Pathophysiology at the molecular and cellular levels and corresponding imaging changes, American Journal of Roentgenology. 198 (2012) 63–74. doi:10.2214/AJR.10.7312.

[6] A.K. Saenger, R.H. Christenson, Stroke biomarkers: progress and challenges for diagnosis, prognosis, differentiation, and treatment, Clin Chem. 56 (2010) 21–33. doi:10.1373/clinchem.2009.133801.

[7] R.J. MacKay, Brain injury after head trauma: Pathophysiology, diagnosis, and treatment, Veterinary Clinics of North America - Equine Practice. 20 (2004) 199–216. doi:10.1016/j.cveq.2003.11.006.

[8] C. Bryan-Hancock, J. Harrison, The global burden of traumatic brain injury: preliminary results from the Global Burden of Disease Project, Injury Prevention. 16 (2011) A17–A17. doi:10.1136/ip.2010.029215.61.

[9] J.A. Langlois, W. Rutland-Brown, M.M. Wald, The epidemiology and impact of traumatic brain injury: a brief overview, J Head Trauma Rehabil. 21 (2006) 375–378.

[10] G.W. Hergenroeder, J.B. Redell, A.N. Moore, P.K. Dash, Biomarkers in the Clinical Diagnosis and Management of Traumatic Brain Injury, Mol Diagn Ther. 12 (2008) 345–358.

[11] C. Werner, K. Engelhard, Pathophysiology of traumatic brain injury, Journal of Anaesthesia 99 (2007) 4–9. doi:10.1093/bja/aem131.

[12] A.I.R. Maas, N. Stocchetti, R. Bullock, Moderate and severe traumatic brain injury in adults, The Lancet Neurology. 7 (2008) 728–741. doi:10.1016/S1474-4422(08)70164-9.

[13] W. Rosamond, K. Flegal, G. Friday, K. Furie, A. Go, K. Greenlund, et al., Heart disease and stroke statistics - 2007 update - A report from the American Heart Association Statistics Committee and Stroke Statistics Subcommittee, Circulation. 115 (2007) E69–E171. doi:10.1161/CIRCULATIONAHA.106.179918.

[14] V.L. Feigin, S. Barker-Collo, R. Krishnamurthi, A. Theadom, N. Starkey, Epidemiology of ischaemic stroke and traumatic brain injury, Best Pract Res Clin

Anaesthesiol. 24 (2010) 485–494. doi:10.1016/j.bpa.2010.10.006.

[15] D. Shlosberg, M. Benifla, D. Kaufer, A. Friedman, Blood-brain barrier breakdown as a therapeutic target in traumatic brain injury, 6 (2010) 393–403. doi:10.1038/nrneurol.2010.74.

[16] T. Wieloch, K. Nikolich, Mechanisms of neural plasticity following brain injury, Curr Opin Neurobiol. 16 (2006) 258–264. doi:10.1016/j.conb.2006.05.011.

[17] J.L. Alves, Blood-brain barrier and traumatic brain injury, Journal of Neuroscience Research. 92 (2013) 141–147. doi:10.1002/jnr.23300.

[18] A.E. Davis, Mechanisms of traumatic brain injury: biomechanical, structural and cellular considerations, Crit Care Nurs Q. 23 (2000) 1–13.

[19] T.A. Gennarelli, The Pathobiology of Traumatic Brain Injury, Neuroscientist. 3 (1997) 73–81. doi:10.1177/107385849700300117.

[20] A.C. McKee, D.H. Daneshvar, The neuropathology of traumatic brain injury, 1st ed., Elsevier B.V, (2014). doi:10.1016/B978-0-444-52892-6.00004-0.

[21] A. Chodobski, B.J. Zink, J. Szmydynger-Chodobska, Blood-brain barrier pathophysiology in traumatic brain injury, Transl. Stroke Res. 2 (2011) 492–516. doi:10.1007/s12975-011-0125-x.

[22] R.L. Macdonald, M. Stoodley, Pathophysiology of cerebral ischemia, Neurol. Med. Chir. (Tokyo). 38 (1998) 1–11.

[23] H.M. Bramlett, W.D. Dietrich, Pathophysiology of cerebral ischemia and brain trauma: similarities and differences, J. Cereb. Blood Flow Metab. 24 (2004) 133–150. doi:10.1097/01.WCB.0000111614.19196.04.

[24] B.J. Thompson, P.T. Ronaldson, Drug delivery to the ischemic brain, Adv Pharmacol. 71 (2014) 165–202. doi:10.1016/bs.apha.2014.06.013.

[25] J. Wang, W. Yang, H. Xie, Y. Song, Y. Li, L. Wang, Ischemic stroke and repair: current trends in research and tissue engineering treatments, Regen Med Res. 2 (2014) 3. doi:10.1186/2050-490X-2-3.

[26] L. Price, C. Wilson, G. Grant, Blood–Brain Barrier Pathophysiology following Traumatic Brain Injury, CRC Press, (2015) doi:10.1201/b18959-5.

[27] S.A. Baldwin, I. Fugaccia, D.R. Brown, L.V. Brown, S.W. Scheff, Blood-brain barrier breach following cortical contusion in the rat, Journal of Neurosurgery. 85 (1996) 476–481. doi:10.3171/jns.1996.85.3.0476.

[28] P.D. Adelson, M.J. Whalen, P.M. Kochanek, P. Robichaud, T.M. Carlos, Blood Brain Barrier Permeability and Acute Inflammation in Two Models of Traumatic Brain Injury in the Immature Rat: A Preliminary Report, in: Intracranial Pressure and Neuromonitoring in Brain Injury, Springer Vienna, Vienna, (1998) pp. 104–106. doi:10.1007/978-3-7091-6475-4_31.

[29] G. Lotocki, J.P. de Rivero Vaccari, E.R. Perez, J. Sanchez-Molano, O. Furones-Alonso, H.M. Bramlett, et al., Alterations in blood-brain barrier permeability to large and small molecules and leukocyte accumulation after traumatic brain injury: effects

of post-traumatic hypothermia, J Neurotrauma. 26 (2009) 1123–1134. doi:10.1089/neu.2008.0802.

[30] R. Härtl, M. Medary, M. Ruge, K.E. Arfors, J. Ghajar, Blood-Brain Barrier Breakdown Occurs Early After Traumatic Brain Injury and is not Related to White Blood Cell Adherence, in: Brain Edema X, Springer, Vienna, Vienna, (1997) pp. 240–242. doi:10.1007/978-3-7091-6837-0_74.

[31] K.E. Sandoval, K.A. Witt, Blood-brain barrier tight junction permeability and ischemic stroke, Neurobiology of Disease. 32 (2008) 200–219. doi:10.1016/j.nbd.2008.08.005.

[32] W.-Y. Liu, Z.-B. Wang, L.-C. Zhang, X. Wei, L. Li, Tight Junction in Blood-Brain Barrier: An Overview of Structure, Regulation, and Regulator Substances, CNS Neurosci Ther. 18 (2012) 609–615. doi:10.1111/j.1755-5949.2012.00340.x.

[33] W.M. Pardridge, Blood-brain barrier biology and methodology, J. Neurovirol. 5 (1999) 556–569. doi:10.3109/13550289909021285.

[34] Y. Chen, R.A. Swanson, Astrocytes and Brain Injury, J. Cereb. Blood Flow Metab. 23 (2003) 137–149. doi:10.1097/01.WCB.0000044631.80210.3C.

[35] I.P. Karve, J.M. Taylor, P.J. Crack, The contribution of astrocytes and microglia to traumatic brain injury, British Journal of Pharmacology. (2016). doi:10.1111/bph.2016.173.issue-4.

[36] G. Esposito, J.D. Van Horn, D.R. Weinberger, K.F. Berman, Gender differences in cerebral blood flow as a function of cognitive state with PET, Journal of Nuclear Medicine. 37 (1996) 559–564.

[37] T. Rabinowicz, D.E. Dean, J.M.-C. Petetot, G.M. de Courten-Myers, Gender Differences in the Human Cerebral Cortex: More Neurons in Males; More Processes in Females:, Journal of Child Neurology. 14 (2016) 98–107. doi:10.1177/088307389901400207.

[38] J.M. Goldstein, L.J. Seidman, N.J. Horton, N. Makris, D.N. Kennedy, V.S. Caviness, et al., Normal sexual dimorphism of the adult human brain assessed by in vivo magnetic resonance imaging, Cereb. Cortex. 11 (2001) 490–497. doi:10.1093/cercor/11.6.490.

[39] R.K.R. Salokangas, Gender and the use of neuroleptics in schizophrenia further testing of the oestrogen hypothesis, Schizophrenia Research. 16 (1995) 7–16. doi:10.1016/0920-9964(94)00059-H.

[40] B. Oztas, Sex and blood-brain barrier, Pharmacol. Res. 37 (1998) 165–167. doi:10.1006/phrs.1997.0243.

[41] R.J. Mathew, W.H. Wilson, S.R. Tant, Determinants of resting regional cerebral blood flow in normal subjects, Biol. Psychiatry. 21 (1986) 907–914.

[42] G. Rodriguez, S. Warkentin, J. Risberg, G. Rosadini, Sex Differences in Regional Cerebral Blood Flow, J. Cereb. Blood Flow Metab. 8 (2016) 783–789. doi:10.1038/jcbfm.1988.133.

[43] D.G. Daniel, R.J. Mathew, W.H. Wilson, Sex roles and regional cerebral blood flow,

Psychiatry Research. 27 (1989) 55–64.

[44] B. Öztas, S. Ćmurcu, M. Kaya, Influence of Sex on the Blood Brain Barrier Permeability During Bicuculline-Induced Seizures, International Journal of Neuroscience. 65 (1992) 131–139. doi:10.3109/00207459209003284.

[45] B. Oztas, S. Akgul, F.B. Seker, Gender Difference in the Influence of Antioxidants on the Blood–Brain Barrier Permeability During Pentylenetetrazol-Induced Seizures in Hyperthermic Rat Pups, Biol Trace Elem Res. 118 (2007) 77–83. doi:10.1007/s12011-007-0020-1.

[46] B. Oztas, Asymmetrical changes in blood–brain barrier permeability during pentylenetetrazol-induced seizures and in acute hypertension, Psychiatry Research: Neuroimaging. 82 (1998) 129–133. doi:10.1016/S0925-4927(98)00014-6.

[47] R. Roof, Estrogen-Related Gender Difference in Survival Rate and Cortical Blood Flow After Impact-Acceleration Head Injury in Rats, (2008) 1–22.

[48] R.L. Roof, R. Duvdevani, D.G. Stein, Gender influences outcome of brain injury: progesterone plays a protective role, Brain Research. 607 (1993) 333–336.

[49] S. Villapol, D.J. Loane, M.P. Burns, Sexual dimorphism in the inflammatory response to traumatic brain injury, Glia. 65 (2017) 1423–1438. doi:10.1002/glia.23171.

[50] S. Margulies, R. Hicks, Combination Therapies for Traumatic Brain Injury: Prospective Considerations, Http://Www.Liebertpub.com/Neu. 26 (2009) 925–939. doi:10.1089/neu.2008.0794.

[51] Y. Xiong, A. Mahmood, M. Chopp, Animal models of traumatic brain injury, Nature Reviews Neuroscience. 14 (2013) 128–142. doi:10.1038/nrn3407.

[52] Y. Xiong, A. Mahmood, M. Chopp, Emerging treatments for traumatic brain injury, Expert Opin Emerg Drugs. 14 (2009) 67–84. doi:10.1517/14728210902769601.

[53] V.E. Johnson, D.F. Meaney, D.K. cullen, D.H. Smith, Animal models of traumatic brain injury, Handb Clin Neurol. 127 (2015) 115–128. doi:10.1016/B978-0-444-52892-6.00008-8.

[54] M.C. LaPlaca, C.M. Simon, G.R. Prado, D.K. Cullen, CNS injury biomechanics and experimental models, in: Neurotrauma: New Insights Into Pathology and Treatment, Elsevier, 2007: pp. 13–26. doi:10.1016/S0079-6123(06)61002-9.

[55] W.T. O'Connor, A. Smyth, M.D. Gilchrist, Animal models of traumatic brain injury: A critical evaluation, Pharmacology and Therapeutics. 130 (2011) 106–113. doi:10.1016/j.pharmthera.2011.01.001.

[56] D.H. Smith, H.D. SOARES, J.S. PIERCE, K.G. PERLMAN, K.E. Saatman, D.F. MEANEY, et al., A Model of Parasagittal Controlled Cortical Impact in the Mouse - Cognitive and Histopathologic Effects, J Neurotrauma. 12 (1995) 169–178. doi:10.1089/neu.1995.12.169.

[57] S. Yu, Y. Kaneko, E. Bae, C.E. Stahl, Y. Wang, H. van Loveren, et al., Severity of controlled cortical impact traumatic brain injury in rats and mice dictates degree of behavioral deficits, Brain Research. 1287 (2009) 157–163.

doi:10.1016/j.brainres.2009.06.067.

[58] B. Jennett, Epidemiology of head injury, Arch. Dis. Child. 78 (1998) 403–406.

[59] M. Faul, V. Coronado, Epidemiology of traumatic brain injury, 1st ed., Elsevier B.V, (2014) doi:10.1016/B978-0-444-52892-6.00001-5.

[60] I. Cernak, Animal models of head trauma, Neurotherapeutics. 2 (2005) 410–422. doi:10.1602/neurorx.2.3.410.

[61] J. Lifshitz, R.K. Rowe, D.R. Griffiths, M.N. Evilsizor, T.C. Thomas, P.D. Adelson, et al., Clinical relevance of midline fluid percussion brain injury: Acute deficits, chronic morbidities and the utility of biomarkers, Brain Injury. 30 (2016) 1293–1301. doi:10.1080/02699052.2016.1193628.

[62] B. Fehily, M. Fitzgerald, Repeated Mild Traumatic Brain Injury, Cell Transplant. 26 (2017) 1131–1155. doi:10.1177/0963689717714092.

[63] C. Goddeyne, J. Nichols, C. Wu, T. Anderson, Repetitive mild traumatic brain injury induces ventriculomegaly and cortical thinning in juvenile rats, J Neurophysiol. 113 (2015) 3268–3280. doi:10.1152/jn.00970.2014.

[64] M.J. Kane, M. Angoa-Pérez, D.I. Briggs, D.C. Viano, C.W. Kreipke, D.M. Kuhn, A mouse model of human repetitive mild traumatic brain injury, Journal of Neuroscience Methods. 203 (2012) 41–49. doi:10.1016/j.jneumeth.2011.09.003.

[65] M.W. Wojnarowicz, A.M. Fisher, O. Minaeva, L.E. Goldstein, Considerations for Experimental Animal Models of Concussion, Traumatic Brain Injury, and Chronic Traumatic Encephalopathy-These Matters Matter, Front Neurol. 8 (2017) 240. doi:10.3389/fneur.2017.00240.

[66] M.J. McGinn, J.T. Povlishock, Cellular and molecular mechanisms of injury and spontaneous recovery, 1st ed., Elsevier B.V, (2014). doi:10.1016/B978-0-444-52892-6.00005-2.

[67] G. Orive, R.M. Hernández, A.R. Gascón, A. Domínguez-Gil, J.L. Pedraz, Drug delivery in biotechnology: present and future, Current Opinion in Biotechnology. 14 (2003) 659–664. doi:10.1016/j.copbio.2003.10.007.

[68] S. Parveen, R. Misra, S.K. Sahoo, Nanoparticles: a boon to drug delivery, therapeutics, diagnostics and imaging, Nanomedicine: Nanotechnology, Biology, and Medicine. 8 (2012) 147–166. doi:10.1016/j.nano.2011.05.016.

[69] R.K. Narayan, M.E. Michel, B. Ansell, A. Baethmann, A. Biegon, M.B. Bracken, et al., Clinical Trials in Head Injury, Http://Www.Liebertpub.com/Neu. 19 (2004) 503–557. doi:10.1089/089771502753754037.

[70] R.M. Adibhatla, Citicoline in stroke and TBI clinical trials, Nat Rev Neurol. 9 (2013) 173. doi:10.1038/nrneurol.2012.166-c1.

[71] R. Vink, A.J. Nimmo, Multifunctional drugs for head injury, Neurotherapeutics. 6 (2009) 28–42. doi:10.1016/j.nurt.2008.10.036.

[72] V.J. Mohanraj, Y. Chen, Nanoparticles - A review, Trop. J. Pharm Res. 5 (2006) 561–573. doi:10.4314/tjpr.v5i1.14634.

[73] W.H. De Jong, P.J.A. Borm, Drug delivery and nanoparticles: Applications and hazards, Ijn. 3 (2008) 133–149.

[74] A. Agarwal, N. Lariya, G. Saraogi, N. Dubey, H. Agrawal, G.P. Agrawal, Nanoparticles as novel carrier for brain delivery: a review, Curr. Pharm. Des. 15 (2009) 917–925. doi:10.2174/138161209787582057.

[75] A.G. de Boer, P.J. Gaillard, Drug targeting to the brain, Annu. Rev. Pharmacol. Toxicol. 47 (2007) 323–355. doi:10.1146/annurev.pharmtox.47.120505.105237.

[76] G.A. Silva, Nanotechnology approaches for the regeneration and neuroprotection of the central nervous system, Surgical Neurology. 63 (2005) 301–306. doi:10.1016/j.surneu.2004.06.008.

[77] J. Kreuter, Nanoparticles—a historical perspective, International Journal of Pharmaceutics. 331 (2007) 1–10. doi:10.1016/j.ijpharm.2006.10.021.

[78] S.R. Mudshinge, A.B. Deore, S. Patil, C.M. Bhalgat, Nanoparticles: Emerging carriers for drug delivery, Saudi Pharmaceutical Journal. 19 (2011) 129–141. doi:10.1016/j.jsps.2011.04.001.

[79] J.R. Kanwar, X. Sun, V. Punj, B. Sriramoju, R.R. Mohan, S.-F. Zhou, et al., Nanoparticles in the treatment and diagnosis of neurological disorders: untamed dragon with fire power to heal, Nanomedicine: Nanotechnology, Biology, and Medicine. 8 (2012) 399–414. doi:10.1016/j.nano.2011.08.006.

[80] R. Singh, J.W. Lillard Jr, Nanoparticle-based targeted drug delivery, Experimental and Molecular Pathology. 86 (2009) 215–223. doi:10.1016/j.yexmp.2008.12.004.

[81] M.L. Hans, A.M. Lowman, Biodegradable nanoparticles for drug delivery and targeting, Current Opinion in Solid State and Materials Science. 6 (2002) 319–327. doi:10.1016/S1359-0286(02)00117-1.

[82] V. Gadhvi, K. Brijesh, A. Gupta, K. Roopchandani, N. Patel, Nanoparticles for Brain Targeting, Research Journal of Pharmacy and Technology. 6 (2013) 454–458.

[83] R.A. Petros, J.M. DeSimone, Strategies in the design of nanoparticles for therapeutic applications, Nat Rev Drug Discov. 9 (2010) 615–627. doi:10.1038/nrd2591.

[84] J. Shi, A.R. Votruba, O.C. Farokhzad, R. Langer, Nanotechnology in drug delivery and tissue engineering: from discovery to applications, Nano Lett. 10 (2010) 3223–3230. doi:10.1021/nl102184c.

[85] A.C. Anselmo, S. Mitragotri, Nanoparticles in the clinic, Bioengineering & Translational Medicine. 1 (2016) 10–29. doi:10.1002/btm2.10003.

[86] M.E. Davis, Z.G. Chen, D.M. Shin, Nanoparticle therapeutics: an emerging treatment modality for cancer, Nat Rev Drug Discov. 7 (2008) 771–782. doi:10.1038/nrd2614.

[87] J.L. Gilmore, X. Yi, L. Quan, A.V. Kabanov, Novel Nanomaterials for Clinical Neuroscience, J Neuroimmune Pharmacol. 3 (2008) 83–94. doi:10.1007/s11481-007-9099-6.

[88] H.H. Gustafson, D. Holt-Casper, D.W. Grainger, H. Ghandehari, Nanoparticle uptake: The phagocyte problem, Nano Today. 10 (2015) 487–510. doi:10.1016/j.nantod.2015.06.006.

[89] Y.-N. Zhang, W. Poon, A.J. Tavares, I.D. McGilvray, W.C.W. Chan, Nanoparticle-liver interactions: Cellular uptake and hepatobiliary elimination, J Control Release. 240 (2016) 332–348. doi:10.1016/j.jconrel.2016.01.020.

[90] D.E. Owens, N.A. Peppas, Opsonization, biodistribution, and pharmacokinetics of polymeric nanoparticles, International Journal of Pharmaceutics. 307 (2006) 93–102. doi:10.1016/j.ijpharm.2005.10.010.

[91] E. Polo, M. Collado, B. Pelaz, P. del Pino, Advances toward More Efficient Targeted Delivery of Nanoparticles in Vivo: Understanding Interactions between Nanoparticles and Cells, ACS Nano. 11 (2017) 2397–2402. doi:10.1021/acsnano.7b01197.

[92] M. Masserini, Nanoparticles for Brain Drug Delivery, ISRN Biochem. (2013) 1–18. doi:10.1155/2013/238428.

[93] A. Kumari, S.K. Yadav, S.C. Yadav, Biodegradable polymeric nanoparticles based drug delivery systems, Colloids and Surfaces B: Biointerfaces. 75 (2010) 1–18. doi:10.1016/j.colsurfb.2009.09.001.

[94] M. Johnsson, K. Edwards, Liposomes, Disks, and Spherical Micelles: Aggregate Structure in Mixtures of Gel Phase Phosphatidylcholines and Poly(Ethylene Glycol)-Phospholipids, Biophysical Journal. 85 (2003) 3839–3847. doi:10.1016/S0006-3495(03)74798-5.

[95] B. Klajnert, M. Bryszewska, Dendrimers: properties and applications, Acta Biochim. Pol. 48 (2001) 199–208.

[96] J.J. Wang, Z.W. Zeng, R.Z. Xiao, T. Xie, G.L. Zhou, X.R. Zhan, et al., Recent advances of chitosan nanoparticles as drug carriers, Ijn. 6 (2011) 765–774. doi:10.2147/IJN.S17296.

[97] A. Puri, K. Loomis, B. Smith, J.-H. Lee, A. Yavlovich, E. Heldman, et al., Lipid-Based Nanoparticles as Pharmaceutical Drug Carriers: From Concepts to Clinic, Crit Rev Ther Drug Carrier Syst. 26 (2009) 523–580.

[98] M. Cho, W.-S. Cho, M. Choi, S.J. Kim, B.S. Han, S.H. Kim, et al., The impact of size on tissue distribution and elimination by single intravenous injection of silica nanoparticles, Toxicol Lett. 189 (2009) 177–183. doi:10.1016/j.toxlet.2009.04.017.

[99] J. Conde, A. Ambrosone, V. Sanz, Y. Hernandez, V. Marchesano, F. Tian, et al., Design of multifunctional gold nanoparticles for in vitro and in vivo gene silencing, ACS Nano. 6 (2012) 8316–8324. doi:10.1021/nn3030223.

[100] K.J. Watson, J. Zhu, S.T. Nguyen, C.A. Mirkin, Hybrid Nanoparticles with Block Copolymer Shell Structures, J. Am. Chem. Soc. 121 (1999) 462–463. doi:10.1021/ja983173l.

[101] K. Hadinoto, A. Sundaresan, W.S. Cheow, Lipid–polymer hybrid nanoparticles as a new generation therapeutic delivery platform: A review, Eur J Pharm Biopharm. 85

(2013) 427–443. doi:10.1016/j.ejpb.2013.07.002.

[102] V.P. Torchilin, V.G. Omelyanenko, M.I. Papisov, A.A. Bogdanov, V.S. Trubetskoy, J.N. Herron, et al., Poly(ethylene glycol) on the liposome surface: on the mechanism of polymer-coated liposome longevity, Biochim. Biophys. Acta. 1195 (1994) 11–20. doi:10.1016/0005-2736(94)90003-5.

[103] W.-L. Lu, X.-R. Qi, Q. Zhang, R.-Y. Li, G.-L. Wang, R.-J. Zhang, et al., A pegylated liposomal platform: pharmacokinetics, pharmacodynamics, and toxicity in mice using doxorubicin as a model drug, J. Pharmacol. Sci. 95 (2004) 381–389.

[104] M.J. Ernsting, M. Murakami, A. Roy, S.-D. Li, Factors controlling the pharmacokinetics, biodistribution and intratumoral penetration of nanoparticles, Journal of Controlled Release. 172 (2013) 782–794. doi:10.1016/j.jconrel.2013.09.013.

[105] M.D. Scott, K.L. Murad, Cellular camouflage: fooling the immune system with polymers, Curr. Pharm. Des. 4 (1998) 423–438.

[106] Y. Sadzuka, S. Hirotsu, S. Hirota, Effect of liposomalization on the antitumor activity, side-effects and tissue distribution of CPT-11, Cancer Lett. 127 (1998) 99–106. doi:10.1016/S0304-3835(98)00031-7.

[107] H.S. Choi, W. Liu, P. Misra, E. Tanaka, J.P. Zimmer, B.I. Ipe, et al., Renal clearance of quantum dots, Nature Biotechnology. 25 (2007) 1165–1170. doi:10.1038/nbt1340.

[108] K. Nicolay, G. Strijkers, H. Grull, Gd-Containing Nanoparticles as MRI Contrast Agents, John Wiley & Sons, Ltd, Chichester, UK, (2013). doi:10.1002/9781118503652.ch11.

[109] D.H. Jo, J.H. Kim, T.G. Lee, J.H. Kim, Size, surface charge, and shape determine therapeutic effects of nanoparticles on brain and retinal diseases, Nanomedicine: Nanotechnology, Biology, and Medicine. 11 (2015) 1603–1611. doi:10.1016/j.nano.2015.04.015.

[110] C. Saraiva, C. Praça, R. Ferreira, T. Santos, L. Ferreira, L. Bernardino, Nanoparticle-mediated brain drug delivery: Overcoming blood–brain barrier to treat neurodegenerative diseases, Journal of Controlled Release. 235 (2016) 34–47. doi:10.1016/j.jconrel.2016.05.044.

[111] G. Sonavane, K. Tomoda, K. Makino, Biodistribution of colloidal gold nanoparticles after intravenous administration: effect of particle size, Colloids and Surfaces B: Biointerfaces. 66 (2008) 274–280. doi:10.1016/j.colsurfb.(2008).07.004.

[112] R.H. Müller, C. Jacobs, O. Kayser, Nanosuspensions as particulate drug formulations in therapy. Rationale for development and what we can expect for the future, Advanced Drug Delivery Reviews. 47 (2001) 3–19.

[113] S. Honary, F. Zahir, Effect of Zeta Potential on the Properties of Nano-Drug Delivery Systems - A Review (Part 1), Trop. J. Pharm Res. 12 (2013) 1–10. doi:10.4314/tjpr.v12i2.19.

[114] S.-D. Li, L. Huang, Pharmacokinetics and biodistribution of nanoparticles, Mol. Pharmaceutics. 5 (2008) 496–504. doi:10.1021/mp800049w.

[115] P.R. Lockman, J.M. Koziara, R.J. Mumper, D.D. Allen, Nanoparticle surface charges alter blood-brain barrier integrity and permeability, Journal of Drug Targeting. 12 (2004) 635–641. doi:10.1080/10611860400015936.

[116] L.E. Euliss, J.A. DuPont, S. Gratton, J. DeSimone, Imparting size, shape, and composition control of materials for nanomedicine, Chem. Soc. Rev. 35 (2006) 1095–1104. doi:10.1039/b600913c.

[117] Y. Li, M. Kröger, W.K. Liu, Shape effect in cellular uptake of PEGylated nanoparticles: comparison between sphere, rod, cube and disk, Nanoscale. 7 (2015) 16631–16646. doi:10.1039/c5nr02970h.

[118] Y. Li, T. Yue, K. Yang, X. Zhang, Molecular modeling of the relationship between nanoparticle shape anisotropy and endocytosis kinetics, Biomaterials. 33 (2012) 4965–4973. doi:10.1016/j.biomaterials.2012.03.044.

[119] H. Herd, N. Daum, A.T. Jones, H. Huwer, H. Ghandehari, C.-M. Lehr, Nanoparticle geometry and surface orientation influence mode of cellular uptake, ACS Nano. 7 (2013) 1961–1973. doi:10.1021/nn304439f.

[120] P. Kolhar, A.C. Anselmo, V. Gupta, K. Pant, B. Prabhakarpandian, E. Ruoslahti, et al., Using shape effects to target antibody-coated nanoparticles to lung and brain endothelium, Proc Natl Acad Sci U S A. 110 (2013) 10753–10758. doi:10.1073/pnas.1308345110.

[121] P. Chaturbedy, M. Kumar, K. Salikolimi, S. Das, S.H. Sinha, S. Chatterjee, et al., Shape-directed compartmentalized delivery of a nanoparticle-conjugated small-molecule activator of an epigenetic enzyme in the brain, J Control Release. 217 (2015) 151–159. doi:10.1016/j.jconrel.2015.08.043.

[122] D. Liu, A. Mori, L. Huang, Role of liposome size and RES blockade in controlling biodistribution and tumor uptake of GM1-containing liposomes, Biochimica Et Biophysica Acta (BBA) - Biomembranes. 1104 (1992) 95–101. doi:10.1016/0005-2736(92)90136-A.

[123] S. Hanada, K. Fujioka, Y. Inoue, F. Kanaya, Y. Manome, K. Yamamoto, Cell-Based in Vitro Blood–Brain Barrier Model Can Rapidly Evaluate Nanoparticles' Brain Permeability in Association with Particle Size and Surface Modification, Ijms. 15 (2014) 1812–1825. doi:10.3390/ijms15021812.

[124] G. Fricker, M. Ott, A. Mahringer, The Blood Brain Barrier (BBB), Springer, 2014.

[125] W.M. Pardridge, The blood-brain barrier: bottleneck in brain drug development, Neurotherapeutics. 2 (2005) 3–14. doi:10.1602/neurorx.2.1.3.

[126] V. Torchilin, Tumor delivery of macromolecular drugs based on the EPR effect, Advanced Drug Delivery Reviews. 63 (2011) 131–135. doi:10.1016/j.addr.2010.03.011.

[127] T. Geelen, L.E. Paulis, B.F. Coolen, K. Nicolay, G.J. Strijkers, Passive targeting of lipid-based nanoparticles to mouse cardiac ischemia-reperfusion injury, Contrast Media Mol. Imaging. 8 (2012) 117–126. doi:10.1002/cmmi.1501.

[128] M.A. Clond, B.-S. Lee, J.J. Yu, M.B. Singer, T. Amano, A.W. Lamb, et al., Reactive oxygen species-activated nanoprodrug of Ibuprofen for targeting traumatic brain

injury in mice, PLoS ONE. 8 (2013) e61819–e61819. doi:10.1371/journal.pone.0061819.

[129] W.M. Pardridge, Drug transport across the blood-brain barrier, Journal of Cerebral Blood Flow & Metabolism. 32 (2012) 1959–1972. doi:10.1038/jcbfm.2012.126.

[130] W. Lu, Q. Sun, J. Wan, Z. She, X.-G. Jiang, Cationic albumin-conjugated pegylated nanoparticles allow gene delivery into brain tumors via intravenous administration, Cancer Res. 66 (2006) 11878–11887. doi:10.1158/0008-5472.CAN-06-2354.

[131] A.M. Grabrucker, R. Chhabra, D. Belletti, F. Forni, M.A. Vandelli, B. Ruozi, et al., Nanoparticles as Blood–Brain Barrier Permeable CNS Targeted Drug Delivery Systems, in: The Blood Brain Barrier (BBB), Springer Berlin Heidelberg, Berlin, Heidelberg, 2013: pp. 71–89. doi:10.1007/7355_2013_22.

[132] M. Shilo, M. Motiei, P. Hana, R. Popovtzer, Transport of nanoparticles through the blood-brain barrier for imaging and therapeutic applications, Nanoscale. 6 (2014) 2146–2152. doi:10.1039/c3nr04878k.

[133] D.T. Wiley, P. Webster, A. Gale, M.E. Davis, Transcytosis and brain uptake of transferrin-containing nanoparticles by tuning avidity to transferrin receptor, Proc Natl Acad Sci U S A. 110 (2013) 8662–8667. doi:10.1073/pnas.1307152110.

[134] A. Ćurić, J.P. Möschwitzer, G. Fricker, Development and characterization of novel highly-loaded itraconazole poly(butyl cyanoacrylate) polymeric nanoparticles, Eur J Pharm Biopharm. 114 (2017) 175–185. doi:10.1016/j.ejpb.2017.01.014.

[135] H. Tu, H. Hsuchou, A.J. Kastin, X. Wu, W. Pan, Unique leptin trafficking by a tailless receptor, Faseb J. 24 (2010) 2281–2291. doi:10.1096/fj.09-143487.

[136] R.L. McCall, J. Cacaccio, E. Wrabel, M.E. Schwartz, T.P. Coleman, R.W. Sirianni, Pathogen-inspired drug delivery to the central nervous system, Tissue Barriers. 2 (2014) e944449. doi:10.4161/21688362.2014.944449.

[137] J.B. Fishman, J.B. Rubin, J.V. Handrahan, J.R. Connor, R.E. Fine, Receptor-mediated transcytosis of transferrin across the blood-brain barrier, Journal of Neuroscience Research. 18 (1987) 299–304. doi:10.1002/jnr.490180206.

[138] C. Fillebeen, L. Descamps, M.P. Dehouck, L. Fenart, M. Benaïssa, G. Spik, et al., Receptor-mediated transcytosis of lactoferrin through the blood-brain barrier, J. Biol. Chem. 274 (1999) 7011–7017. doi:10.1074/jbc.274.11.7011.

[139] I. Cabezón, G. Manich, R. Martín-Venegas, A. Camins, C. Pelegrí, J. Vilaplana, Trafficking of Gold Nanoparticles Coated with the 8D3 Anti-Transferrin Receptor Antibody at the Mouse Blood-Brain Barrier, Mol. Pharmaceutics. 12 (2015) 4137–4145. doi:10.1021/acs.molpharmaceut.5b00597.

[140] N. Bien-Ly, Y.J. Yu, D. Bumbaca, J. Elstrott, C.A. Boswell, Y. Zhang, et al., Transferrin receptor (TfR) trafficking determines brain uptake of TfR antibody affinity variants, J Exp Med. 211 (2014) 233–244. doi:10.1084/jem.20131660.

[141] J. Niewoehner, B. Bohrmann, L. Collin, E. Urich, H. Sade, P. Maier, et al., Increased Brain Penetration and Potency of a Therapeutic Antibody Using a Monovalent Molecular Shuttle, Neuron. 81 (2014) 49–60. doi:10.1016/j.neuron.2013.10.061.

[142] Y. Lin, Y. Pan, Y. Shi, X. Huang, N. Jia, J.-Y. Jiang, Delivery of large molecules via poly(butyl cyanoacrylate) nanoparticles into the injured rat brain, Nanotechnology. 23 (2012) 165101. doi:10.1088/0957-4484/23/16/165101.

[143] B.M. Johnson, W.N. Charman, C.J.H. Porter, An in vitro examination of the impact of polyethylene glycol 400, pluronic P85, and vitamin E d-a-tocopheryl polyethylene glycol 1000 succinate on P-glycoprotein efflux and enterocyte-based metabolism in excised rat intestine, AAPS PharmSci. 4 (2002) 193–205. doi:10.1208/ps040440.

[144] B. Petri, A. Bootz, A. Khalansky, T. Hekmatara, R. Müller, R. Uhl, et al., Chemotherapy of brain tumour using doxorubicin bound to surfactant-coated poly(butyl cyanoacrylate) nanoparticles: revisiting the role of surfactants, Journal of Controlled Release. 117 (2007) 51–58. doi:10.1016/j.jconrel.2006.10.015.

[145] S. Wohlfart, S. Gelperina, J. Kreuter, Transport of drugs across the blood–brain barrier by nanoparticles, Journal of Controlled Release. 161 (2012) 264–273. doi:10.1016/j.jconrel.2011.08.017.

[146] L.-X. Zhao, A.-C. Liu, S.-W. Yu, Z.-X. Wang, X.-Q. Lin, G.-X. Zhai, et al., The Permeability of Puerarin Loaded Poly(butylcyanoacrylate) Nanoparticles Coated with Polysorbate 80 on the Blood-Brain Barrier and Its Protective Effect against Cerebral Ischemia/Reperfusion Injury, Biological and Pharmaceutical Bulletin. 36 (2013) 1263–1270. doi:10.1248/bpb.b12-00769.

[147] J. Kreuter, P. Ramge, V. Petrov, S. Hamm, S.E. Gelperina, B. Engelhardt, et al., Direct evidence that polysorbate-80-coated poly(butylcyanoacrylate) nanoparticles deliver drugs to the CNS via specific mechanisms requiring prior binding of drug to the nanoparticles, Current Opinion in Solid State and Materials Science. 20 (2003) 409–416. doi:10.1023/A:1022604120952.

[148] R.M. Koffie, C.T. Farrar, L.-J. Saidi, C.M. William, B.T. Hyman, T.L. Spires-Jones, Nanoparticles enhance brain delivery of blood-brain barrier-impermeable probes for in vivo optical and magnetic resonance imaging, Proc Natl Acad Sci U S A. 108 (2011) 18837–18842. doi:10.1073/pnas.1111405108.

[149] M.K. Baskaya, A. Muralikrishna Rao, A. Dogan, D. Donaldson, R.J. Dempsey, The biphasic opening of the blood–brain barrier in the cortex and hippocampus after traumatic brain injury in rats, Neurosci. Lett. 226 (1997) 33–36. doi:10.1016/S0304-3940(97)00239-5.

[150] P.D. Adelson, M.J. Whalen, P.M. Kochanek, P. Robichaud, T.M. Carlos, Blood brain barrier permeability and acute inflammation in two models of traumatic brain injury in the immature rat: a preliminary report, 71 (1998) 104–106.

[151] M.D. Habgood, N. Bye, K.M. Dziegielewska, C.J. Ek, M.A. Lane, A. Potter, et al., Changes in blood-brain barrier permeability to large and small molecules following traumatic brain injury in mice, Eur. J. Neurosci. 25 (2007) 231–238. doi:10.1111/j.1460-9568.2006.05275.x.

[152] Y. Ban, L.J. Rizzolo, A culture model of development reveals multiple properties of RPE tight junctions, Mol Vis. 3 (1997) 18–18.

[153] A. Phinikaridou, M.E. Andia, A. Protti, A. Indermuehle, A. Shah, A. Smith, et al., Noninvasive magnetic resonance imaging evaluation of endothelial permeability in murine atherosclerosis using an albumin-binding contrast agent, Circulation. 126

(2012) 707–719. doi:10.1161/CIRCULATIONAHA.112.092098.

[154] W. Cai, X. Chen, Nanoplatforms for Targeted Molecular Imaging in Living Subjects, Small. 3 (2007) 1840–1854. doi:10.1002/smll.200700351.

[155] A.A. Gabizon, Pegylated Liposomal Doxorubicin: Metamorphosis of an Old Drug into a New Form of Chemotherapy, Cancer Investigation. 19 (2001) 424–436. doi:10.1081/CNV-100103136.

[156] A.A. Gabizon, Liposome circulation time and tumor targeting: implications for cancer chemotherapy, Advanced Drug Delivery Reviews. 16 (1995) 285–294. doi:10.1016/0169-409X(95)00030-B.

[157] T.S. Levchenko, R. Rammohan, A.N. Lukyanov, K.R. Whiteman, V.P. Torchilin, Liposome clearance in mice: the effect of a separate and combined presence of surface charge and polymer coating, International Journal of Pharmaceutics. 240 (2002) 95–102. doi:10.1016/S0378-5173(02)00129-1.

[158] C.E. Mora-Huertas, H. Fessi, A. Elaissari, Polymer-based nanocapsules for drug delivery, International Journal of Pharmaceutics. 385 (2010) 113–142. doi:10.1016/j.ijpharm.2009.10.018.

[159] J. Lipka, M. Semmler-Behnke, R.A. Sperling, A. Wenk, S. Takenaka, C. Schleh, et al., Biodistribution of PEG-modified gold nanoparticles following intratracheal instillation and intravenous injection, Biomaterials. 31 (2010) 6574–6581. doi:10.1016/j.biomaterials.2010.05.009.

[160] I. Brigger, Poly(ethylene glycol)-Coated Hexadecylcyanoacrylate Nanospheres Display a Combined Effect for Brain Tumor Targeting, Journal of Pharmacology and Experimental Therapeutics. 303 (2002) 928–936. doi:10.1124/jpet.102.039669.

[161] X. Gao, L. Yang, J.A. Petros, F.F. Marshall, J.W. Simons, S. Nie, In vivo molecular and cellular imaging with quantum dots, Current Opinion in Biotechnology. 16 (2005) 63–72. doi:10.1016/j.copbio.2004.11.003.

[162] X. Ping, K. Jiang, S.-Y. Lee, J.-X. Cheng, X. Jin, PEG-PDLLA micelle treatment improves axonal function of the corpus callosum following traumatic brain injury, J Neurotrauma. 31 (2014) 1172–1179. doi:10.1089/neu.2013.3147.

[163] T. Yardeni, M. Eckhaus, H.D. Morris, M. Huizing, S. Hoogstraten-Miller, Retro-orbital injections in mice, Lab Anim. 40 (2011) 155–160. doi:10.1038/laban0511-155.

[164] W.D. Dietrich, O. Alonso, M. Halley, Early microvascular and neuronal consequences of traumatic brain injury: a light and electron microscopic study in rats, J Neurotrauma. 11 (1994) 289–301.

[165] F. Alexis, E. Pridgen, L.K. Molnar, O.C. Farokhzad, Factors Affecting the Clearance and Biodistribution of Polymeric Nanoparticles, Mol. Pharmaceutics. 5 (2008) 505–515. doi:10.1021/mp800051m.

[166] Y. Yamamoto, Y. Nagasaki, Y. Kato, Y. Sugiyama, K. Kataoka, Long-circulating poly(ethylene glycol)-poly(D,L-lactide) block copolymer micelles with modulated surface charge, Journal of Controlled Release. 77 (2001) 27–38.

[167] H. Tanno, R.P. Nockels, L.H. Pitts, L.J. Noble, Breakdown of the blood-brain barrier after fluid percussive brain injury in the rat. Part 1: Distribution and time course of protein extravasation, J Neurotrauma. 9 (1992) 21–32.

[168] A.J. Sawyer, T.R. Kyriakides, Nanoparticle-based evaluation of blood–brain barrier leakage during the foreign body response, J. Neural Eng. 10 (2013) 016013–18. doi:10.1088/1741-2560/10/1/016013.

[169] S. Sangiorgi, A. De Benedictis, M. Protasoni, A. Manelli, M. Reguzzoni, A. Cividini, et al., Early-stage microvascular alterations of a new model of controlled cortical traumatic brain injury: 3D morphological analysis using scanning electron microscopy and corrosion casting Laboratory investigation, Journal of Neurosurgery. 118 (2013) 763–774. doi:10.3171/2012.11.JNS12627.

[170] L.-D.D. Pham, K. Hayakawa, J.H. Seo, M.-N. Nguyen, A.T. Som, B.J. Lee, et al., Crosstalk between oligodendrocytes and cerebral endothelium contributes to vascular remodeling after white matter injury, Glia. 60 (2012) 875–881. doi:10.1002/glia.22320.

[171] B. Chertok, B.A. Moffat, A.E. David, F. Yu, C. Bergemann, B.D. Ross, et al., Iron oxide nanoparticles as a drug delivery vehicle for MRI monitored magnetic targeting of brain tumors, Biomaterials. 29 (2008) 487–496. doi:10.1016/j.biomaterials.2007.08.050.

[172] J. Fang, H. Nakamura, H. Maeda, The EPR effect: Unique features of tumor blood vessels for drug delivery, factors involved, and limitations and augmentation of the effect, Advanced Drug Delivery Reviews. 63 (2011) 136–151. doi:10.1016/j.addr.2010.04.009.

[173] D. Liu, A. Mori, L. Huang, Role of liposome size and RES blockade in controlling biodistribution and tumor uptake of GM1-containing liposomes, Biochim. Biophys. Acta. 1104 (1992) 95–101.

[174] H. Cabral, Y. Matsumoto, K. Mizuno, Q. Chen, M. Murakami, M. Kimura, et al., Accumulation of sub-100 nm polymeric micelles in poorly permeable tumours depends on size, Nature Nanotechnology. 6 (2011) 815–823. doi:10.1038/nnano.2011.166.

[175] P.S. Tsai, J.P. Kaufhold, P. Blinder, B. Friedman, P.J. Drew, H.J. Karten, et al., Correlations of neuronal and microvascular densities in murine cortex revealed by direct counting and colocalization of nuclei and vessels, Journal of Neuroscience. 29 (2009) 14553–14570. doi:10.1523/JNEUROSCI.3287-09.2009.

[176] B. Klein, W. Kuschinsky, H. Schröck, F. Vetterlein, Interdependency of local capillary density, blood flow, and metabolism in rat brains, Am. J. Physiol. 251 (1986) H1333–40.

[177] F.M. Faraci, D.D. Heistad, Regulation of large cerebral arteries and cerebral microvascular pressure, Circ. Res. 66 (1990) 8–17.

[178] S. Herculano-Houzel, C. Watson, G. Paxinos, Distribution of neurons in functional areas of the mouse cerebral cortex reveals quantitatively different cortical zones, Front Neuroanat. 7 (2013) 35. doi:10.3389/fnana.2013.00035.

[179] L.O. Ostergaard, T.O.R.S. Engedal, R. Aamand, R. Mikkelsen, N.K. Iversen, M.

Anzabi, et al., Capillary transit time heterogeneity and flow-metabolism coupling after traumatic brain injury, Journal of Cerebral Blood Flow &Amp; Metabolism. 34 (2014) 1585–1598. doi:10.1038/jcbfm.2014.131.

[180] A. Dorr, J.G. Sled, N. Kabani, Three-dimensional cerebral vasculature of the CBA mouse brain: A magnetic resonance imaging and micro computed tomography study, 35 (2007) 1409–1423. doi:10.1016/j.neuroimage.2006.12.040.

[181] F. Szoka, D. Papahadjopoulos, Procedure for preparation of liposomes with large internal aqueous space and high capture by reverse-phase evaporation, Proc Natl Acad Sci U S A. 75 (1978) 4194–4198.

[182] N. Nishiyama, H. Takemoto, Polymeric Micelles, in: S. Kobayashi, K. Müllen (Eds.), Encyclopedia of Polymeric Nanomaterials, Springer Berlin Heidelberg, Berlin, Heidelberg, 2015: pp. 1958–1963. doi:10.1007/978-3-642-29648-2_226.

[183] C. Fang, B. Shi, Y.-Y. Pei, M.-H. Hong, J. Wu, H.-Z. Chen, In vivo tumor targeting of tumor necrosis factor-α-loaded stealth nanoparticles: Effect of MePEG molecular weight and particle size, European Journal of Pharmaceutical Sciences. 27 (2006) 27–36. doi:10.1016/j.ejps.2005.08.002.

[184] C.-K. Kim, P. Ghosh, V.M. Rotello, Multimodal drug delivery using gold nanoparticles, Nanoscale. 1 (2009) 61–67. doi:10.1039/b9nr00112c.

[185] D.-F. Liu, C. Qian, Y.-L. An, Di Chang, S.-H. Ju, G.-J. Teng, Magnetic resonance imaging of post-ischemic blood-brain barrier damage with PEGylated iron oxide nanoparticles, Nanoscale. 6 (2014) 15161–15167. doi:10.1039/c4nr03942d.

[186] A.Y. Jin, U.I. Tuor, D. Rushforth, R. Filfil, J. Kaur, F. Ni, et al., Magnetic resonance molecular imaging of post-stroke neuroinflammation with a P-selectin targeted iron oxide nanoparticle, Contrast Media Mol. Imaging. 4 (2009) 305–311. doi:10.1002/cmmi.292.

[187] F.H. Kobeissy, M.S. Kindy, A. Vertegel, Nanoparticles for Neurotherapeutic Drug Delivery in Neurodegenerative Disorders *Application in Neurotrauma*, CRC Press/Taylor & Francis, Boca Raton (FL), 2015. doi:10.1517/14728210902769601.

[188] B.J. Kelley, J. Lifshitz, J.T. Povlishock, Neuroinflammatory responses after experimental diffuse traumatic brain injury, Journal of Neuropathology & Experimental Neurology. 66 (2007) 989–1001. doi:10.1097/NEN.0b013e3181588245.

[189] C.E. Dixon, J.W. Lighthall, T.E. Anderson, Physiologic, histopathologic, and cineradiographic characterization of a new fluid-percussion model of experimental brain injury in the rat, J Neurotrauma. 5 (1988) 91–104. doi:10.1089/neu.1988.5.91.

[190] R.H. Schmidt, M.S. Grady, Regional patterns of blood-brain barrier breakdown following central and lateral fluid percussion injury in rodents, J Neurotrauma. 10 (1993) 415–430.

[191] T.K. McIntosh, L. Noble, B. Andrews, A.I. Faden, Traumatic brain injury in the rat: characterization of a midline fluid-percussion model, Cent Nerv Syst Trauma. 4 (1987) 119–134.

[192] A.H. Hosseini, J. Lifshitz, Brain injury forces of moderate magnitude elicit the

fencing response, Med Sci Sports Exerc. 41 (2009) 1687–1697. doi:10.1249/MSS.0b013e31819fcd1b.

[193] X. Yun, V.D. Maximov, J. Yu, H. Zhu, A.A. Vertegel, M.S. Kindy, Nanoparticles for targeted delivery of antioxidant enzymes to the brain after cerebral ischemia and reperfusion injury, J. Cereb. Blood Flow Metab. 33 (2013) 583–592. doi:10.1038/jcbfm.2012.209.

[194] B. Ruozi, D. Belletti, H.S. Sharma, A. Sharma, D.F. Muresanu, H. Mössler, et al., PLGA Nanoparticles Loaded Cerebrolysin: Studies on Their Preparation and Investigation of the Effect of Storage and Serum Stability with Reference to Traumatic Brain Injury, Mol. Neurobiol. 52 (2015) 899–912. doi:10.1007/s12035-015-9235-x.

[195] E.J. Kwon, M. Skalak, R. Lo Bu, S.N. Bhatia, Neuron-Targeted Nanoparticle for siRNA Delivery to Traumatic Brain Injuries, ACS Nano. 10 (2016) 7926–7933. doi:10.1021/acsnano.6b03858.

[196] I. Khalin, R. Alyautdin, T.W. Wong, J. Gnanou, G. Kocherga, J. Kreuter, Brain-derived neurotrophic factor delivered to the brain using poly (lactide-co-glycolide) nanoparticles improves neurological and cognitive outcome in mice with traumatic brain injury, Drug Delivery. 23 (2016) 3520–3528. doi:10.1080/10717544.2016.1199609.

[197] J. Xu, M. Ypma, P.A. Chiarelli, J. Park, R.G. Ellenbogen, P.S. Stayton, et al., Theranostic Oxygen Reactive Polymers for Treatment of Traumatic Brain Injury, Adv. Funct. Mater. 26 (2016) 4124–4133. doi:10.1002/adfm.201504416.

[198] K.M. Guskiewicz, N.L. Weaver, D.A. Padua, W.E. Garrett, Epidemiology of Concussion in Collegiate and High School Football Players, The American Journal of Sports Medicine. 28 (2000) 643–650. doi:10.1177/03635465000280050401.

[199] S. Okie, Traumatic brain injury in the war zone, N Engl J Med. 352 (2005) 2043–2047. doi:10.1056/NEJMp058102.

[200] A.C. McKee, R.C. Cantu, C.J. Nowinski, E.T. Hedley-Whyte, B.E. Gavett, A.E. Budson, et al., Chronic traumatic encephalopathy in athletes: progressive tauopathy after repetitive head injury, Journal of Neuropathology & Experimental Neurology. 68 (2009) 709–735. doi:10.1097/NEN.0b013e3181a9d503.

[201] R. Villaseñor, L. Ozmen, N. Messaddeq, F. Grüninger, H. Loetscher, A. Keller, et al., Trafficking of Endogenous Immunoglobulins by Endothelial Cells at the Blood-Brain Barrier, Sci. Rep. (2016) 1–10. doi:10.1038/srep25658.

[202] B.R. Bitner, D.C. Marcano, J.M. Berlin, R.H. Fabian, L. Cherian, J.C. Culver, et al., Antioxidant carbon particles improve cerebrovascular dysfunction following traumatic brain injury, ACS Nano. 6 (2012) 8007–8014. doi:10.1021/nn302615f.

[203] Z.S. Bailey, E. Nilson, J.A. Bates, A. Oyalowo, K.S. Hockey, V.S.S.S. Sajja, et al., Cerium Oxide Nanoparticles Improve Outcome After In Vitro and In Vivo Mild Traumatic Brain Injury, J Neurotrauma. (2016). doi:10.1089/neu.2016.4644.

[204] I. Yamakami, T.K. McIntosh, Effects of traumatic brain injury on regional cerebral blood flow in rats as measured with radiolabeled microspheres, J. Cereb. Blood Flow Metab. 9 (1989) 117–124. doi:10.1038/jcbfm.1989.16.

[205] Y. Lin, Y. Pan, M. Wang, X. Huang, Y. Yin, Y. Wang, et al., Blood-brain barrier permeability is positively correlated with cerebral microvascular perfusion in the early fluid percussion-injured brain of the rat, Lab Invest. 92 (2012) 1623–1634. doi:10.1038/labinvest.2012.118.

[206] Á. Nyúl-Tóth, M. Suciu, J. Molnár, C. Fazakas, J. Haskó, H. Herman, et al., Differences in the molecular structure of the blood-brain barrier in the cerebral cortex and white matter: an in silico, in vitro, and ex vivo study, Am J Physiol Heart Circ Physiol. 310 (2016) H1702–H1714. doi:10.1152/ajpheart.00774.2015.

[207] I. Wilhelm, Á. Nyúl-Tóth, M. Suciu, A. Hermenean, I.A. Krizbai, Heterogeneity of the blood-brain barrier, Tissue Barriers. 4 (2016) e1143544–8. doi:10.1080/21688370.2016.1143544.

[208] A.H. Faraji, P. Wipf, Nanoparticles in cellular drug delivery, Bioorg Med Chem. 17 (2009) 2950–2962. doi:10.1016/j.bmc.2009.02.043.

[209] F. Brabazon, C.M. Wilson, D.K. Shukla, S. Mathur, S. Jaiswal, S. Bermudez, et al., [18F]FDG-PET Combined with MRI Elucidates the Pathophysiology of Traumatic Brain Injury in Rats, J Neurotrauma. 34 (2017) 1074–1085. doi:10.1089/neu.2016.4540.

[210] P. Lee, J. Kim, R. Williams, R. Sandhir, E. Gregory, W.M. Brooks, et al., Effects of aging on blood brain barrier and matrix metalloproteases following controlled cortical impact in mice, Experimental Neurology. 234 (2012) 50–61. doi:10.1016/j.expneurol.2011.12.016.

[211] K. Vagnerova, I.P. Koerner, P.D. Hurn, Gender and the Injured Brain, Anesthesia & Analgesia. 107 (2008) 201–214. doi:10.1213/ane.0b013e31817326a5.

[212] H.W. Caplan, C.S. Cox, S.S. Bedi, Do microglia play a role in sex differences in TBI? Journal of Neuroscience Research. 95 (2017) 509–517. doi:10.1002/jnr.23854.

[213] R.C. Gur, R.E. Gur, W.D. Obrist, J.P. Hungerbuhler, D. Younkin, A.D. Rosen, et al., Sex and handedness differences in cerebral blood flow during rest and cognitive activity, Science. 217 (1982) 659–661.

[214] K.M. Lenz, M.M. McCarthy, A Starring Role for Microglia in Brain Sex Differences, Neuroscientist. 21 (2015) 306–321. doi:10.1177/1073858414536468.

[215] M.M. McCarthy, G.J. De Vries, N.G. Forger, Sexual Differentiation of the Brain: Mode, Mechanisms, and Meaning, in: Hormones, Brain and Behavior, Elsevier, 2009: pp. 1707–1746. doi:10.1016/B978-008088783-8.00054-1.

[216] J.P. Niemeier, P.B. Perrin, M.G. Holcomb, C.D. Rolston, L.K. Artman, J. Lu, et al., Gender Differences in Awareness and Outcomes During Acute Traumatic Brain Injury Recovery, Journal of Women's Health. 23 (2014) 573–580. doi:10.1089/jwh.2013.4535.

[217] V. Chan, T. Mollayeva, K.J. Ottenbacher, A. Colantonio, Sex-Specific Predictors of Inpatient Rehabilitation Outcomes After Traumatic Brain Injury, Archives of Physical Medicine and Rehabilitation. 97 (2016) 772–780. doi:10.1016/j.apmr.2016.01.011.

[218] V. Chan, T. Mollayeva, K.J. Ottenbacher, A. Colantonio, Clinical profile and comorbidity of traumatic brain injury among younger and older men and women: a brief research notes, BMC Res Notes. 10 (2017) 1529–7. doi:10.1186/s13104-017-2682-x.

[219] R. Rahimian, P. Cordeau Jr, J. Kriz, Brain Response to Injuries: When Microglia Go Sexist, Neuroscience. (2018) 1–10. doi:10.1016/j.neuroscience.2018.02.048.

[220] N. Sollmann, P.S. Echlin, V. Schultz, P.V. Viher, A.E. Lyall, Y. Tripodis, et al., Sex differences in white matter alterations following repetitive subconcussive head impacts in collegiate ice hockey players, Neuroimage Clin. 17 (2018) 642–649. doi:10.1016/j.nicl.2017.11.020.

[221] R. Duvdevani, R.L. Roof, Z. FULOP, S.W. HOFFMAN, D.G. Stein, Blood-Brain-Barrier Breakdown and Edema Formation Following Frontal Cortical Contusion - Does Hormonal Status Play a Role, J Neurotrauma. 12 (1995) 65–75. doi:10.1089/neu.1995.12.65.

[222] H. Tanno, R.P. Nockels, L.H. Pitts, L.J. Noble, Breakdown of the blood-brain barrier after fluid percussion brain injury in the rat: Part 2: Effect of hypoxia on permeability to plasma proteins, J Neurotrauma. 9 (1992) 335–347.

[223] A.K. Beery, I. Zucker, Sex bias in neuroscience and biomedical research, Neuroscience & Biobehavioral Reviews. 35 (2011) 565–572. doi:10.1016/j.neubiorev.2010.07.002.

[224] R. Mostany, C. Portera-Cailliau, A craniotomy surgery procedure for chronic brain imaging, JoVE. (2008) –. doi:10.3791/680.

[225] A. Holtmaat, T. Bonhoeffer, D.K. Chow, J. Chuckowree, V. De Paola, S.B. Hofer, et al., Long-term, high-resolution imaging in the mouse neocortex through a chronic cranial window, Nat Protoc. 4 (2009) 1128–1144. doi:10.1038/nprot.2009.89.

[226] P.A. Stewart, C.R. Farrell, C.L. Farrell, E. Hayakawa, Horseradish peroxidase retention and washout in blood-brain barrier lesions, Journal of Neuroscience Methods. 41 (1992) 75–84. doi:10.1016/0165-0270(92)90125-W.

[227] Z.G. Huang, D. Xue, E. Preston, H. Karbalai, A.M. Buchan, Biphasic opening of the blood-brain barrier following transient focal ischemia: effects of hypothermia, Can J Neurol Sci. 26 (1999) 298–304.

[228] A. Chodobski, B.J. Zink, J. Szmydynger-Chodobska, Blood–Brain Barrier Pathophysiology in Traumatic Brain Injury, Transl. Stroke Res. 2 (2011) 492–516. doi:10.1007/s12975-011-0125-x.

[229] L.R. Baxter Jr., J.C. Mazziotta, M.E. Phelps, C.E. Selin, B.H. Guze, L. Fairbanks, Cerebral glucose metabolic rates in normal human females versus normal males, Psychiatry Research. 21 (1987) 237–245. doi:10.1016/0165-1781(87)90028-X.

[230] J.-P. Dollé, A. Jaye, S.A. Anderson, H. Ahmadzadeh, V.B. Shenoy, D.H. Smith, Newfound sex differences in axonal structure underlie differential outcomes from in vitro traumatic axonal injury, Experimental Neurology. 300 (2018) 121–134. doi:10.1016/j.expneurol.2017.11.001.

[231] S.F. Witelson, I.I. Glezer, D.L. Kigar, Women have greater density of neurons in

posterior temporal cortex, Journal of Neuroscience. 15 (1995) 3418–3428.

[232] D.N. Krause, S.P. Duckles, D.A. Pelligrino, Influence of sex steroid hormones on cerebrovascular function, Journal of Applied Physiology. 101 (2006) 1252–1261. doi:10.1152/japplphysiol.01095.2005.

[233] S. Tobet, J.G. Knoll, C. Hartshorn, E. Aurand, M. Stratton, P. Kumar, et al., Brain Sex Differences and Hormone Influences: A Moving Experience? Journal of Neuroendocrinology. 21 (2009) 387–392. doi:10.1111/j.1365-2826.2009.01834.x.

[234] C.M. Mack, G.W. Boehm, A.S. Berrebi, V.H. Denenberg, Sex differences in the distribution of axon types within the genu of the rat corpus callosum, Brain Research. 697 (1995) 152–156. doi:10.1016/0006-8993(95)00804-Y.

[235] M. Pesaresi, R. Soon-Shiong, L. French, D R Kaplan, F.D. Miller, T. Paus, Axon diameter and axonal transport: In vivo and in vitro effects of androgens, NeuroImage. 115 (2015) 191–201. doi:10.1016/j.neuroimage.2015.04.048.

[236] D.C. Alexander, P.L. Hubbard, M.G. Hall, E.A. Moore, M. Ptito, G.J.M. Parker, et al., Orientationally invariant indices of axon diameter and density from diffusion MRI, NeuroImage. 52 (2010) 1374–1389. doi:10.1016/j.neuroimage.2010.05.043.

[237] H.V.O. Carswell, I.M. Macrae, L. Gallagher, E. Harrop, K.J. Horsburgh, Neuroprotection by a selective estrogen receptor β agonist in a mouse model of global ischemia, Am J Physiol Heart Circ Physiol. 287 (2004) H1501–H1504. doi:10.1152/ajpheart.00227.2004.

[238] R. Liu, Y. Wen, E. Perez, X. Wang, A.L. Day, J.W. Simpkins, et al., 17β-Estradiol attenuates blood–brain barrier disruption induced by cerebral ischemia–reperfusion injury in female rats, Brain Research. 1060 (2005) 55–61. doi:10.1016/j.brainres.2005.08.048.

[239] M.E. O'Donnell, T.I. Lam, L.Q. Tran, S. Foroutan, S.E. Anderson, Estradiol Reduces Activity of the Blood–Brain Barrier Na–K–Cl Cotransporter and Decreases Edema Formation in Permanent Middle Cerebral Artery Occlusion, J. Cereb. Blood Flow Metab. 26 (2006) 1234–1249. doi:10.1038/sj.jcbfm.9600278.

[240] J.A. Shin, S.J. Yang, S.I. Jeong, H.J. Park, Y.H. Choi, E.M. Park, Activation of estrogen receptor β reduces blood-brain barrier breakdown following ischemic injury, Neuroscience. 235 (2013) 165–173. doi:10.1016/j.neuroscience.2013.01.031.

[241] I. Harukuni, P.D. Hurn, B.C.B. research, 2001, Deleterious effect of β-estradiol in a rat model of transient forebrain ischemia, Elsevier
. 900 (2001) 137–142. doi:10.1016/S0006-8993(01)02278-8.

[242] V.E. Thiel, K.L. Audus, Nitric oxide and blood-brain barrier integrity, Antioxidants & Redox Signaling. 3 (2001) 273–278. doi:10.1089/152308601300185223.

[243] Y. Gu, G. Zheng, M. Xu, Y. Li, X. Chen, W. Zhu, et al., Caveolin-1 regulates nitric oxide-mediated matrix metalloproteinases activity and blood-brain barrier permeability in focal cerebral ischemia and reperfusion injury, J Neurochem. 120 (2012) 147–156. doi:10.1111/j.1471-4159.2011.07542.x.

[244] A.S. Diler, G. Üzüm, K. Akgün Dar, U. Aksu, P. Atukeren, Y.Z. Ziylan, Sex

differences in modulating blood brain barrier permeability by NO in pentylenetetrazol-induced epileptic seizures, Life Sciences. 80 (2007) 1274–1281. doi:10.1016/j.lfs.2006.12.039.

[245] G. Üzüm, K. Akgün Dar, N. BAHÇEKAPILI, A.S. Diler, Y.Z. Ziylan, Nitric oxide involvement in seizures elicited by pentylentetrazol and sex dependence, International Journal of Neuroscience. 115 (2005) 1503–1514. doi:10.1080/00207450590957782.

[246] R. Gref, M. Lück, P. Quellec, M. Marchand, E. Dellacherie, S. Harnisch, et al., “Stealth” corona-core nanoparticles surface modified by polyethylene glycol (PEG): influences of the corona (PEG chain length and surface density) and of the core composition on phagocytic uptake and plasma protein adsorption, Colloids and Surfaces B: Biointerfaces. 18 (2000) 301–313. doi:10.1016/S0927-7765(99)00156-3.

[247] R. Gref, G. Miralles, É. Dellacherie, Polyoxyethylene-coated nanospheres: effect of coating on zeta potential and phagocytosis, Polymer International. 48 (1999) 251–256. doi:10.1002/(SICI)1097-0126(199904)48:4<251::AID-PI104>3.0.CO;2-4.

[248] E.A. Nance, G.F. Woodworth, K.A. Sailor, T.Y. Shih, Q. Xu, G. Swaminathan, et al., A Dense Poly(Ethylene Glycol) Coating Improves Penetration of Large Polymeric Nanoparticles Within Brain Tissue, Sci Transl Med. 4 (2012) 149ra119–149ra119. doi:10.1126/scitranslmed.3003594.

[249] D.G. Stein, Brain damage, sex hormones and recovery: a new role for progesterone and estrogen? Trends in Neurosciences. 24 (2001) 386–391.

[250] D.I. Shreiber, A.C. Bain, D.F. Meaney, In Vivo Thresholds for Mechanical Injury to the Blood-Brain Barrier, 1 (1997) 973335. doi:10.4271/973335.

[251] V.E. Johnson, M.T. Weber, R. Xiao, D.K. cullen, D.F. Meaney, W. Stewart, et al., Mechanical disruption of the blood–brain barrier following experimental concussion, Acta Neuropathol. (2018) 1–16. doi:10.1007/s00401-018-1824-0.

[252] S. Chen, Time course of cellular pathology after controlled cortical impact injury, Experimental Neurology. 182 (2003) 87–102. doi:10.1016/S0014-4886(03)00002-5.

[253] J.M. Ziebell, R.K. Rowe, J.L. Harrison, K.C. Eakin, T. Colburn, F.A. Willyerd, et al., Experimental diffuse brain injury results in regional alteration of gross vascular morphology independent of neuropathology, Brain Injury. 30 (2016) 217–224. doi:10.3109/02699052.2015.1090012.

[254] R.K. Rowe, D.R. Griffiths, J. Lifshitz, Midline (Central) Fluid Percussion Model of Traumatic Brain Injury, Methods Mol. Biol. 1462 (2016) 211–230. doi:10.1007/978-1-4939-3816-2_13.

[255] M.D. Habgood, D.J. Begley, N.J. Abbott, Determinants of passive drug entry into the central nervous system, Cell. Mol. Neurobiol. 20 (2000) 231–253. doi:10.1023/A:1007001923498.

[256] J.D. Meyers, T. Doane, C. Burda, J.P. Basilion, Nanoparticles for imaging and treating brain cancer, Nanomedicine. 8 (2013) 123–143. doi:10.2217/nnm.12.185.

[257] C. Berry, E.J. Ley, A. Tillou, G. Cryer, D.R. Margulies, A. Salim, The Effect of

Gender on Patients With Moderate to Severe Head Injuries, Journal of Trauma and Acute Care Surgery. 67 (2009) 950–953. doi:10.1097/TA.0b013e3181ba3354.

[258] Z. Groswasser, M. Cohen, O. Keren, Female TBI patients recover better than males, Brain Injury. 12 (2009) 805–808. doi:10.1080/026990598122197.

[259] J. Leitgeb, W. Mauritz, A.B., Effects of gender on outcomes after traumatic brain injury, Journal of neurotrauma. 6 (2011) 1620-6. doi: 10.1097/TA.0b013e318226ea0e

[260] C. Renner, H. Hummelsheim, A. Kopczak, D. Steube, H.J. Schneider, M. Schneider, et al., The influence of gender on the injury severity, course and outcome of traumatic brain injury, Brain Injury. 26 (2012) 1360–1371. doi:10.3109/02699052.2012.667592.

[261] Elana Farace, Wayne M Alves, Do women fare worse: a metaanalysis of gender differences in traumatic brain injury outcome, Http://Dx.Doi.org/10.3171/Jns.2000.93.4.0539. 93 (2009) 539–545. doi:10.3171/jns.2000.93.4.0539.

[262] M. Ottochian, A. Salim, C. Berry, L.S. Chan, M.T. Wilson, D.R. Margulies, Severe traumatic brain injury: is there a gender difference in mortality? The American Journal of Surgery. 197 (2009) 155–158. doi:10.1016/j.amjsurg.2008.09.008.

[263] C.W. Majerske, J.P. Mihalik, D. Ren, M.W. Collins, C.C. Reddy, M.R. Lovell, et al., Concussion in sports: postconcussive activity levels, symptoms, and neurocognitive performance, J Athl Train. 43 (2008) 265–274. doi:10.4085/1062-6050-43.3.265.

[264] J.H. Miller, C. Gill, E.N. Kuhn, B.G. Rocque, J.Y. Menendez, J.A. O'Neill, et al., Predictors of delayed recovery following pediatric sports-related concussion: a case-control study, J Neurosurg Pediatr. 17 (2016) 491–496. doi:10.3171/2015.8.PEDS14332.

[265] Scott L Zuckerman, Rachel P Apple, Mitchell J Odom, Young M Lee, Gary S Solomon, Allen K Sills, Effect of sex on symptoms and return to baseline in sport-related concussion, 13 (2014) 72–81. Doi.org/10.3171/2013.9.PEDS13257.

[266] S. Bodhankar, A. Lapato, Y. Chen, A.A. Vandenbark, J.A. Saugstad, H. Offner, Role for microglia in sex differences after ischemic stroke: importance of M2, Metab Brain Dis. 30 (2015) 1515–1529.

[267] A.L. Dotson, J. Wang, Y. Chen, D. Manning, H. Nguyen, J.A. Saugstad, et al., Sex differences and the role of PPAR alpha in experimental stroke, Metab Brain Dis. 31 (2015) 539–547.

[268] X. Xiong, L. Xu, L. Wei, R.E. White, Y.B. Ouyang, R.G. Stroke, et al., IL-4 is required for sex differences in vulnerability to focal ischemia in mice, Am Heart Assoc. DOI: 10.1161/STROKEAHA.115.008897

[269] F. Sohrabji, M.J. Park, A.H. Mahnke, Sex differences in stroke therapies, Journal of Neuroscience Research. 95 (2017) 681–691. doi:10.1002/jnr.23855.

[270] J.M. Schwarz, P.W. Sholar, S.D. Bilbo, Sex differences in microglial colonization of the developing rat brain, J Neurochem. 7 (2012) no–no. doi:10.1111/j.1471-4159.2011.07630.x.

[271] C.A. O'Connor, I. Cernak, R. Vink, Both estrogen and progesterone attenuate edema formation following diffuse traumatic brain injury in rats, Brain Research. 1062 (2005) 171–174. doi:10.1016/j.brainres.2005.09.011.

[272] A.J. Bruce-Keller, F.O. Dimayuga, J.L. Reed, C. Wang, R. Angers, M.E. Wilson, et al., Gender and estrogen manipulation do not affect traumatic brain injury in mice, Http://Www.Liebertpub.com/Neu. 24 (2007) 203–215. doi:10.1089/neu.2006.0163.

[273] C.H. Gleiter, U. Gundert-Remy, Gender differences in pharmacokinetics, European Journal of Drug Metabolism and Pharmacokinetics. 21 (1996) 123–128. doi:10.1007/BF03190260.

[274] P. Thuermann, Gender-related differences in pharmacokinetics and pharmacodynamics, Gender Medicine. 3 (2006) S27–S28. doi:10.1016/S1550-8579(06)80044-6.

[275] X.-D. Zhang, Chen, Song, Wang, Shen, Wu, et al., Sex differences in the toxicity of polyethylene glycol-coated gold nanoparticles in mice, Ijn. (2013) 2409–11. doi:10.2147/IJN.S46376.

[276] Y.S. Kim, J.S. Kim, H.S. Cho, D.S. Rha, J.M. Kim, J.D. Park, et al., Twenty-Eight-Day Oral Toxicity, Genotoxicity, and Gender-Related Tissue Distribution of Silver Nanoparticles in Sprague-Dawley Rats, Inhalation Toxicology. 20 (2008) 575–583.

[277] W.-Y. Kim, J. Kim, J.D. Park, H.Y. Ryu, Il Je Yu, Histological Study of Gender Differences in Accumulation of Silver Nanoparticles in Kidneys of Fischer 344 Rats, Journal of Toxicology and Environmental Health, Part A. 72 (2009) 1279–1284. doi:10.1080/15287390903212287.

[278] H. Chen, F. Spagnoli, M. Burris, W.B. Rolland, A. Fajilan, H. Dou, et al., Nanoerythropoietin is 10-times more effective than regular erythropoietin in neuroprotection in a neonatal rat model of hypoxia and ischemia, Stroke. 43 (2012) 884–887. doi:10.1161/STROKEAHA.111.637090.

[279] S.R. Popielarski, S.H. Pun, M.E. Davis, A nanoparticle-based model delivery system to guide the rational design of gene delivery to the liver. 1. Synthesis and characterization, Bioconjugate Chem. 16 (2005) 1063–1070. doi:10.1021/bc050113d.

[280] Q. Xu, L.M. Ensign, N.J. Boylan, A. Schön, X. Gong, J.-C. Yang, et al., Impact of Surface Polyethylene Glycol (PEG) Density on Biodegradable Nanoparticle Transport in Mucus ex Vivoand Distribution in Vivo, ACS Nano. 9 (2015) 9217–9227. doi:10.1021/acsnano.5b03876.

[281] A.T. Bauer, H.F.B.U. rgers, T. Rabie, H.H. Marti, Matrix metalloproteinase-9 mediates hypoxia-induced vascular leakage in the brain via tight junction rearrangement, J. Cereb. Blood Flow Metab. 30 (2009) 837–848. doi:10.1038/jcbfm.2009.248.

[282] C. Kilkenny, W. Browne, I. Cuthill, M. Emerson, D. Altman, Improving Bioscience Research Reporting: The ARRIVE Guidelines for Reporting Animal Research, Animals. 4 (2014) 35–44. doi:10.3390/ani4010035.

[283] J. Lifshitz, Fluid Percussion Injury Model, in: Animal Models of Acute Neurological

Injuries, Humana Press, Totowa, NJ, (2009): pp. 369–384. doi:10.1007/978-1-60327-185-1_32.

[284] R.K. Rowe, J.L. Harrison, B.F. O'Hara, J. Lifshitz, Recovery of Neurological Function Despite Immediate Sleep Disruption Following Diffuse Brain Injury in the Mouse: Clinical Relevance to Medically Untreated Concussion, Sleep. 37 (2014) 743–752. doi:10.5665/sleep.3582.

[285] R.K. Rowe, J.L. Harrison, B.F. O'Hara, J. Lifshitz, Diffuse brain injury does not affect chronic sleep patterns in the mouse, Brain Injury. 28 (2014) 504–510. doi:10.3109/02699052.2014.888768.

[286] R.K. Rowe, M. Striz, A.D. Bachstetter, L.J. Van Eldik, K.D. Donohue, B.F. O'Hara, et al., Diffuse Brain Injury Induces Acute Post-Traumatic Sleep, PLoS ONE. 9 (2014). doi:10.1371/journal.pone.0082507.

[287] J.L. Harrison, R.K. Rowe, B.F. O'Hara, P.D. Adelson, J. Lifshitz, Acute over-the-counter pharmacological intervention does not adversely affect behavioral outcome following diffuse traumatic brain injury in the mouse, Exp Brain Res. 232 (2014) 2709–2719. doi:10.1007/s00221-014-3948-3.

[288] R.K. Rowe, D.R. Griffiths, J. Lifshitz, Midline (Central) Fluid Percussion Model of Traumatic Brain Injury, Methods Mol. Biol. 1462 (2016) 211–230. doi:10.1007/978-1-4939-3816-2_13.

[289] R.K. Rowe, J.L. Harrison, T.C. Thomas, J.R. Pauly, P.D. Adelson, J. Lifshitz, Using anesthetics and analgesics in experimental traumatic brain injury, Lab Anim. 42 (2013) 286–291. doi:10.1038/laban.257.

APPENDIX A

A. SUPPLEMENTARY FROM CHAPTER 2

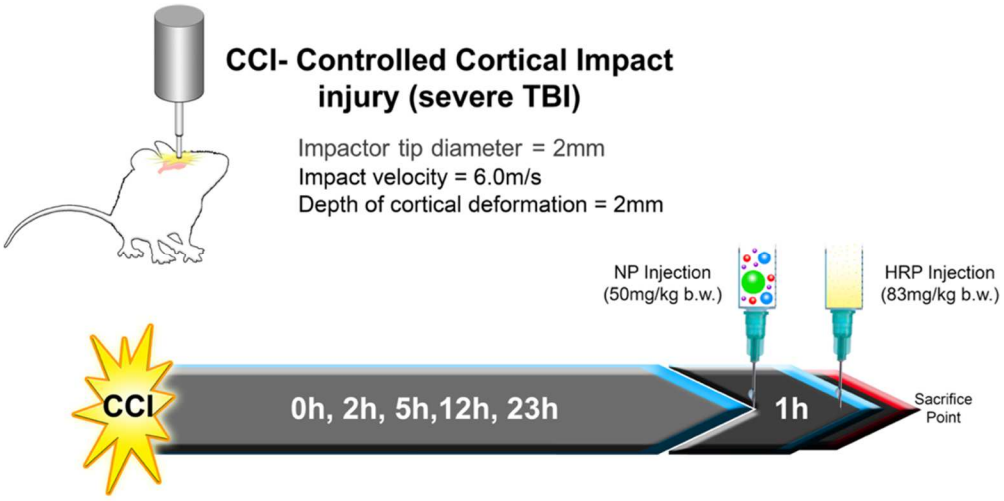

Figure A.1 In vivo experimental study design: Cocktail of different size nanoparticles (NP: 20 nm, 40 nm, 100 nm and 500 nm) was injected intravenously at various time points post CCI and animals were sacrificed one-hour post injection. HRP was injected intravenously, 10 min before sacrifice.

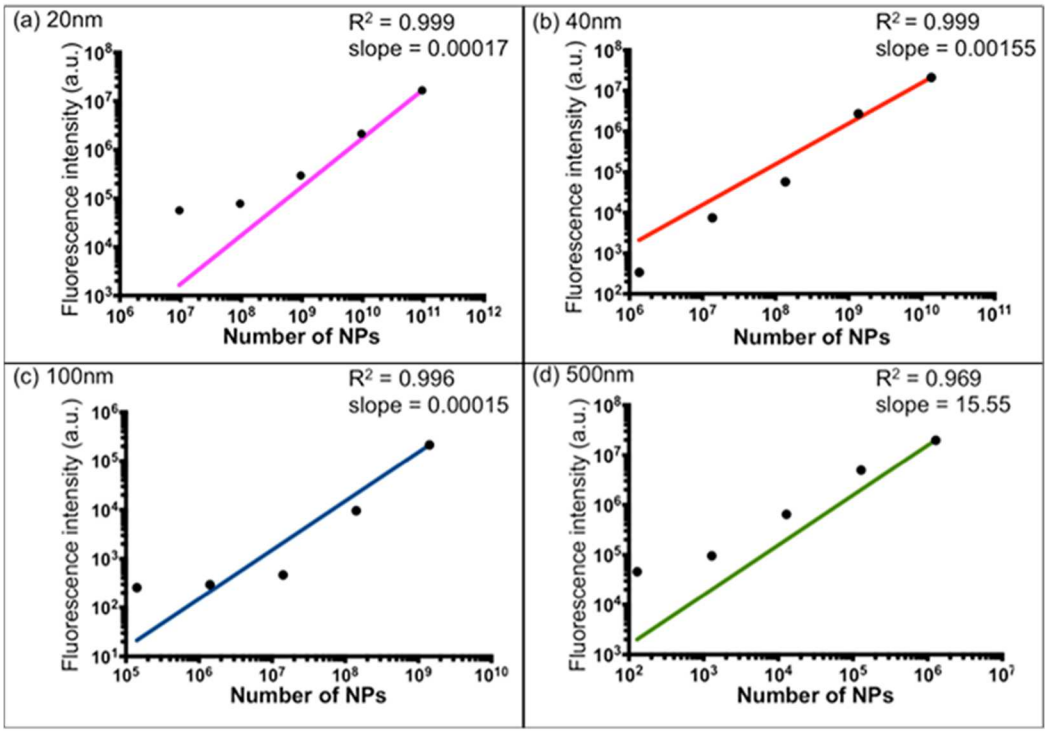

Figure A.2 Calibration curves for each NPs. (a) – (d) Linear fit calibration curves for 20 nm, 40 nm, 100 nm and 500 nm NP (a.u. arbitrary units). Data (n =5) and fits presented on a log-log scale for clarity, with R^2 ranging from 0.969 – 0.999.

Known concentrations of NPs with five dilutions: 1333 µg/ml, 133.3 µg/ml, 13.33 µg/ml, 1.333 µg/ml, and 0.1333 µg/ml were used, in triplicates. 1ul of solution was carefully pipetted into hemocytometer and measured using 20X magnification of confocal microscope. The confocal microscopy parameters were kept consistent with that used for the brain tissue sections. Two regions for each four of the channels were measured in three different samples. The amount of solution in these regions was determined by dividing the total volume of solution added and total number of squares on hemocytometer. The amount of solution (µg) was then converted to the number of NPs using the information provided by the manufactures for each NP size. A calibration curve with the intensity on y-axis and number of NP on x-axis was plotted (Figure S1). Each NP showed linear trend, with R^2 ranging between 0.96-0.99. The reciprocal of slopes

obtained from each curve was multiplied with the intensity obtained for the brain tissue measurement, to calculate the number of each NP.

APPENDIX B

B. SUPPLEMENTARY FROM CHAPTER 3

B.1 Nanoparticle (NP) PEG conjugation

As presented in our previous study[2], carboxylated NPs were PEGylated using EDC/NHS chemistry. Briefly, mPEGamine 750 Da was mixed with 20 nm NPs (NH_2:COOH at 2:1 mole excess) whereas mPEGamine 2 kDa was mixed with 40 nm, 100 nm and 500 nm NPs; (NH_2:COOH at 5:1 mole excess). EDC/NHS (in MES buffer) was added to NP / PEG mixture (8 mM/4 mM for 20 nm and 200 mM/100 mM for other NPs) and HEPES buffer was added to obtain a final pH of 7.8 before incubating for 3 h at room temperature. Glycine (100 mM) was added to quench the reaction. Unbound PEG was removed via dialysis (20 kDa MW). PEGylated NPs were suspended in a 20 mM HEPES (pH 7.4). The concentration of each NP solution was determined with fluorescent standard curves generated from known concentrations of as-received Fluorospheres (FLUOstar Omega fluorescence plate reader; BMG Labtech, Ortenberg, Germany). Yields of NPs ranged between 40-60 %. A concentration of 13.3 mg/ml for each NP was used for all *in vivo* studies.

B.2 Nanoparticle characterization

The hydrodynamic diameter and zeta potential of NPs in 20 mM HEPES (pH 7.4) were measured pre- and post-PEGylation with a dynamic light scattering (DLS) device (Zetasizer Nano Malvern; Malvern, UK). For each NP, three measurements were made and the mean ± standard error of mean (s.e.m.) was reported (Table B.1).

B.3 Animals and Study Design

Mice were housed in a 14h light/10h dark cycle at a constant temperature (23°C ± 2° C) with food and water available *ad libitum* according to the Association for Assessment and Accreditation of Laboratory Animal Care International. All mice used in this study were group housed. Mice were acclimated to their environment following shipment for at least three days prior to any experiments. All animal studies were conducted in accordance with the guidelines established by the internal IACUC (Institutional Animal Care and Use Committee) and the NIH guidelines for the care and use of laboratory animals. Studies are reported following the ARRIVE

(Animal Research: Reporting In Vivo experiments) guidelines[282]. Randomization of animals was achieved by assigning animals to time points before the initiation of the study to ensure equal distribution across groups. A power analysis was performed to calculate group sizes based on preliminary data and previously published work from our group investigating nanoparticle accumulation following controlled cortical impact in the mouse[2]. Data collection stopped at pre-determined final endpoints based on time post-injury for each animal.

B.4 Midline Fluid Percussion Injury (FPI)- Craniotomy

Mice were subjected to midline fluid percussion injury (FPI) consistent with methods previously described [283-288]. Group sizes are indicated in the results section and figure legends for individual studies. Mice were anesthetized using 5% isoflurane in 100% oxygen for five minutes and the head of the mouse was placed in a stereotaxic frame with continuously delivered isoflurane at 2.5% via nosecone. While anesthetized, body temperature was maintained using a Deltaphase® isothermal heating pad (Braintree Scientific Inc., Braintree, MA). A midline incision was made exposing bregma and lambda, and fascia was removed from the surface of the skull. A trephine (3 mm outer diameter) was used for the craniotomy, centered on the sagittal suture between bregma and lambda without disruption of the dura. An injury cap prepared from the female portion of a Luer-Loc needle hub was fixed over the craniotomy using cyanoacrylate gel and methyl-methacrylate (Hygenic Corp., Akron, OH). The incision was sutured at the anterior and posterior edges and topical Lidocaine ointment was applied. The injury hub was closed using a Luer-Loc cap and mice were placed in a heated recovery cage and monitored until ambulatory before being returned to their home cage.

After injury induction, the injury hub was removed and the brain was inspected for uniform herniation and integrity of the dura. The dura was intact in all mice; none were excluded as technical failures. The incision was cleaned using saline and closed using sutures. Diffuse brain-injured mice had righting reflex recovery times greater than five minutes and a positive fencing response. Sham injured mice recovered a righting reflex within 20 seconds. After spontaneously righting, mice were placed in a heated recovery cage and monitored until

ambulatory (approximately 5 to 15 additional minutes) before being returned to their home cage. Adequate measures were taken to minimize pain or discomfort[289].

B.5 Analysis of HRP and NP accumulation after mCHI/RmCHI

Tissue sections were incubated in PBS buffer for 20 mins at room temperature prior to use. The tissue sampling regions were directly under the impact, specifically, -1 mm to -3 mm Bregma (three sections per animal, three animals per cohort). For HRP analysis, freshly prepared DAB substrate solution (200 µl) was added to the tissue and incubated for ten mins at room temperature. Slides were then washed in PBS buffer three times (two mins each) and coversliped after adding a drop of aqueous mounting media. Sections were imaged using Slide Scanner (PathScan Enabler IV, Meyer Instruments, TX, USA).

For NP analysis, slides containing the frozen sections were incubated at room temperature for 20 mins in 1X PBS to rehydrate the tissue and remove OCT compound. Slides were coverslipped after adding one drop of fluorescent mounting media (Vectashield). The tissue sections sampling under the impact region, specifically, -1 mm to -3 mm Bregma (three sections per animal, three animals per cohort) were used. The whole brain sections were imaged with conventional epifluorescent microscopy at 10X objective.

B.6 Analysis/quantification of HRP extravasation after midline FPI

The tissue sections were incubated in PBS buffer for 20 mins at room temperature. Freshly prepared DAB substrate solution (200 µl) was added and incubated for ten mins at room temperature. Slides were then washed in PBS buffer three times (two mins each) and coverslipped after adding a drop of aqueous mounting media. Sections (three sections per animal, three animals per group) were imaged using Slide Scanner. Sections were located ~-1.65 mm Bregma. Quantitative analysis of HRP staining was accomplished by defining two regions of interest (ROI) based on previously established HRP staining patterns for FPI: (1) cortex (includes primary somatosensory and primary, and secondary motor cortex) and (2) corpus callosum [190], (S1). Specifically, ImageJ software (National institute of health, Bethesda, MD, USA) was used to

draw ROIs manually and grid lines were used as a reference tool. The full brain scan images were rotated such that the midline was oriented at the center of the grid. Next, the horizontal line tangential to the ventral aspect of the corpus callosum was used to mark the maximum extent of ROI Next, the line just below the corpus callosum was used to mark the maximum extent of the ROI (Figure S1). The ROI for the corpus callosum was drawn spanning through the entire corpus callosum above the maximum extent line. The images were then thresholded to remove background using tissue sections from HRP injected naïve brain. Thresholded images were analyzed using ImageJ to obtain percent area of positive HRP staining. Pixel value higher than that of the threshold value was considered positive for HRP stain.

B.7 Quantification of NP accumulation after midline FPI

The brain tissue was processed and analyzed similar to our previous study[2]. Briefly, slides were incubated at room temperature for 20 mins in 1X PBS to rehydrate the tissue and remove OCT compound. Coverslips were mounted on the section after adding one drop of fluorescent mounting media (Vectashield). The full brain sections (three sections per animal, three animals per group) were scanned using confocal microscopy (ZEISS LSM 800 with Airyscan, Carl Zeiss, CA, USA) at 10X magnification. Sections were located ~-1.65 mm Bregma. Scanning settings for each NP: 20 nm, 40 nm, 100 nm and 500 nm were $\lambda_{ex}/\lambda_{em}$=656 nm/683nm (600 V gain); $\lambda_{ex}/\lambda_{em}$=576 nm/607 nm (600 V gain); $\lambda_{ex}/\lambda_{em}$=357 nm/414 nm (640 V gain), and $\lambda_{ex}/\lambda_{em}$=503 nm/514 nm (600 V gain), respectively. Configuration settings were maintained constant for all the images collected. For brain sections, Z stacking was performed and total Z depth was 20 µm with a slice thickness of 5 µm. The Z stacks were converted to a single image by maximum projection tool using Zeiss software (Zen, Carl Zeiss, CA, USA). Quantitative analysis of NP accumulation was accomplished by defining two regions of interest (ROI) based on previously established HRP staining patterns for FPI: (1) cortex (includes primary somatosensory and primary, and secondary motor cortex) and (2) corpus callosum [190], (Figure S1). Specifically, ImageJ software was used to draw ROIs manually and grid lines were used as a reference tool. The full brain scan images were rotated such that the midline was oriented at the

center of the grid. Next, the horizontal line tangential to the ventral aspect of the corpus callosum was used to mark the maximum extent of ROI (Figure S1). The ROI for cortex was manually drawn spanning through the entire cortex above the maximum extent line. The ROI for corpus callosum was drawn spanning through the entire corpus callosum above the maximum extent line. The ROI images were thresholded to remove background fluorescence using tissue sections from NP injected naïve brain. The percent area of total positive NP pixels was calculated using ImageJ software. Pixel intensity value higher than that of the threshold value was considered positive for NP.

B.8 Immunohistochemical analysis for mCHI/RmCHI

Due to the complex pathophysiology of the mCHI and RmCHI models, we assessed the integrity of the BBB by the presence of intracerebral mouse IgG (immunoglobulin). A positive IgG stain within the brain parenchyma indicated the BBB was compromised at some point after injury. Brain sections from the mCHI study with single and multiple CHI impacts were used. The sections (stored at -80°C) were incubated at room temperature for 20 mins before placing them in PBS bath and washed 3 times. The slides were incubated with a solution made up of anti-mouse IgG secondary antibody 488 (1:200) with 2% goat serum and 0.1% triton X-100 for 2h at room temperature in the dark. The sections were rinsed with PBS (4 times, 5 min each) before placing the coverslip with fluorescent mounting media (Vectashield). A conventional epifluorescent microscope (Leica DMI6000 B, Leica Microsystems, Wetzlar, Germany) was used to image the stained sections.

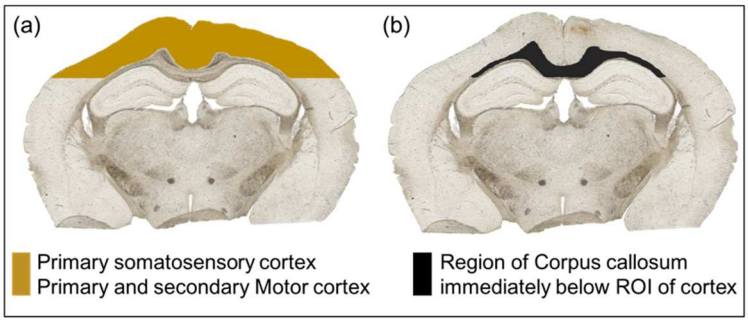

Figure B.1 Region of interest for quantification of FPI cohorts for HRP staining and NP accumulation. (a) Colored area shows the primary somatosensory, primary and secondary motor cortex. (b) Colored area shows the region of the corpus callosum immediately below the ROI of cortex.

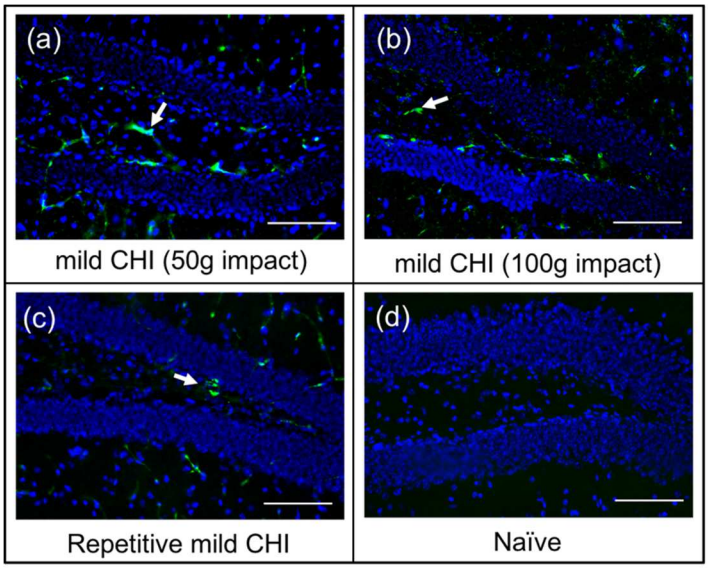

Figure B.2 Immunostain for endogenous IgG after mild/repetitive mild CHI. Positive staining of IgG shown in hippocampus (green, white arrows) and DAPI (blue) at 1h post mild CHI (50g)

(a), mild CHI (100g) (b), and repetitive mild CHI (c). As a control, naïve tissue displays no IgG but only DAPI stain (d). Scale bar = 100 μm. Note: IgG stain was observed in cortex as well (data not shown).

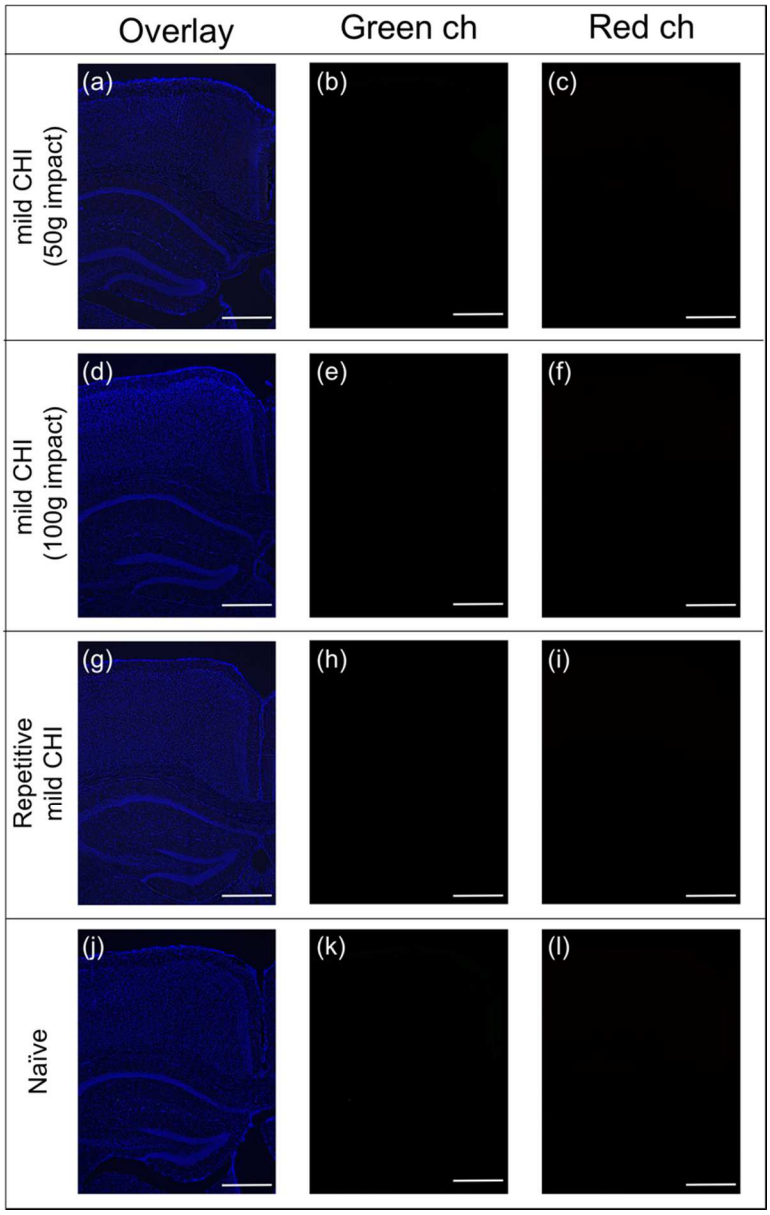

Figure B.3 Representative images from epifluorescent microscopy after mild/repetitive mild CHI. No fluorescence is observed in green (λ_{ex} 488 nm) and red (λ_{ex} 555 nm) channels (ch) after mild 50g CHI ((a)-(c)), mild 100g CHI ((d)-(f)), repetitive mild CHI ((g)-(i)), and in control

naïve groups ((j)-(l)). Overlay images were obtained by overlaying DAPI, green and red channel. Scale bar = 500 μm.

Nominal NP size (nm)	**Hydrodynamic size (nm)**	**Zeta potential (mV)**
20	23.9±2.0	-26.7±4.1
40	56.9±3.5	-10.1±5.0
100	102.3±5.6	-24.4±4.4
500	519.1±29.1	-27.1±2.2

Table B.1 PEGylated nanoparticle characterization for diffuse TBI study: Hydrodynamic diameter and zeta potential of PEGylated NP, mean±standard error of mean (n=3). Measurements in 20 mM HEPES (pH 7.4).

1	HRP - Cortex	Comparison	F (DFn, DFd)	P value	Significant
		Interaction	F (2, 12) = 7.76	P=0.0069	Yes
		Injured vs Sham	F (1, 12) = 29.02	P=0.0002	Yes
		Time points	F (2, 12) = 7.814	P=0.0067	Yes
2		Comparison	F (DFn, DFd)	P value	Significant
		Interaction	F (2, 12) = 6.619	P=0.0116	Yes

	HRP - Corpus callosum	Injured vs Sham	F (1, 12) = 6.457	P=0.0259	Yes
		Time points	F (2, 12) = 6.585	P=0.0117	Yes
NP - Cortex					
3	20 nm	Comparison	F (DFn, DFd)	P value	Significant
		Interaction	F (2, 12) = 17.71	P=0.0003	Yes
		Injured vs Sham	F (1, 12) = 27.49	P=0.0002	Yes
		Time points	F (2, 12) = 18.14	P=0.0002	Yes
4	40 nm	Comparison	F (DFn, DFd)	P value	Significant
		Interaction	F (2, 12) = 13.94	P=0.0007	Yes
		Injured vs Sham	F (1, 12) = 20.97	P=0.0006	Yes
		Time points	F (2, 12) = 14.72	P=0.0006	Yes
5	100 nm	Comparison	F (DFn, DFd)	P value	Significant
		Interaction	F (2, 12) = 5.373	P=0.0216	Yes
		Injured vs Sham	F (1, 12) = 10.47	P=0.0071	Yes
		Time points	F (2, 12) = 7.76	P=0.0069	Yes

6	500 nm	Comparison	F (DFn, DFd)	P value	Significant
		Interaction	F (2, 12) = 11.15	P=0.0018	Yes
		Injured vs Sham	F (1, 12) = 26.16	P=0.0003	Yes
		Time points	F (2, 12) = 12.23	P=0.0013	Yes
NP - Corpus callosum					
7	20 nm	Comparison	F(DFn, DFd)	P value	Significant
		Interaction	F (2, 12) = 0.4299	P=0.6602	No
		Injured vs Sham	F (1, 12) = 0.7643	P=0.3991	No
		Time points	F (2, 12) = 1.736	P=0.2176	No
8	40 nm	Comparison	F(DFn, DFd)	P value	Significant
		Interaction	F (2, 12) = 1.015	P=0.3915	No
		Injured vs Sham	F (1, 12) = 1.502	P=0.2438	No
		Time points	F (2, 12) = 1.081	P=0.3701	No
9	100 nm	Comparison	F (DFn, DFd)	P value	Significant
		Interaction	F (2, 12) = 3.555	P=0.0613	No
		Injured vs Sham	F (1, 12) = 2.893	P=0.1147	No
		Time points	F (2, 12) = 3.106	P=0.0818	No

10	500 nm	Comparison	F (DFn, DFd)	P value	Significant
		Interaction	F (2, 12) = 0.8051	P=0.4698	No
		Injured vs Sham	F (1, 12) = 1.491	P=0.2455	No
		Time points	F (2, 12) = 1	P=0.3965	No

Table B.2 Statistical analysis for HRP and NP after FPI study: Tabular results of two-way ANOVA for HRP extravasation in the cortex (row 1) and corpus callosum (row 2). The two-way ANOVA results of Nanoparticle accumulation in the cortex for 20 nm (row 3), 40 nm (row 4), 100 nm (row 5) and 500 nm (row 6) are displayed. The two-way ANOVA results for nanoparticle analysis in the corpus callosum for 20 nm (row 7), 40 nm (row 8), 100 nm (row 9) and 500 nm (row 10) are shown.